International Scientific-Technical and Production Journal

The Paton WELDING JOURNAL

March
2008
3

English translation of the monthly «Avtomaticheskaya Svarka» (Automatic Welding) journal published in Russian since 1948

Founders: *E.O. Paton Electric Welding Institute of the NAS of Ukraine*
International Association «Welding»

Publisher: *International Association «Welding»*

Editor-in-Chief B.E.Paton

Editorial board:

Yu.S.Borisov V.F.Grabin
A.Ya.Ishchenko V.F.Khorunov
B.V.Khitrovskaya I.V.Krivtsun
S.I.Kuchuk-Yatsenko
Yu.N.Lankin V.K.Lebedev
V.N.Lipodaev L.M.Lobanov
V.I.Makhnenko A.A.Mazur
O.K.Nazarenko I.K.Pokhodnya
I.A.Ryabtsev Yu.A.Sterenbogen
N.M.Voropai K.A.Yushchenko
A.T.Zelnichenko

International editorial council:

N.P.Alyoshin (Russia)
U.Diltey (Germany)
Guan Qiao (China)
D. von Hofe (Germany)
V.I.Lysak (Russia)
N.I.Nikiforov (Russia)
B.E.Paton (Ukraine)
Ya.Pilarczyk (Poland)
P.Seyffarth (Germany)
G.A.Turichin (Russia)
Zhang Yanmin (China)
A.S.Zubchenko (Russia)

Promotion group:

V.N.Lipodaev, V.I.Lokteva
A.T.Zelnichenko (exec. director)
Translators:
I.N.Kutianova, V.F.Orets,
T.K.Vasilenko, N.V.Yalanskaya
Editor
N.A.Dmitrieva
Electron galley:
I.S.Dmitruk, T.Yu.Snegiryova

Address:
E.O. Paton Electric Welding Institute,
International Association «Welding»,
11, Bozhenko str., 03680, Kyiv, Ukraine
Tel.: (38044) 287 67 57
Fax: (38044) 528 04 86
E-mail: journal@paton.kiev.ua
http://www.nas.gov.ua/pwj

State Registration Certificate
KV 4790 of 09.01.2001

Subscriptions:
$324, 12 issues per year,
postage and packaging included.
Back issues available.

All rights reserved.
This publication and each of the articles contained herein are protected by copyright. Permission to reproduce material contained in this journal must be obtained in writing from the Publisher.
Copies of individual articles may be obtained from the Publisher.

CONTENTS

© PWI, International Association «Welding», 2008

TAKING INTO ACCOUNT OF HIGH-FREQUENCY MECHANICAL PEENING INFLUENCE ON CYCLIC WORKING LIFE OF WELDED JOINTS AT DOUBLE-FREQUENCY LOADING

V.S. KOVALCHUK
E.O. Paton Electric Welding Institute, NASU, Kiev, Ukraine

Methodology, analytical dependences and nomograms for determining area of efficient use of hardening of the 09G2S steel welded joints by high-frequency mechanical peening and estimation of its influence on increase of cyclic working life at double-frequency loading are proposed.

Keywords: arc welding, welded steel structures, double-frequency loading, welded joints, increase of cyclic working life, high-frequency mechanical peening

Increase of cyclic working life of welded metal structures at the stage of their manufacturing and after repair and restoration of joints by means of welding is an important and actual task. There are different methods for increasing resistance to fatigue of welded joints. As a rule, they are based on removal of tensile or artificial induction of favorable compression residual stresses in the area of the weld transition to the base metal.

One of the most efficient, productive and economical methods of creation of residual compression stresses, reduction of stress concentration and surface hardening of the weld metal or area of the weld transition to the base metal is high-frequency mechanical peening (HFMP) with application of ultrasonic converters [1–3]. At single-frequency loading such additional treatment may increase 2–10 times cyclic working life of welded joints of structural steels depending upon a type of the joints, class of the material strength and asymmetry of the cycle. However, a real loading spectrum of many elements of structures consists of two and more simultaneously acting variable components of different amplitude and frequency. Previously obtained results of experimental investigations showed that cyclic working life of materials and welded joints at double-frequency loading depends upon amplitude and frequency ratios of stresses, as well as mechanical characteristics of the metals [4], whereby by means of increase of the latter working life significantly reduces. As far as in mechanical peening surface hardening of the metal occurs due to elastic-plastic strain [3], one may expect reduction of efficiency of this kind of treatment of the items, which operate under conditions of variable loading with additional stresses from vibrations.

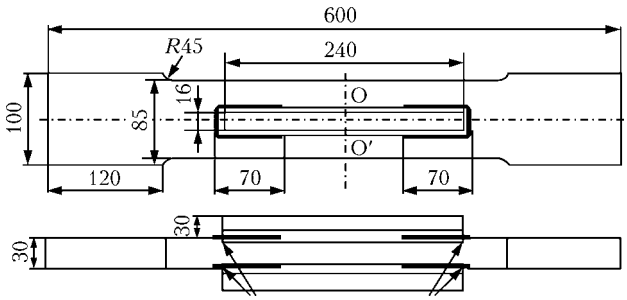

Figure 1. View of specimen for assessment of HFMP efficiency in increase of resistance to fatigue of welded joints at loading cycles of simple and complex forms (arrows show position of zones treated by peening)

For assessing influence of HFMP on enhanced resistance to fatigue of welded joints under conditions of double-frequency loading, experimental investigations of large-scale specimens from the 09G2S low-alloy steel with longitudinal ribs (Figure 1), having high values of concentration of stresses and level of residual tensile welding stresses in initial state, comparable with those in real structures, were carried out. Welds on longitudinal ribs of the specimens were produced by manual arc welding using the UONI-13 / 55 stick electrodes with full penetration.

For obtaining initial data on resistance to fatigue of the joints at single- and double-frequency loading the samples were tested in the post-welding state. For estimating influence of hardening on enhancement of working life of the joints under similar conditions of tests, areas of the weld transition to the base metal within 70 mm length from edge of ribs of the specimens were additionally treated by HFMP. Fatigue tests were continued under the same conditions of loading till formation of new cracks of the same size. On the specimens in initial state, after they were tested at double-frequency loading till formation of fatigue cracks of critical size, role of forging was determined on the repaired welds. For this purpose metal around the cracks was removed by the finger-type cutter, recesses were welded up by the UONI-13 / 55 electrodes, and transition zone from the weld to the base metal was treated by HFMP.

© V.S. KOVALCHUK, 2008

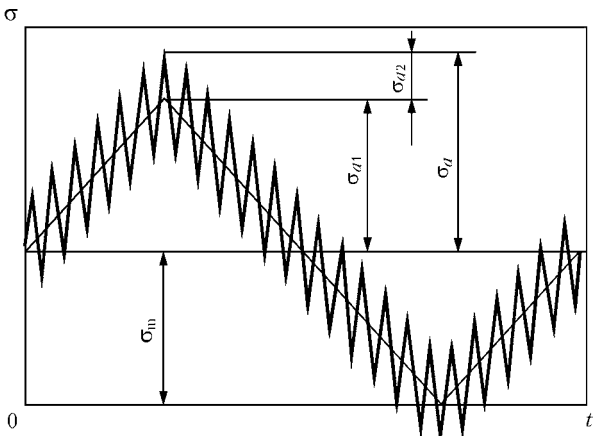

Figure 2. Form of loading cycle: σ_{a2} / σ_{a1} — amplitudes of low- and high-frequency stresses, respectively; σ_a — total amplitude of stresses; σ_m — mean stress of cycle; t — time

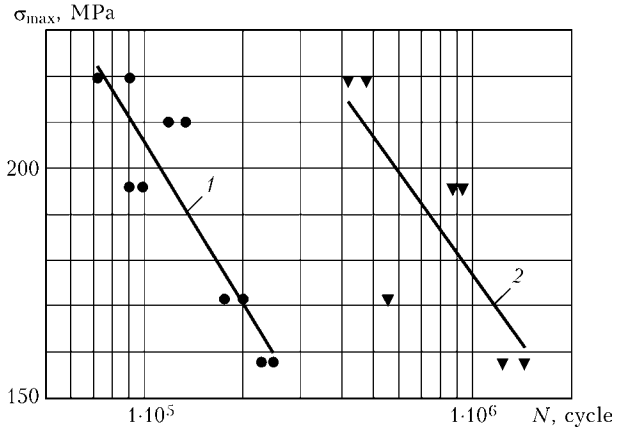

Figure 3. Resistance to fatigue of welded joints of 09G2S steel with longitudinal stiffening ribs at zeroed single-frequency extension in initial state (*1*) and after HFMP (*2*)

Fatigue tests of the specimens were carried out under mild conditions of zeroed single- and double-frequency axial extension on the URS 200 / 20 servo-hydraulic machine. In process of the tests fatigue cracks, as a rule, originated over fusion line of the end-lap weld with the base metal. Criterion for termination of the tests was a developing fatigue crack of 20 mm length.

Fatigue tests at a single-frequency loading were carried out at frequency f_1 = 5 Hz, frequency of additional vibrations under conditions of a double-frequency loading (Figure 2) was f_2 = 10 Hz. Low-frequency component of the double-frequency loading with ratio of frequencies f_2 / f_1 = 100 was f_1 = 0.1 Hz. Tests at the double-frequency loading were carried out at ratio of amplitudes of high- and low-frequency components σ_{a2} / σ_{a1} ≈ 0.2 and 0.4.

The results obtained of the fatigue tests at a single-frequency loading of the specimens in initial state *1* and after HFMP *2* are presented in Figure 3. Comparison of these data shows that HFMP of the 09G2S steel welded joints with longitudinal stiffening ribs increases cyclic working life at a single-frequency loading 5 times:

$$K_{1WLI} = N_{1h} / N_{1i}, \quad (1)$$

where K_{1WLI} is the coefficient of working life increase at single-frequency loading after forging of the joint; N_{1h}, N_{1i}, is the cyclic working life (number of cycles) at a single-frequency loading of a welded joint hardened by peening and in initial state, respectively.

Results of investigations of resistance to fatigue at double-frequency loading of similar 09G2S steel specimens in initial state and after HFMP of the areas of transition from the weld to the base metal of the joints in initial state and after welding repair are presented in the Table.

Coefficient of the cyclic working life reduction of the welded joints at double-frequency loading in initial after the welding state and after high-frequency peening was determined using previously obtained for steels of different classes of strength and types of joints analytical dependence, invariant to concentra-

Resistance to fatigue of 09G2S steel welded joints with longitudinal stiffening ribs under conditions of axial zeroed double-frequency tension

State of specimen	Maximal stress σ_{1max}, MPa	σ_{a2}/σ_{a1}	Number of loading cycles		æ (experimental)	ϑ (calculated)	ϑ (mean)
			$N_2 \cdot 10^{-3}$	$N_1 \cdot 10^{-3}$			
Initial after welding	202.8	0.177	25.396	97	3.82	1.60	1.4
	206.0	0.193	22.492	90	4.00	1.53	
	203.6	0.380	8.700	95	10.92	1.37	
	210.3	0.430	7.105	76	10.70	1.19	
After peening in initial state	230.0	0.220	36.646	300	8.19	2.10	2.1
	206.0	0.193	79.916	500	6.26	2.00	
	222.5	0.190	26.200	340	13.00	2.80	
	203.6	0.380	17.270	530	30.68	1.96	
	210.3	0.430	14.825	430	29.00	1.70	
After welding repair and peening	230.0	0.200	37.250	300	8.10	2.20	2.0
	206.0	0.193	71.400	500	7.00	2.18	
	203.6	0.380	19.890	530	26.60	1.87	
	210.3	0.430	15.330	430	28.10	1.67	

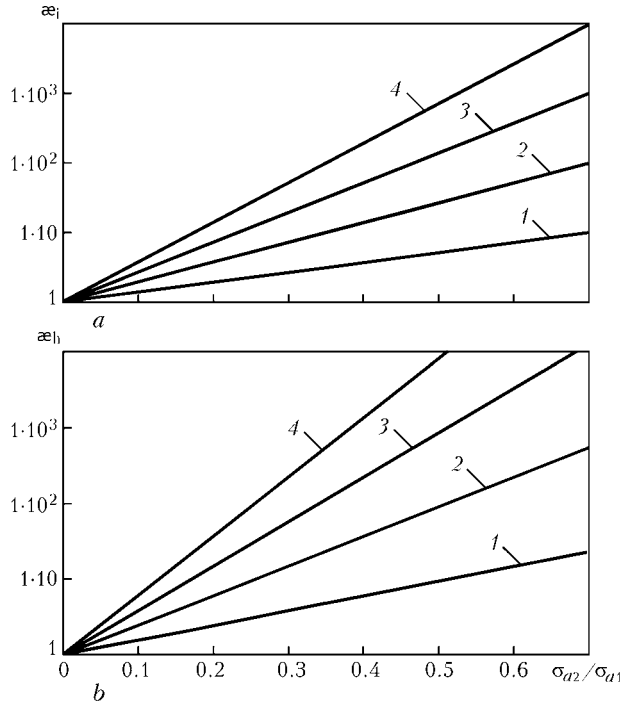

Figure 4. Nomograms for determining coefficient of cyclic working life reduction of welded joints of 09G2S steel at double-frequency extension in initial state (*a*) and after hardening by HFMP in initial state and after welding repair (*b*), obtained at different ratios of frequencies: *1* — $f_2 / f_1 = 1 \cdot 10$; *2* — $1 \cdot 10^2$; *3* — $1 \cdot 10^3$; *4* — $1 \cdot 10^4$

tions of stresses, residual stress level, temperature, cycle characteristic, kind and level of loading, and a number of other factors [5]:

$$æ = (f_2 / f_1)^{\vartheta(\sigma_{a2}/\sigma_{a1})}, \quad (2)$$

where $æ = N_1 / N_2$ is the coefficient of cyclic working life reduction at a double-frequency loading determined by ratio of working lives under conditions of single- and double-frequency loading at the same levels of low-frequency stress, coefficient of the cycle asymmetry, residual stresses, temperature and other parameters; N_1 is the working life (number of cycles) of a welded joint at a single-frequency loading; N_2 is the same at a double-frequency loading estimated by the number of the low-frequency component cycles; ϑ is the correction coefficient, depending upon mechanical properties of the material.

As one can see from the Table, the ϑ values for hardened by peening welded joints are higher than

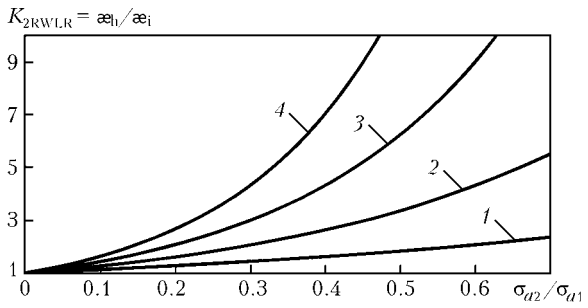

Figure 5. Nomogram for determining coefficient K_{2RWLR} of relative working life reduction at double-frequency loading of welded joints hardened by peening (*1–4* are the same as in Figure 4)

for the joints in initial state. On basis of these data nomograms are built using dependence (2) for determining coefficients of working life reduction of the 09G2S steel welded joints at a double-frequency loading in initial state (Figure 4, *a*) in the form of the ratio of working lives:

$$æ_h = N_{1i} / N_{2i}, \quad (3)$$

and after hardening by HFMP of the joints in initial state or after welding repair (Figure 4, *b*):

$$æ_i = N_{1h} / N_{2h}, \quad (4)$$

where N_{2i} and N_{2h} are the working life at the double-frequency loading of a welded joint, calculated by number of cycles of the low-frequency component in initial state and after hardening of the joint by high-frequency peening, respectively.

As one can see from Figure 4, at fixed values of ratios of amplitudes and frequencies, values of the working life reduction coefficient $æ_h$ of welded joints, strengthened by high-frequency peening, are in initial state or after repair welding higher than of the coefficient $æ_i$ of welded joints in initial state without hardening. As far as coefficients of the working life reduction at the double-frequency loading $æ_h$ and $æ_i$ in the considered cases are determined by the analytical dependence (2) and differ only by values of coefficient ϑ, coefficient K_{2RWLR} of relative working life reduction at the double-frequency loading of welded joints after their hardening by HFMP may be presented in the following form:

$$K_{2RWLR} = æ_h / æ_i = (f_2 / f_1)^{(\sigma_{a2}/\sigma_{a1})(\vartheta_h - \vartheta_i)}. \quad (5)$$

Taking into account obtained values ϑ_h and ϑ_i, this analytical dependence in graphic form is presented in Figure 5. One can see from this Figure that by means of growth of the amplitude and frequency ratios of the double-frequency loading components, cyclic working life of the 09G2S steel welded joints, treated by HFMP, reduces more intensively than of the joints in initial state. Due to this efficiency of the peening reduces and beginning from certain values of the double-frequency loading parameters HFMP may become useless or even harmful.

Evidently, at double-frequency loading additional peening is efficient only in case, when values of coefficient K_{1WLI} of working life increase under conditions of a single-frequency loading are higher than coefficient of relative working life reduction K_{2RWLR} under conditions of double-frequency loading.

Real values of the efficient coefficient of cyclic working life increase at the double-frequency loading K_{2EWLI} of hardened by HFMP welded joints of the 09G2S steel may be found from the dependence

$$K_{2EWLI} = K_{1WLI} / K_{2RWLR}, \quad (6)$$

having substituted into it actual values from expressions (1) and (5).

For the investigated welded joints of the 09G2S steel, $\vartheta_h = 2.1$, $\vartheta_i = 1.4$ and $K_{1WLI} = 5$ were experimentally determined. After substitution of these data in expression (5), efficient coefficient of working life increase by HFMP of welded joints of the 09G2S steel at the double-frequency loading is determined from the analytical expression

$$K_{2EWLI} = 5/(f_2/f_1)^{0.7(\sigma_{a2}/\sigma_{a1})}, \quad (7)$$

or from its dependences, presented in Figure 6.

It is evident that additional high-frequency peening of welded joints at the double-frequency loading is expedient, if value K_{2EWLI} significantly exceeds 1. However, proceeding from technical and economic reasons one may recommend using its minimal value at the level $K_{2EWLI} = 1.5$ (in Figure 6 this level is indicated by the dashed line).

At values of efficient coefficient of the working life increase $K_{2EWLI} = 1.5 \div 1.0$, HFMP gets ineffective, and at $K_{2EWLI} < 1$ — harmful. As one can see from Figure 6, in this case in the area of efficient use of HFMP, maximal value σ_{a2}/σ_{a1} reduces from 0.9 to 0.2 for the purpose of increasing working life of the 09G2S steel welded joints when ratio f_2/f_1 increases from $1 \cdot 10$ to $1 \cdot 10^4$.

On basis of the results obtained of the investigations one may recommend for increasing cyclic working life at the double-frequency loading the following procedure for determining the need and taking into account hardening by HFMP of welded joints of the 09G2S steel in initial state or after repair welding:

- proceeding from the preset parameters of the double-frequency loading, values of efficient coefficient K_{2EWLI} of the working life increase by HFMP of welded joints of the 09G2S steel are determined by analytical dependence (7) or a nomogram presented in Figure 6 for the investigated type of a joint or taking into account values K_{1WLI} for other types of joints and asymmetry of the loading cycle;
- application of HFMP is considered expedient, provided coefficient of cyclic working life increase by high-frequency peening $K_{2EWLI} = 1.5$ or more;
- using fatigue curve *1* (see Figure 3) for investigated type of the joint or respective dependences or fatigue curves of other types of joints and asymmetry of cycle of stresses, number of cycles N_{1i} is found at single-frequency loading by the level of stresses, corresponding to the low-frequency component of the double-frequency loading;
- coefficient of the cyclic working life reduction $æ_h$ is calculated using formula (2) or nomogram (see Figure 4, *b*), where coefficient, depending upon properties of the material for welded joints of the 09G2S steel after HFMP, equals $\vartheta = 2.1$;
- calculated number of the low-frequency component of the stress cycles at double-frequency loading of a welded joint, hardened by high-frequency peening, is found, taking into account influence of the high-frequency component from the expression $N_{2h} = N_{1i}/æ_h$.

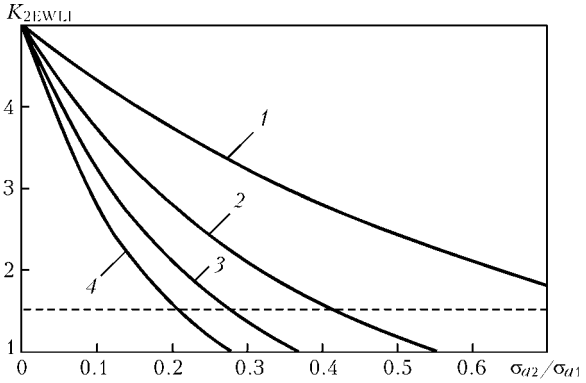

Figure 6. Nomogram for determining area of efficient application of HFMP for purpose of increasing working life of welded joints of 09G2S steel at different parameters of double-frequency loading (*1*–*4* are the same as in Figure 4)

CONCLUSIONS

1. Coefficient of the cyclic working life reduction at the double-frequency peening of welded joints of the 09G2S steel after HFMP is determined by the same analytical expression, which is used without peening, but with different values of correction coefficients ϑ.

2. In analytical expression of reduction of the cyclic working life coefficient, index of the power for the joints treated by peening, is 1.5 times higher than for the untreated ones. Due to this cyclic working life of welded joints of the 09G2S steel, hardened by HFMP, reduces under conditions of double-frequency loading to a greater degree than without peening; this difference increases by means of increase of the ratios of amplitudes and frequencies.

3. Depending upon ratio of frequencies of the double-frequency loading components f_2/f_1 (from $1 \cdot 10$ to $1 \cdot 10^4$) area of efficient application of high-frequency peening for the purpose of increasing working life of welded joints of the 09G2S steel is limited by ratio of the σ_{a2}/σ_{a1} stresses from 0.9 to 0.2 respectively.

4. For additional high-frequency peening of welded joints of the 09G2S steel to be justified, recommended minimal value of efficient coefficient of the working life increase K_{2EWLI} should be not less than 1.5.

1. Mikheev, P.P. (1990) Increase in fatigue strength of structure welded joints by ultrasonic percussion treatment. In: *Transact. on Problems of Welding and Special Electrometallurgy*. Kiev: Naukova Dumka.
2. Knysh, V.V., Kuzmenko, A.Z. (2005) Increase in fatigue strength of welded joints by high-frequency mechanical peening. *Svarshchik*, **2**, 19–21.
3. Lobanov, L.M., Kirian, V.I., Knysh, V.V. (2006) Increase in life of welded metal structures by high-frequency mechanical peening. *Fiziko-Khim. Mekhanika Materiala*, **1**, 56–61.
4. Trufyakov, V.I., Kovalchuk, V.S. (1982) Determination of service life at two-frequency loading. Report 2: Procedure. *Problemy Prochnosti*, **10**, 15–20.
5. Kovalchuk, V.S. (1993) Fatigue strength of welded joints at two-frequency loading. In: *Welded building structures*. Ed. by L.M. Lobanov. Vol. 1: Basis of structure design. Kiev: Naukova Dumka.

CALCULATION PREDICTION OF OVERALL DISTORTIONS IN LASER WELDED BEAMS

O.V. MAKHNENKO[1] and **P. SEYFFARTH**[2]
[1]E.O. Paton Electric Welding Institute, NASU, Kiev, Ukraine
[2]IMG, Germany

Mathematical model is described, which was developed for prediction of overall bending distortions of long beams in laser welding to optimise the distance between the fixing supports, at which deviation of the laser beam from the joint site is not in excess of the admissible value.

Keywords: laser welding, welded beams, overall bending distortions, fixation system, numerical investigation

Intensively widening application of laser technologies, in particular, in fabrication of welded structures, made it necessary to address new problems, one of which is ensuring a high accuracy of positioning of the weld. A beam is distorted during welding, and deviation of the laser beam moving along the preset path may exceed the admissible value. Allowance for deviation of the laser beam in welding beams with a wall thickness of 4–19 mm is approximately ±0.3 mm. Fixations are used to limit distortions of the beams during welding. In welding long beams (up to 6000 mm long), a large number of fixations increases the labour intensity and, correspondingly, decreases the productivity of the technological process. Under conditions of modern flexible small-lot (at the customer's request) manufacturing of different profiles of welded beams, experimental setting of optimal distances between the fixations is unprofitable. That led to the need to develop a mathematical model, which would allow prediction of temporary and residual welding bending distortions of different profiles of beams, as well as optimisation of a distance between fixations along the length of a beam at a preset allowance for deviation of the laser beam.

Application of a general approach of 3-D modelling by the finite element method to determine overall distortions of long beams is time-consuming and requires substantial computer resources. Therefore, the following assumptions were made in the calculation model used.

To calculate temperature fields, the use is made of an assumption of a fast-moving heat source, where the 3-D problem is reduced to a set of 2-D problems solved by the finite element method for the cross sections considered along the length of a beam.

The mechanical problem for determination of stresses and strains in the cross sections considered at a preset temperature field is solved by the finite element methods within the framework of a beam hypothesis of plane sections using the thermoplasticity theory methods [1]. It is reported [2] that the use of the beam hypotheses or hypotheses of plane sections for determination of stresses and strains in long welded beams makes it possible to achieve the satisfactory results, compared with the results obtained by 3-D modelling. The results may differ to some extent in regions of the beginning and end of the beam. At the same time, the calculation model can be substantially simplified. The solution is found by successive tracing of development of elasto-plastic strains in each section of the beam. At each tracing stage, physical non-linearity related to plastic strains is realised by means of the iteration process with respect to material state function $\psi(x, y, z, t)$ at each considered point of the beam at time moment t. Therefore, the non-linear problem at each tracing stage is replaced by a set of the successively solved linearised problems.

To determine the «shrinkage function» for a case of bending distortions in welding of the beams hinged at the ends, or preset axial forces at the edges and bending moments, it is usually enough to consider characteristic section x = const, within which the known temperature field of heating and cooling is $T(y, z, t)$, as well as the external axial force is $N_{xx}(t)$ and moments are $M_{yy}(t)$ and $M_{zz}(t)$. This is a statically determined problem, where at each tracing stage the increments of curvature $\Delta\kappa_{yy}(t)$ and $\Delta\kappa_{zz}(t)$, and those of longitudinal shortening $\Delta\varepsilon^0_{xx}(t) = \Delta\varepsilon_{xx}(0, 0, t)$, are determined within the framework of the beam hypotheses from the following equilibrium equations [1]:

$$\Delta\varepsilon^0_{xx}L_{j1} + \Delta\kappa_{zz}L_{jz} + \Delta\kappa_{yy}L_{jy} + P_j = \overline{M}_j \quad (j = 1, z, y), \quad (1)$$

where $L_{iq} = \int\limits_F \frac{jq}{B_1}\, dF(i, q = 1, z, y)$; $P_j = \int\limits_F b_{xx}\frac{dF}{B_1} \times$ $\times (j = 1, z, y)$; F is the cross section area of the beam; $\overline{M}_j$ is the external load, i.e. at $j = 1$ it is force $N_{xx}(t)$, and at $j = z, y$ these are moments $M_{zz}(t)$ and $M_{yy}(t)$, respectively, which act in a given section at time moment t; $B_1 = \frac{2\psi + K}{3}$; ψ is the material state function; and $K = \frac{1 - 2\nu}{E}$ is the volumetric compression modulus for the plane stressed state.

At normal stresses other than zero, σ_{xx} also corresponds to the plane stressed state, i.e.

© O.V. MAKHNENKO and P. SEYFFARTH, 2008

$$b_{xx} = \left(\frac{\sigma_{xx} - \frac{1}{3}\sigma_{xx}}{2G} + K\frac{\sigma_{xx}}{3} \right)_{t-\Delta t} - \Delta\varphi = \left(\frac{\sigma_{xx}}{E} \right)_{t-\Delta t} - \Delta\varphi. \quad (2)$$

Stresses $\sigma_{xx}(y, z, t)$ are determined by the following relationship:

$$\sigma_{xx}(y, z, t) = \frac{1}{B_1} [\Delta\varepsilon^0_{xx}(t) + \Delta\kappa_{zz}(t)z + \Delta\kappa_{yy}(t)y - b_{xx}]. \quad (3)$$

State function $\psi(y, z, t)$ is found by the iteration method using the known algorithm [1]. At each iteration by ψ, it is necessary to solve the system of equilibrium equations (1), the matrix of which is symmetrical and positively defined, which is a sufficient condition for existence and uniqueness of the solution for this system at preset $\overline{M}_j$.

In the case of a multiple-support beam (Figure 1), the forces at the supports, $Q_{ji}(t)$ ($j = y, z$; $i = 0, 1, 2, \ldots, N$), depend upon the stressed state, providing that at the supports the increments of displacements are

$$\Delta U_{ji} = 0 \quad (j = y, z; \quad i = 0, 1, \ldots, N). \quad (4)$$

As the solution with respect to function $\Delta U_j(x, t)$ at each iteration by ψ is determined at the preset values of $\psi(x, y, z, t)$, it is more convenient to find it in the form of a sum

$$\Delta U_j(x, t) = \Delta U_j^{(T)}(x, t) + \Delta U_j^{(Q)}(x, t) \ (j = z, y). \quad (5)$$

Accordingly, the increment of curvature, $\Delta\kappa_{ij}(x, t)$, can be represented by the following sum:

$$\Delta\kappa_{ij}(x, t) = \Delta\kappa_{ij}^{(T)}(x, t) + \Delta\kappa_{ij}^{(Q)}(x, t). \quad (6)$$

In this case, $\Delta\kappa_{ij}^{(T)}(x, t)$ satisfies the equilibrium equations in section x = const at $\overline{M}_j \equiv 0$, and $\Delta\kappa_{ij}^{(Q)}(x, t)$ can be determined, accordingly, from equations (1) in the following form:

$$\Delta\kappa_{zz}^{Q_j} L_{jz} + \Delta\kappa_{yy}^{Q_j} L_{jy} = \overline{M}_j(Q_j) (j = y, z), \quad (7)$$

i.e.

$$\Delta\kappa_{yy}^{Q} = \frac{L_{zz}\overline{M}_y - \overline{M}_z L_{zy}}{L_{zz}L_{yy} - L_{zy}^2} = \overline{M}_y A_y - M_z D;$$

$$\Delta\kappa_{zz}^{Q} = \frac{L_{yy}\overline{M}_z - \overline{M}_y L_{zy}}{L_{zz}L_{yy} - L_{zy}^2} = \overline{M}_z A_z - M_y D, \quad (8)$$

where $\overline{M}_y$ and $\overline{M}_z$ are the bending moments in section x = const by caused unknown forces $Q_{yi}(t)$, $Q_{zi}(t)$ ($i = 0, 1, \ldots, N$) at the supports

$$A_y = \frac{L_{zz}}{\Delta}; \quad D = \frac{L_{zy}}{\Delta}; \quad A_z = \frac{L_{yy}}{\Delta}; \quad \Delta = L_{zz}L_{yy} - I_{zy}^2.$$

Considering the static equation for forces $Q_{ji}(t)$, i.e.

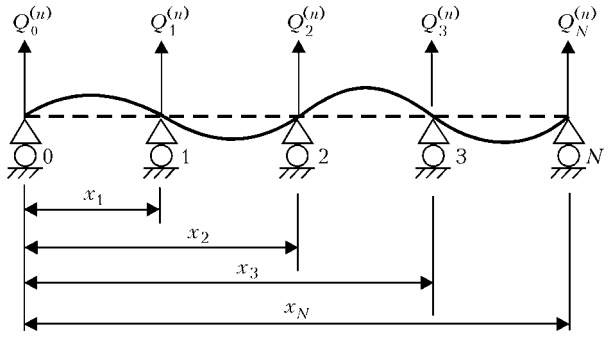

Figure 1. Conditions of fixation of multiple-support beam (n = y, z)

$$\sum_{i=0}^{N} Q_{ji} = 0, \quad \sum_{i=0}^{N} Q_{ji} l_i = 0, \quad (9)$$

where l_i is the distance from the i-th support to the zero one, it can be written down that

$$\overline{M}_j(x) = Q_{0j} l_1 + Q_{1j}(x - l_1) \quad \text{for} \quad l_1 < x < l_2,$$
$$\overline{M}_j(x) = Q_{0j} x + Q_{1j}(x - l_1) + Q_{2j}(x - l_2) \quad \text{for} \quad l_2 < x < l_3,$$

and so on, i.e. for $l_i < x < l_i + 1$

$$\overline{M}_j(x, t) = \sum_{n=0}^{i} Q_{nj}(t)(x - l_n) \quad (10)$$

at $j = y, z$; $i = 1, 2, \ldots, N - 1$; $l_0 = 0$.

Using condition (4), as well as dependencies $\Delta\kappa_{jj} = -(\partial^2 \Delta U_j)/(\partial x^2)$, integration allowing for expressions (1), (7), (8) yields a system of two ($N - 1$) equations with respect to known Q_{ji} and integration constant C_{0j}:

$$C_{0y} l_i + \int_0^{l_i}\int_0^{x} \Delta\kappa_{jj}^{(T)}(t, x)\, dx\, dx + \sum_{n=0}^{i} [Q_{ny}(t)\Phi_{in}^{(y)} - Q_{nz}R_{in}] = 0,$$
$$C_{0z} l_i + \int_0^{l_i}\int_0^{x} \Delta x_{zz}^{(T)}(t, x)\, dx dx + \sum_{n=0}^{i} [Q_{nz}(t)\Phi_{in}^{(z)} - Q_{ny}R_{in}] = 0, \quad (11)$$

where

$$\Phi_{in}^{(j)} = \int_{l_{i-1}}^{l_i}\int_{l_{i-1}}^{x} A_j(x, t)(x - l_{i-1})\, dx dx;$$
$$R_{in} = \int_{l_{i-1}}^{l_i}\int_{l_{i-1}}^{x} D(x, t)(x - l_{i-1})\, dx dx.$$

The rest of the four equations yield static relationships (9).

Upon determining the $Q_i(t)$ values from (11) allowing for (9), at preset $\psi(z, y, t)$, calculate moments $\overline{M}_j$ from (10), and then $\overline{M}_j \Delta\varepsilon_{xx}^0$, $\Delta\kappa_{xx}$ and $\Delta\kappa_{yy}$ from (1) allowing for $\overline{M}_j$. After that, calculate stresses $\sigma_{xx}(t, x, y, z)$ from expression (3), and specify state function $\psi(t, x, y, z)$ from the instability condition. If the condition of convergence by ψ is not met at least at one point, the iteration process for time mo-

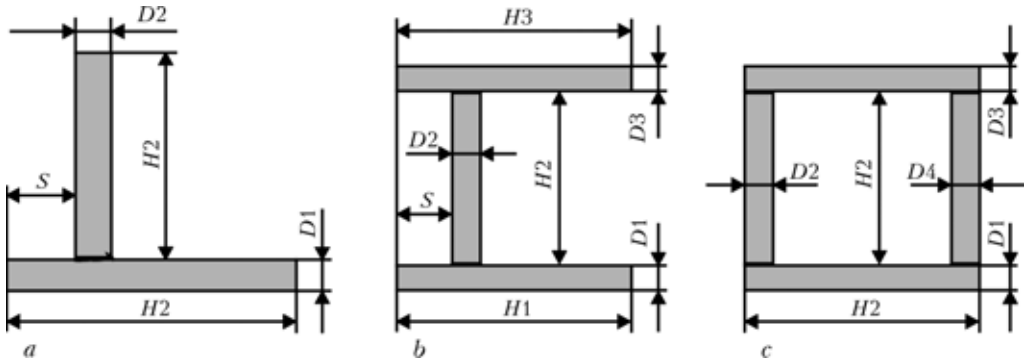

Figure 2. Schematics of different profiles of welded beams: *a*, *b* — T- and H-shaped sections, respectively; *c* — box-shaped section

ment t is continued, i.e. integrals L_{jq}, P_j (1), etc. are calculated. Parameters of shrinkage function in the form of $\Delta\varepsilon^0_{xx}(x, y)$, $\Delta\kappa_{yy}(x, t)$ and $\Delta\kappa_{zz}(x, t)$ after the iteration process by ψ are used to calculate variables $\Delta U_y(x, t)$, $\Delta U_z(x, t)$ and $\Delta U_x(x, t)$, the integration of which by time, starting from $t = 0$, gives a comprehensive information on displacements $U_y(x, t)$, $U_z(x, t)$, $U_x(x, t)$ of points x = const at the beam axis during the heating and cooling processes.

The calculation algorithm was used to determine displacements U_z and U_y of points of the axial line of the beam passing through the centre of gravity of the sections in laser welding of longitudinal welds. Considered were the welded beams 4000 mm long, made from stainless steel and having different profiles (Figure 2): T-, H- and box-shaped sections, with different distances between the fixing supports. An effective power of the laser source was 8.5 kW, and welding speed was 1.3 m / min.

Maximal displacements of points of the axial line of the beam were investigated at the moments of passing of the heat source, which is important for optimisation of distances between the fixing supports along the length of the beam at a preset allowance for deviation of the laser beam. The effect of distances between the fixing supports, welding speed and rigidity of the beam on residual distortions of the beam after removal of fixation was also studied. Maximal forces formed at the fixing supports were determined depending upon the distance between the supports and beam rigidity.

The calculation algorithm was supplemented with the possibility of allowing for the effect of preliminary bend and bend after welding, induced by the fixing supports. That made it possible to investigate the effect of preliminary bend and bend after welding on residual overall distortions of the beam.

To illustrate, Figure 3 shows the calculation results on the kinetics of displacements U_y of points of the axial line of the beam passing through the centre of gravity of the sections in laser welding of longitudinal weld. The calculation was made for a beam of the T-shaped profile (*H1*, *H2* = 80 mm, *D1*, *D2* = 8 mm, *S* = 36 mm). The beam profile and welding heating were symmetrical about axis *Y*. Hence, displacements U_z were equal to zero. Five fixing supports were chosen, which corresponded to a distance of 1000 mm between them. The calculation results showed that maximal displacements of points of the axial line of the beam at the moments of passing of the heat source, $U_{y\ \max\ w}$, were –0.34 mm, which is a bit larger than the allowance for deviation of the laser beam (±0.30 mm) and requires that the fixing supports be increased in number. Residual bend of the beam after removal of the fixing supports was 25.8 mm over a length of 4000 mm. It is apparent that the beam should be subjected to straightening to decrease its bending.

Figure 4 shows the calculated values of maximal displacement U_y of the beam 4000 mm long at the moments of passing of the heat source at different distances between the fixing supports. To compare, the results were determined for five T-shaped beams with one longitudinal weld and different ratios of beam flange *H1* to wall height *H2*: 80 × 160, 80 × 80, 80 × 40, 80 × 25, 40 × 40 mm, as well as for three H-shaped beams with two longitudinal welds: 80 × × 160 × 80, 80 × 80 × 80 and 80 × 40 × 80 mm. Thicknesses of all elements of the beams were equal: *D1* = *D2* = *D3* = 8 mm. Welding conditions and materials of the beams were identical. As shown by the results, the maximal displacement of the beam at the moments of passing of the heat source substantially decreases with decrease in the distance between the fixing supports. At a distance between the fixing supports equal to 500 mm, the maximal displacements of all the beams under consideration were not in excess of the 0.3 mm allowance. For the beams with profiles of 80 × 80 and 80 × 40 mm, requirements for the allowance were met at a distance between the fixing supports equal to 800 mm, and for the beams with profiles of 80 × 160 and 80 × 160 × 80 mm — at a distance of 1000 mm. Therefore, the higher the rigidity of the beam, the lower is the maximal displacement at the moment of passing of the heat source.

Figure 5 shows the calculated values of maximal displacement U_y of the beam 4000 mm long at the moments of passing of the heat source at different welding speeds v_w and constant heat input. The results were obtained for the T-shaped beam (*H1* = *H2* = = 80 mm, *B1* = *B2* = 8 mm) with one longitudinal weld, as well as for the H-shaped beam (*H1* = *H2* = = *H3* = 80 mm, *B1* = *B2* = *B3* = 8 mm) with two longitudinal welds. Results for the T-shaped beam show that the maximal displacement of the beam in-

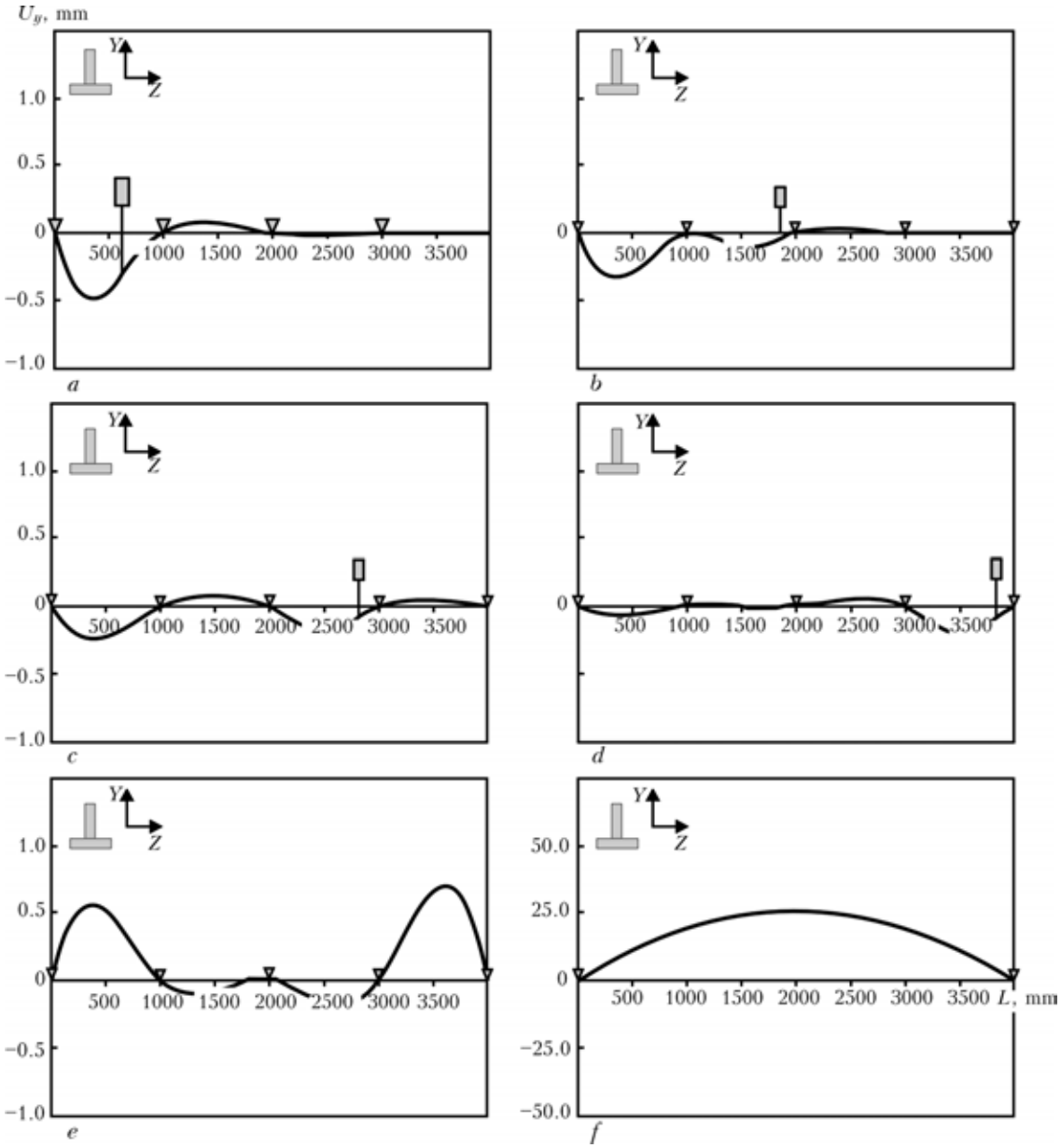

Figure 3. Calculation results on the kinetics of displacements U_y of points of the axial line of the T-shaped beam in laser welding of a longitudinal weld: *a* — t = 28; *b* — 85; *c* — 130; *d* — 176 s; *e* — after complete cooling; *f* — after removal of fixing supports

significantly decreases at the moments of passing of the heat source with increase in the welding speed. For a beam of the H-shaped profile, the welding speed has almost no effect on the maximal displacement of the beam at the moments of passing of the heat source, as the second weld is made after the beam has acquired residual welding distortions caused by the first weld, which determine maximal displacements of the beam.

Figure 6 shows the calculated values of maximal residual bend U_y of the beam 4000 mm long after removal of the fixing supports at different distances between them during welding. The results were obtained for the same T- and H-shaped beams. For the T-shaped beams with profiles of 80 × 80 and 80 × × 40 mm, values of the maximal residual bend hardly depended upon the distance between the fixing supports. However, for the rest of the beams, the effect of the distance between the supports on the maximal residual bend was more substantial. Thus, for the T-shape beam with a profile of 80 × 25 mm and all the H-shaped beams, the maximal residual bend first decreased, and then increased with decrease in the distance between the supports. For the beam with a profile of 40 × 40 mm, the maximal residual bend increased with decrease in the distance between the fixing supports. This is the confirmation of the fact known from practice that fixation of a beam during welding is an inefficient technique to decrease residual bend of the beam. Moreover, for the H-shaped beams, welding with fixation causes a dramatic increase of the residual bend, compared with a beam in a free state (two fixing supports and L_r = 4000 mm). Also, it can be seen that rigidity of the beam promotes decrease in the maximal residual bend. However, the distance between the centre of gravity of the beam profile and weld has a high effect on the residual bend. Thus, in a case of the T-shaped beam with a profile of 80 × 25 mm, the centre of gravity of the profile is close to the weld.

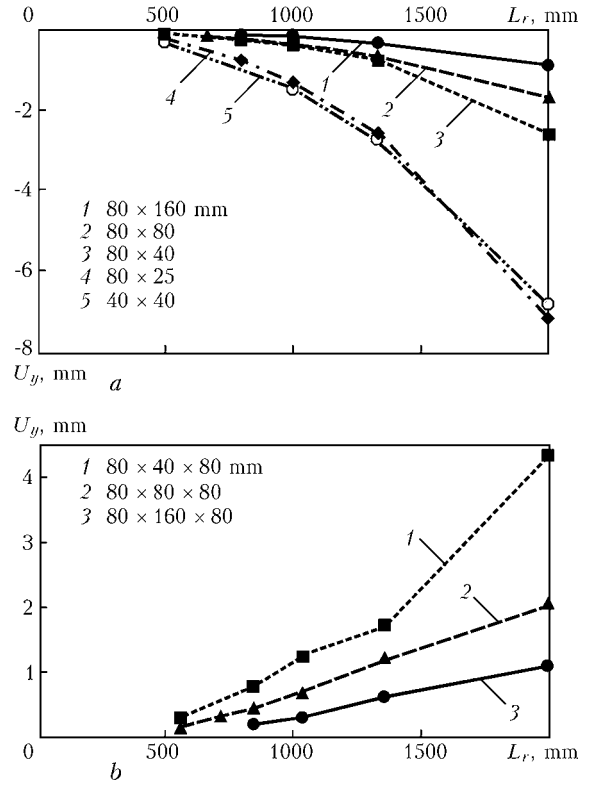

Figure 4. Dependence of maximal displacement of the beam at the moments of passing of the heat source upon the distances between the fixing supports: *a*, *b* — T- and H-shaped beams, respectively

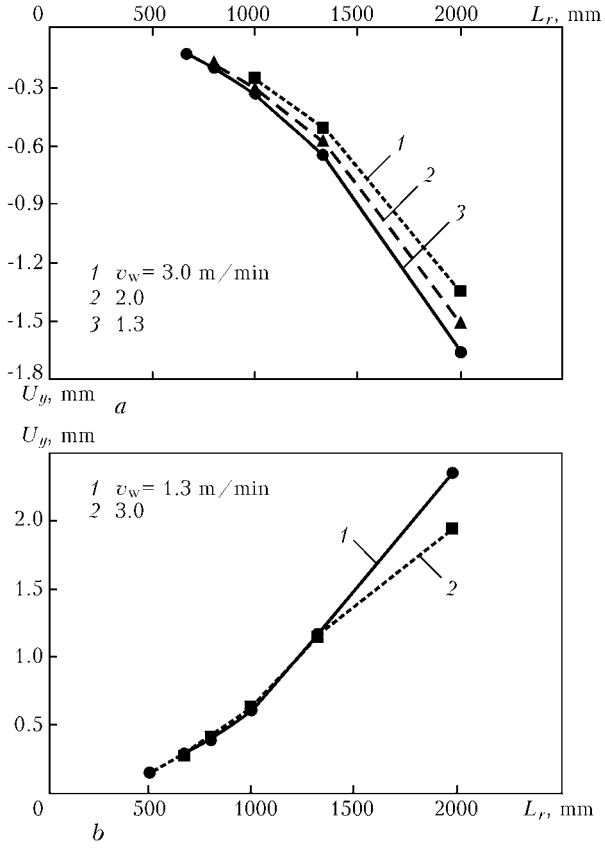

Figure 5. Dependence of maximal displacement of the beam at the moments of passing of the heat source upon the welding speed at Q_h = 380 J / mm: *a* — T-shaped beams 80 × 80 mm; *b* — H-shaped beams 80 × 80 × 80 mm

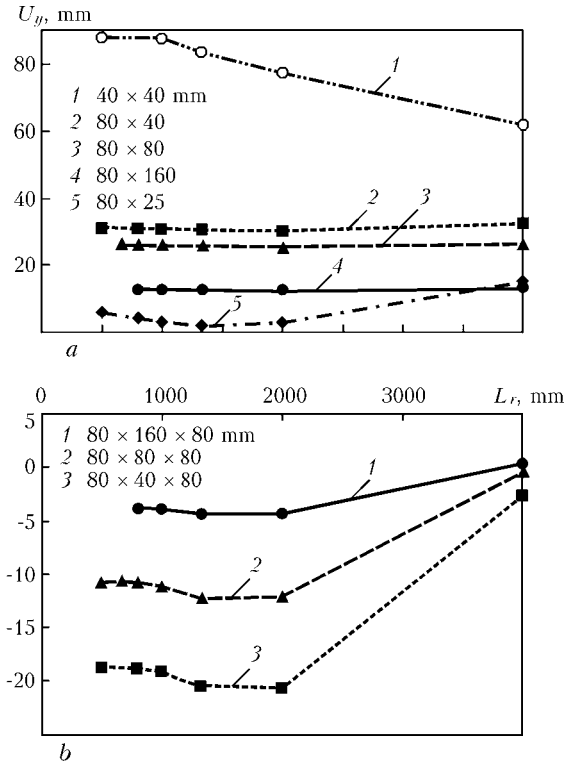

Figure 6. Dependence of maximal residual bend U_y of the beam 4000 mm long after removal of the fixing supports upon the distance between them during welding: *a*, *b* — T- and H-shaped beams, respectively

Therefore, despite a low rigidity of the beam in direction *Y*, residual bend U_y has a low value.

Figure 7 shows the calculated values of maximal forces at the fixing supports during welding and cooling of a beam at different distances between the sup-

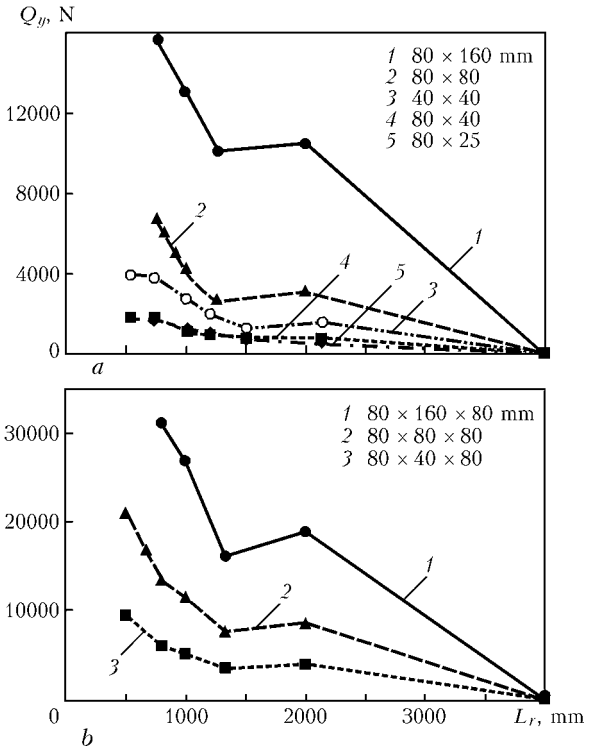

Figure 7. Dependence of maximal forces Q_y at fixing supports during welding and cooling of the beam upon the distance between the supports: *a*, *b* — T- and H-shaped beams, respectively

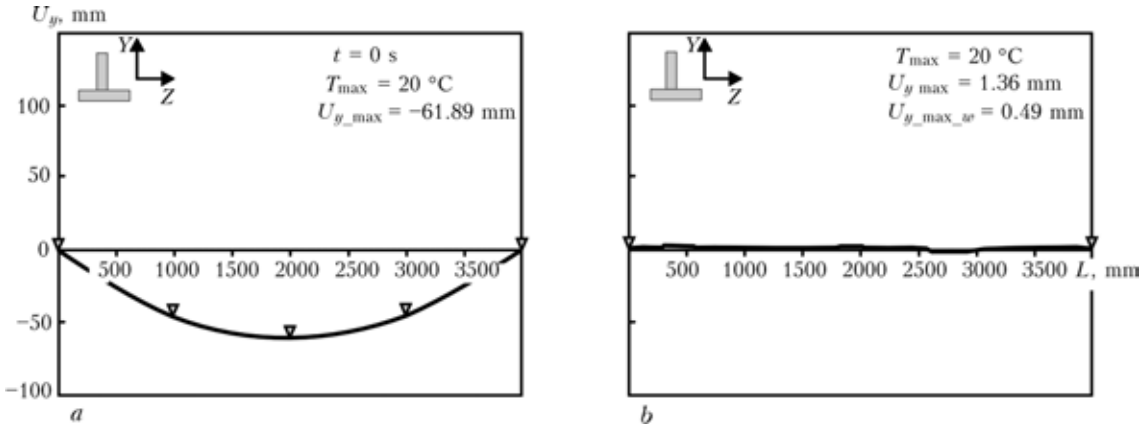

Figure 8. Optimal preliminary bend induced by using fixing supports, at which residual bending distortions of the T-shaped beam are minimal: *a* — bend before welding; *b* — bend after welding and removal of fixing supports

ports for beams with a different rigidity. The results show that the maximal forces at the fixing supports tend to increase with decrease in the distance between the supports and increase in the beam rigidity. It should be noted that the forces at the fixing supports in welding of beams may reach high absolute values, which should be taken into account in development of fixation devices.

In addition to principal functions, the mathematical model allows estimation of the effect of a preliminary bend and bend after welding induced by fixation on the residual overall distortions of a beam. Bend of the beam after welding simulates the process of mechanical straightening. Moreover, the optimal values of the preliminary bend and bend after welding are determined automatically by the method of successive approximations at a preset allowance for the longitudinal bend. Figure 8 shows an example of calculation of the optimal preliminary bend induced by five fixing supports, where residual bending strains of the T-shaped beam ($H1 = H2$ = 80 mm, $D1 = D2$ = 8 mm) 4000 mm long are minimal at the given quantity of the supports. Welding and cooling of the beam in such a bent state, where the bend is –62 mm, lead to the situation where, after removal of fixation, the maximal residual bend of the beam is approximately 1.4 mm. To compare, in the case of welding without preliminary bending (see Figure 3), the bending deflection of the beam is much higher, i.e. 26 mm. Figure 9 shows an example of calculation of the optimal postweld bend induced by five fixations, where residual bending strains of the T-shaped beam are minimal

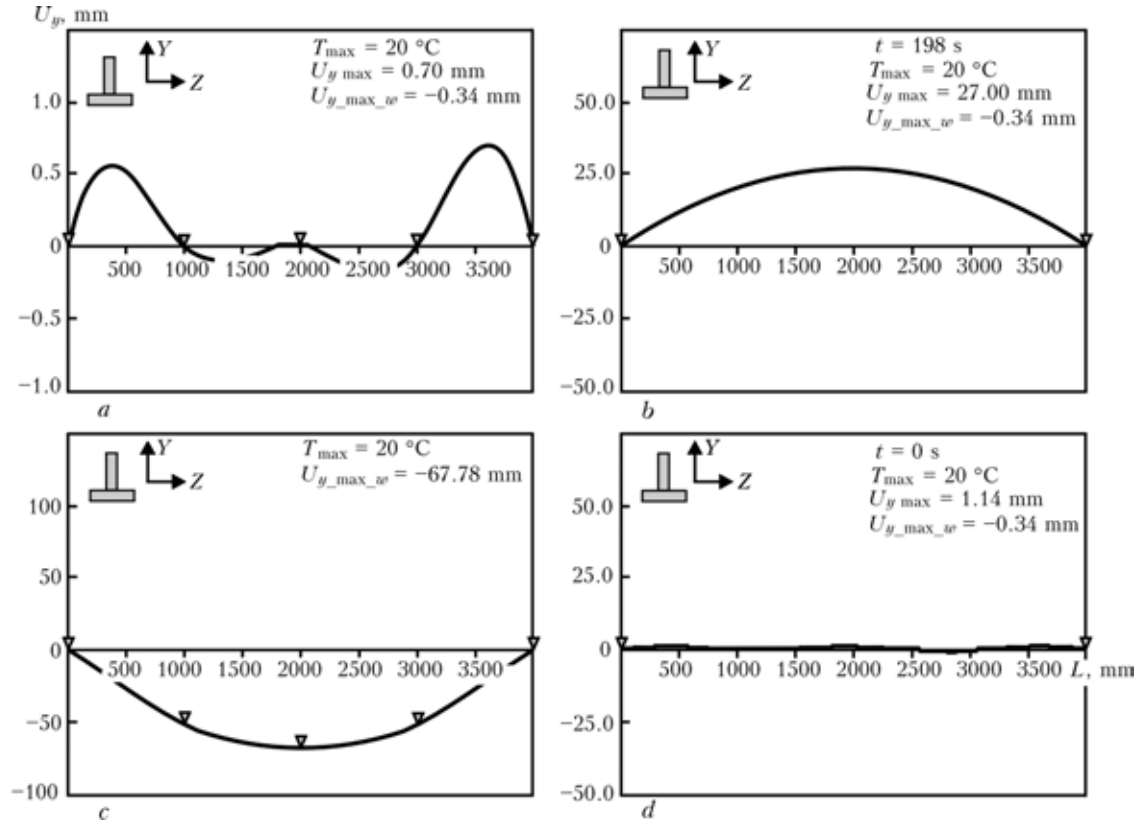

Figure 9. Results of calculation of optimal postweld bend: *a* — distortions after welding; *b* — distortions after removal of fixing supports; *c* — optimal posweld bend; *d* — distortions after bending and removal of fixing supports

(*H1* = *H2* = 80 mm, *D1* = *D2* = 8 mm). Bending to –68 mm decreases the residual maximal bend of the beam to 1.15 mm.

It should be noted that such bends of the beams that cause formation of plastic strains require that high forces be applied at the fixing supports, which makes fixations more complicated. However, this technology for producing welded beams with minimal distortions can find application in certain cases of small-lot production. The model developed can be supplemented with the possibility of determining optimal parameters of thermal straightening of the beams, e.g. by using a defocused laser beam. Thermal straightening does not require any complication of fixation devices, and in this case it is possible to use a welding heat source.

Therefore, application of the developed mathematical model allows:

- prediction of both temporary bending distortions in laser welding of beams of different profiles with a large number of fixing supports, and residual welding distortions after removal of fixations;
- optimisation of distances between the fixing supports to allow for the maximal displacement of the beam at the moments of passing of the laser heat source;
- determination of a value of the optimal preliminary bend and bend after welding, induced by using the fixing supports, at which the residual bending distortions of the beam are minimal.

The above calculations show that:

- the maximal displacement of the beam at the moments of passing of the heat source dramatically decreases with decrease in the distance between the fixing supports;
- the higher the rigidity of the beam, the lower is the maximal displacement of the beam at the moments of passing of the heat source;
- the maximal displacement of the beam at the moments of passing of the heat source insignificantly decreases with increase in the welding speed for the T-shaped beam;
- the welding speed has almost no effect for the H-shaped beam;
- fixation of the beam during welding is inefficient for decreasing residual bend of the beam;
- forces at the fixing supports in welding of the beam may reach high absolute values, which should be taken into account in development of fixation devices.

1. Makhnenko, V.I. (1976) *Calculation methods for investigation of kinetics of welding stresses and strains*. Kiev: Naukova Dumka.
2. Ma, N.X., Ueda, Y., Murakawa, H. et al. (1995) FEM analysis of 3-D welding residual stresses and angular distortion in T-type fillet welds. *J. JWRI*, 24(**2**), 115–122.

DATABANK OF WELDING PARAMETERS

The databank contains information on parameters of CO_2, submerged-arc (with one or two wires) and inert-gas shielded welding of structural steels in different spatial positions depending upon the thickness of base metal, type of a welded joint, groove shape and welding wire diameter. Recommendations on the number of passes for welding the root, filling and decorative beads are given for a case of multipass welding. The recommended welding parameters provide quality weld formation and required amount of deposited metal to ensure structural strength of a welded joint. At the given development stage, the database contains more than two thousand entries of welding conditions.

Figure 1. Selection of welding method, type of welded joint, spatial position and groove shape

Figure 2. Information on CO_2 welding of butt joint

Application. The databank can be used at machine building enterprises for arrangement of computerised work place of a welding production engineer.

Contacts: Prof. Makhnenko V.I.
E-mail: d34@paton.kiev.ua

EFFECT OF LONGITUDINAL MAGNETIC FIELD ON CHARACTERISTICS OF THE ARC IN TIG WELDING IN ARGON ATMOSPHERE

A.D. RAZMYSHLYAEV, M.V. MIRONOVA and **A.A. DELI**
Priazovsky State Technical University, Mariupol, Ukraine

It is demonstrated experimentally, using the split anode method, that diameter of the active (anode) spot on a workpiece decreases with increase in induction of the longitudinal magnetic field within the arc zone, while distribution of density of the current along its radius is more uniform than in welding without the longitudinal magnetic field. It is shown by the probe method that gas-dynamic pressure at the arc centre decreases under the effect of the magnetic field.

Keywords: TIG welding, tungsten electrode, longitudinal magnetic field, arc anode spot, current density, gas-dynamic pressure of the arc

Application of the longitudinal magnetic field (LMF) widens technological capabilities of TIG welding in argon atmosphere and submerged-arc welding using electrode wire [1–3]. In addition to refining of structural components of the weld metal, it improves weld formation, changes sizes of the weld pool (length, width, depth), which are determined to a considerable degree by diameter of the active spot of the arc on a workpiece and distribution of the current density and arc pressure in it.

The simplest welding process for investigation is TIG welding in argon atmosphere. However, even for this process without the application of LMF, the above characteristics of the arc are insufficiently studied, and data on them are often contradictory. For example, as reported in [4–7], current density in the anode spot of the arc on a workpiece decreases along the spot radius following the law close to normal, and at the centre its maximal value ranges from 5 to 100 A / mm^2 for a welding current of about 100–200 A. According to study [8], the current density is distributed in the active spot of the arc on a workpiece almost uniformly, and amounts to about 3–5 A / mm^2. And only study [9] shows that with constant LMF applied to the arc, the current density at the centre of the arc spot on a workpiece decreases to some extent (from 5 to 4.2 A / mm^2 at induction of 20 mT, and to 3.4 A / mm^2 at induction of 50 mT).

With constant and pulsating LMF applied to such an arc, pressure along the arc axis decreases, unless induction within the arc zone is more than 30 mT [10, 11], while vacuum is formed along the arc axis at substantial inductions of LMF (about 80 mT) [3]. As shown in [12], this is associated with rotation of the arc about the longitudinal axis and its transformation into the bell-like (conical) shape. The data of studies [10, 11], which are of a fundamental importance, and which were generated by the gating hole method, require a more detailed study and more accurate definition using other investigation methods, such as the method involving introduction of a probe into the arc [13], which allow determination of distribution of a gas-dynamic component of the arc pressure (velocity head) and, accordingly, rate of the plasma flow in some section of the arc per measurement. As shown in [14], it is the gas-dynamic (some authors call it gas-kinetic) pressure of the argon arc, which is much higher than the magnetostatic one, as well as the rate of the plasma flows associated with this pressure, that are the most important factors determining depth and shape of the welds.

This study is dedicated to experimental investigations of the effect of LMF on such characteristics of the arc in TIG welding in argon atmosphere as diameter of the anode spot of the arc on a workpiece and distribution of the current density in this spot, as well as distribution of pressure in a cross section of the arc.

Welding in all the experiments was performed at a straight polarity using the 4 mm diameter electrode of the VL grade. To ensure minimal penetration of the base metal, the electrode was made with a taper angle of 90° (without blunting). Rectifier of the VSZh-303 type was used as a power supply. Ballast resistors of the RB-301 type were employed to form a drooping characteristic of the welding station and regulate the welding current. Argon of the A grade (GOST 10157–73) was used to shield the arc, the argon flow rate being 5–7 l / min. Solenoid with a carbon steel core was mounted on the tip of the welding torch in alignment with the electrode. The solenoid coil consisted of 104 turns of the 2.0 mm diameter copper wire. Diameter of the anode spot on a workpiece and distribution of the current density along the spot radius were determined by the split anode method, the diagram and description of which are given in studies [5–8]. Two copper plates 6 mm thick with a gap between them equal to 0.2 mm were used as an anode. The current flowing through each of these plates, arc voltage, and current in the solenoid coil were recorded with an oscillograph of the K-115 type. The oscillograph paper speed was 250 mm / s (sometimes 125 mm / s). The current flowing through the

© A.D. RAZMYSHLYAEV, M.V. MIRONOVA and A.A. DELI, 2008

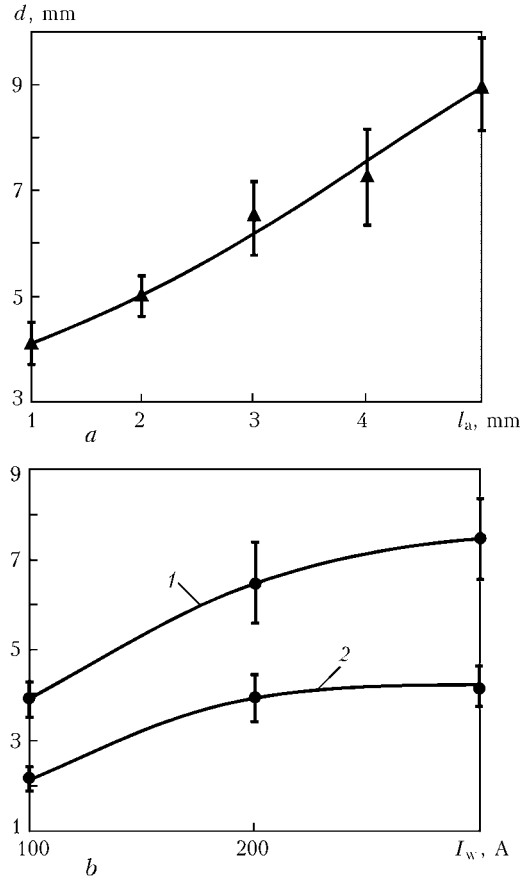

Figure 1. Dependence of diameter of the active spot on a workpiece upon the distance between electrodes (*a*) and welding current (*b*) at l_a = 3 (*1*) and 1 (*2*) mm

split anode plates was recorded, and the oscillograms were processed on the basis of the recommendations given in [4, 8].

It should be noted that, like in study [8], delay of the active spot of the arc was sometimes observed at the first plate in transition through the gap. In this case, part of the current was short-circuited through the second plate earlier than the active spot of the arc

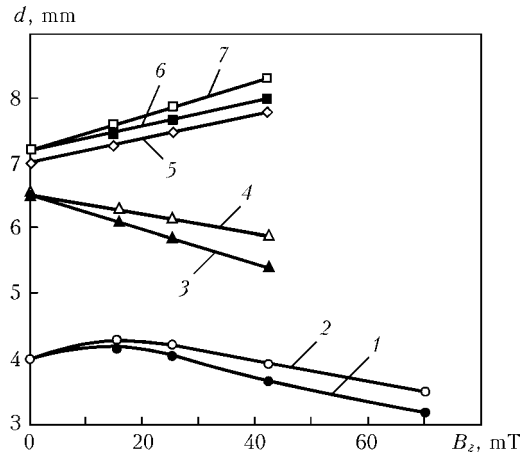

Figure 2. Effect of induction of LMF on diameter of the arc spot on a workpiece and diameter of the arc pressure: *1*, *2* — constant and alternating, 50 Hz frequency LMF, respectively, at l_a = 1 mm; *3*, *4* — same as *1*, *2* but at l_a = 3 mm; *5* — maximal diameter of the arc column at l_a = 3 mm; *6*, *7* — diameter of the arc pressure, respectively, for constant and alternating, 50 Hz frequency LMF at l_a = 3 mm

passed to it. These phenomena were of a random character, i.e. they were not observed in most experiments. In this connection, in every experiment, the moment of passing of the arc through the gap between the plates was recorded with a video camera «Panasonic» at a frequency of 50 frame / s. Oscillograms that clearly showed the above phenomenon were rejected (ignored). Hence, this required that not less than 5–7 experiments be conducted in each mode, and resulted in a certain scatter of the data obtained (Figure 1).

According to the recommendations of study [4], conditional diameter of the anode spot of the arc was determined from the surface area, through which 95 % of the arc current flew. It was established that in welding without LMF an increase in distance between the electrodes, l_a, led to increase in diameter of the anode spot (Figure 1, *a*), and that this diameter grew in the same way with increase in the welding current (Figure 1, *b*). With constant and alternating, 50 Hz frequency LMF applied to the arc, at a distance between the electrodes equal to 1 mm, the axial component of induction grows to 15–20 mT, thus leading to some increase in diameter of the anode spot of the arc on a workpiece (Figure 2, curves *1* and *2*), while with further increase in induction B_z the diameter decreases to some extent. In this case, constant LMF gives a higher effect than the alternating one with a frequency of 50 Hz. If the distance between the electrodes is 3 mm, increase in induction of LMF leads to a monotonous insignificant decrease in diameter of this spot (Figure 2, curves *3* and *4*). According to the data of video recording (at a frequency of 50 frame / s), with increase in induction of both constant and alternating, 50 Hz frequency LMF, the maximal diameter of the arc column observed at a distance of 1.0–1.5 mm from the plate (anode) surface and at l_a = 3 mm increases to some extent (Figure 2, curve *5*).

Distribution of the current density in the arc spot on a workpiece was determined by processing oscillograms using the procedure described in studies [5, 6] (Abel transformation). The oscillograms were scanned, their enlarged images were processed on a computer, and radial distribution of the current density in the arc spot was calculated using the specially developed software. As induction of constant and alternating, 50 Hz frequency LMF increases, the current density at the centre of the anode spot substantially decreases, and distribution of the current density along the spot radius becomes more uniform than in welding without LMF. The current density in the peripheral part of the anode spot under the effect of LMF is higher than without LMF (Figure 3). For a shorter arc (l_a = 1 mm), the above variations in distribution of the current density are more substantial than for a longer arc (l_a = 3 mm). Under the effect of LMF, the centre of the anode spot of the arc is not free from the electric carriers (electrons), as it might be supposed on the basis of the shape and behaviour of the arc in LMF [12], as well as the presence of vacuum in the axial region of its column at considerable in-

ductions of LMF [3, 11]. With LMF of the 1.0–12.5 Hz frequency applied to the arc, diameter of the anode spot had intermediate values relative to the observed ones at constant LMF and 50 Hz frequency LMF, which are shown in Figure 2. The similar effects were observed at the centre of the anode spot and in the current density distribution curves.

To study distribution of the gas-dynamic component of the arc pressure (velocity head of plasma) along the radius of a section normal to the arc axis, as well as diameter of this section (pressure diameter), the use was made of the procedure similar to that described in [13]. The cylindrical probe of a heat-resistant non-magnetic material served as a pressure sensor. Schematic of the measurement device* is shown in Figure 4, *a*. Probe *2* was rigidly attached (normal) to elastic string *9* with a diameter of 0.4 mm. The string was tension mounted on supports *10*. With the arc pressure affecting probe *2*, string *9* twisted, and the beam directed from laser pointer *4* reflected from light mirror *3* and went to screen *5*, which was installed at a substantial distance (about 2 m) from mirror *3* to increase sensitivity of the device. To avoid oscillations of probe *2* under the effect of the arc, damping device *6* was provided for in the system. The process of deviation of the beam (image on the screen) when arc *8* passed through probe *2* was recorded with the video camera (at a frequency of 50 frame / s).

Tungsten, quartz and graphite probes with the 1.5 mm diameter were tested. In welding under conditions: I_w = 200 A, l_a = 3 mm, and v_w = 75 m / h, the maximal heat resistance was exhibited by tungsten (it was not melted by the arc). In this case, the maximal deviation of the beam on the screen was identical, i.e. the probe material did not affect the parameter investigated. It turned out that the tungsten probe with the 1.0 mm diameter was also not melted by the arc under the above conditions. Therefore, considering the expediency of decreasing diameter of the probe introduced into the arc, the probe of the above diameter was used in all the further experiments.

Like in [13], calibration of the device was carried out by affecting the probe with the argon flow fed through a rectangular slot, measuring 8.0 × 1.5 mm, made at the end of a round copper tube. The laminar mode of the argon flow was employed for the calibration. The probe was placed at a distance of 0.4–0.5 mm from the end (slot) of the tube. The gas flow rate was fixed with flow meter RS-3. To determine proportion between the force acting on the probe and deviation of the beam on the screen, weights (milligram pieces) were hung on the probe. Also, the probe drag coefficient required for further data processing was estimated from the following formula:

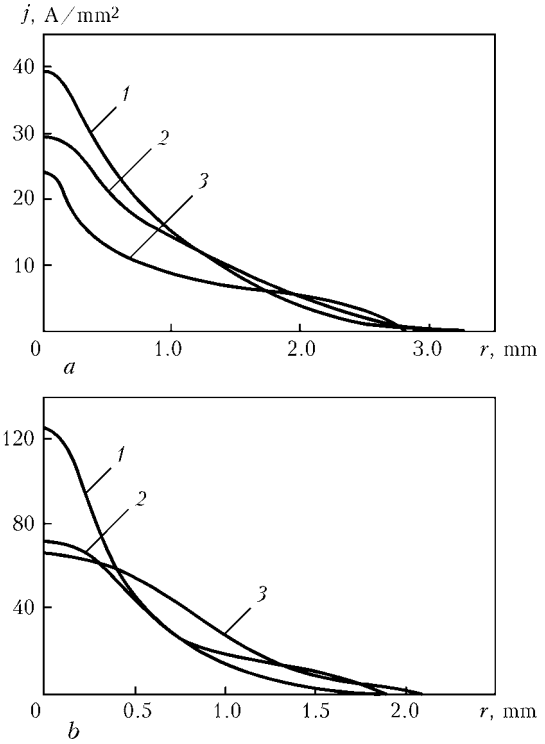

Figure 3. Distribution of current density along axis *r* at an electrode spacing l_a = 3 (*a*) and 1 (*b*) mm without the effect of LMF (*1*), with constant LMF at B_z = 25 mT (*2*) and with 50 Hz frequency LMF at B_z = 25 mT (*3*)

$$F = C_x S_p \frac{\rho v^2}{2},$$

where F is the force acting on the probe, N; C_x is the probe drag coefficient; S_p is the probe drag area, m^2;

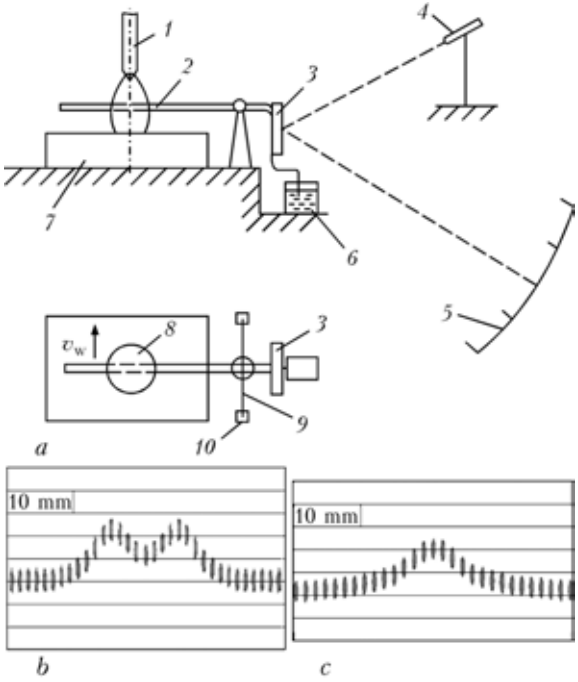

Figure 4. Schematic of the device for measuring the force effect of the arc (*a*), and image of beam deviation on the screen at B_z = 42 (*b*) and 0 (*c*) mT: *1* — electrode; *2* — probe; *3* — mirror; *4* — laser pointer; *5* — screen; *6* — damping device; *7* — workpiece; *8* — arc; *9* — string; *10* — supports

*Schematic of device was offered by Prof. I.V. Pentegov, Doctor of Technical Sciences and staff member of the E.O. Paton Electric Welding Institute.

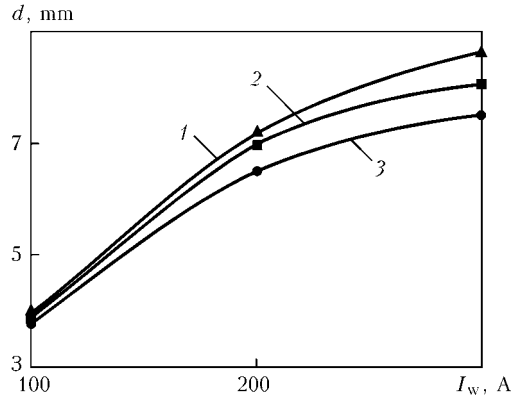

Figure 5. Dependence of diameters of the arc column (*1*), gas-dynamic arc pressure (*2*) and active spot of the arc (*3*) on a workpiece at l_a = 3 mm upon the welding current

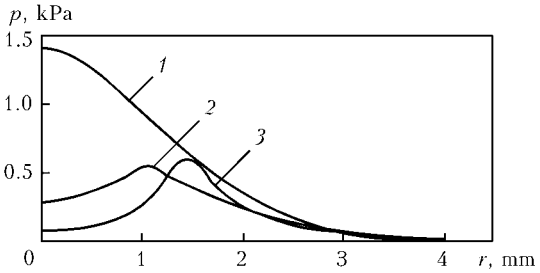

Figure 6. Distribution of gas-dynamic pressure of the arc along axis r at l_a = 3 mm: *1* — without LMF; *2* — constant LMF (B_z = = 25 mT); *3* — alternating, 50 Hz frequency LMF (B_z = 25 mT)

ρ is the argon density, kg / m^3; and ν is the argon flow rate, m / s.

As shown by the calculations, probe grad coefficient C_x within an argon flow rate range of 7–20 m / s has almost identical values.

Typical screen images of the processes of deviation of the beam with time, when the arc crosses the tungsten probe (Figure 4, *b*, *c*), were used to determine distribution of the pressure along the radius of the arc section. Processing was performed by the procedure similar to that described in [13] by using a computer and the specially developed software.

With increase in induction of LMF, diameter of the arc pressure increases to some extent, similar to visible diameter of the arc column in the same section (see Figure 2). Characteristically, the visible diameter of the arc column almost coincides with diameter of the arc pressure at a preset value of induction of both constant and alternating, 50 Hz frequency LMF (see Figure 2, curves *5*–*7*).

For the welding process without the LMF effect, diameters of the arc column, arc pressure and anode spot of the arc on a workpiece grow with increase in the welding current (Figure 5). In this case, diameter of the active spot of the arc on a workpiece is somewhat smaller than diameters of the arc column and arc pressure. As the welding current increases, the difference between diameter of the active spot and diameter of the arc pressure increases (see Figure 5). The similar dependence occurs also with increase in induction of LMF (see Figure 2).

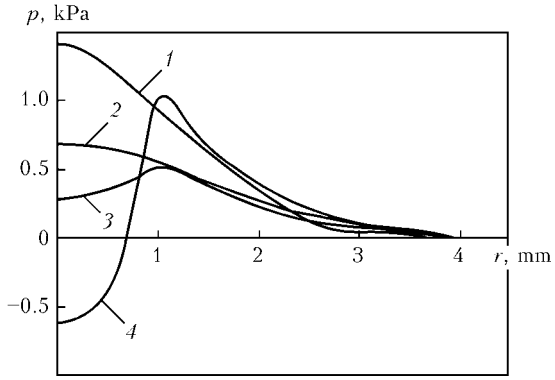

Figure 7. Distribution of gas-dynamic pressure of the arc along axis r at l_a = 3 mm under the effect of constant LMF of differing induction: *1* — B_z = 0; *2* — 18; *3* — 25; *4* — 45 mT

Under the effect of both constant and alternating, 50 Hz frequency LMF, the pressure of the arc at its axis considerably decreases. Also characteristically, alternating LMF influences the arc pressure not less intensively than the constant one (Figure 6). With increase in induction of constant (and, accordingly, alternating, 50 Hz frequency) LMF, the pressure of the arc at its axis decreases. As follows from the data shown in Figure 7, curve *4*, for constant LMF, at an induction of about 40 mT or higher the negative values can be observed at the arc axis, which is incorrect from the physical standpoint. Allowing for the peculiarities, which are typical of the measurement methods applied (probe method), the negative values of the arc pressure are attributable to the fact that within the arc zone adjoining the arc axis the plasma flow is directed from a workpiece to electrode. The positive and negative values of the arc pressure shown in Figure 6 should be regarded as gradients of the gas-dynamic pressures directed from an electrode to workpiece and, accordingly, from a workpiece to electrode.

The data obtained allow widening of the notions on the effect of LMF on such important characteristics of the arc as distribution of the current density in the anode spot of the arc and distribution of the arc pressure, which are determining as to their effect on the efficiency of penetration of the base metal and quality of the weld formation under the effect of LMF.

CONCLUSIONS

1. As induction of constant and alternating, 50 Hz frequency LMF increases, diameter of the active spot of the arc on a workpiece and current density at the spot centre decrease, while distribution of the current density along the radius is more uniform than in welding without the effect of LMF.

2. The method of introducing a probe into the arc confirms the data, which were generated earlier by the gating hole method, that under the effect on the arc by constant and alternating, 50 Hz frequency LMF the gas-dynamic pressure of the arc decreases at its axis and increases in the peripheral regions. At an induction of LMF equal to about 40 mT or higher at axis of the arc, its plasma flow has a velocity component directed from a workpiece to electrode.

1. Chernysh, V.P., Kuznetsov, V.D., Briskman, A.N. et al. (1983) *Welding with electromagnetic stirring*. Kiev: Tekhnika.
2. Razmyshlyaev, A.D. (2000) *Magnetic control of weld formation in arc welding*. Mariupol: Priazovsky GTU.
3. Birzhev, V.A. (1997) *Theoretical and technological principles of increasing the productivity of arc welding and surfacing in external axial magnetic field*: Syn. of Thesis for Dr. of Techn. Sci. Degree. Lipetsk.
4. Gvozdetsky, V.S. (1973) About the function of current density distribution in the anode spot of the arc. *Avtomatich. Svarka*, **12**, 20–24.
5. Shoek, P.A. (1966) Investigation of energy balance at anode of high-current arcs ignited in argon atmosphere. In: *Current problems of heat exchange*. Moscow; Leningrad: Energiya.
6. Erokhin, A.A., Bukarov, V.A., Ishchenko, Yu.S. (1971) Influence of the tungsten cathode geometry on some welding arc characteristics and metal penetration. *Svarochn. Proizvodstvo*, **12**, 17–21.
7. Ostrovsky, O.E., Kryukovsky, V.N., Buk, B.B. et al. (1977) Effect of activating fluxes on penetrating capacity of the welding arc and energy concentration in the anode spot. *Ibid.*, **3**, 3–4.
8. Mechev, V.S., Zamkov, V.N., Prilutsky, V.P. (1971) Radial distribution of current density in anode spot of the argon arc. *Avtomatich. Svarka*, **8**, 7–10.
9. Luo, J., Luo, Q., Lin, Y.H. et al. (2003) A new approach for fluid flow model in gas tungsten arc weld pool using longitudinal electromagnetic control. *Welding J.*, **8**, 202–206.
10. Selyanenkov, V.N., Blinkov, V.A., Kazakov, Yu.V. et al. (1975) On weld formation in longitudinal magnetic field during argon-arc welding. *Svarochn. Proizvodstvo*, **11**, 5–7.
11. Matyash, V.I., Syrovatka, V.V., Florinsky, F.B. (1981) Influence of the longitudinal pulsed electromagnetic field on the gas-kinetic pressure of the arc. *Avtomatich. Svarka*, **5**, 6–7, 12.
12. Kuznetsov, V.D., Malinkin, I.V., Syrovatka, V.V. et al. (1972) Behavior of arc and electrode metal transfer in longitudinal magnetic field welding. *Ibid.*, **4**, 3–4.
13. Lenivkin, V.A., Petrov, P.I., Dyurgerov, N.G. (1984) Determination of dynamic pressure of the welding arc plasma. *Svarochn. Proizvodstvo*, **7**, 3–4.
14. Voropaj, N.M., Krivtsun, I.V. (1978) Gas-dynamic characteristics of plasma flows in welding arcs. *Magnitn. Gidrodinamika*, **1**, 132–136.

SELECTION OF FILLER METALS FOR BRAZING THIN-WALLED HEAT EXCHANGING DEVICES

V.F. KHORUNOV and **S.V. MAKSYMOVA**
E.O. Paton Electric Welding Institute, NASU, Kiev, Ukraine

Peculiarities of structure of seams in thin-sheet stainless steel joints produced by vacuum brazing using copper and nickel alloys as brazing filler metals are considered. Results of metallographic examinations and mechanical tests of the brazed joints are presented. Good prospects for utilisation of brazing filler metals based on the Ni–Mn system are demonstrated for brazing thin-walled structures, in particular, plate-ribbed heat exchangers.

Keywords: vacuum brazing, heat exchanging device, stainless steel, microstructure, brazing filler metal, brazed seam, boron, strength

Production of permanent joints by vacuum brazing is gaining wide acceptance in many industries for the fabrication of different-purpose structures, mainly from corrosion- and heat-resistant steels and alloys, as well as superalloys, applied in aircraft, rocket, space and nuclear power engineering.

Vacuum brazing is characterised by a number of advantages, compared with traditional brazing methods. It is superior to all other brazing methods and technologies, as in vacuum brazing the atmosphere of the vacuum furnace features an almost absolute absence of any substances. Thus, in vacuum at a rarefaction of the working space equal to $1.33 \cdot 10^{-4}$ Pa, 1 cm^3 of the furnace contains $3 \cdot 10^{10}$ molecules, this corresponding to a dew point of –90 °C.

Brazing in vacuum makes it possible to most effectively increase the temperature of unbrazing of the joints due to evaporation of volatile elements contained in brazing filler metals (indium, manganese, etc.), this involving certain technological difficulties, which, however, are fully compensated for by the high quality of the products.

The most significant peculiarity of brazing in vacuum is the possibility of performing the process using no fluxes. This provides high strength, corrosion resistance and vacuum tightness of the joints, which is especially important for the fabrication of many structures, e.g. high-efficiency heat exchanging devices from stainless steels. High-efficiency heat exchange, decreased thermal stresses and reduced weight of heat exchangers are achieved in manufacture of plate-type heat exchangers from thin-sheet (0.05–0.30 mm) materials. Wide possibilities for selection of channel shapes and methods for intensification of heat exchange exist in design of such heat exchangers. The degree of compactness of aircraft plate-type heat exchangers, which implies the ratio of an area of the heat-exchange surface to its volume, amounts to 4000 m^2 / m^3, which is much higher than that of the best samples of tubular heat exchangers (2275 m^2 / m^3). For conventional tubular structures this indicator is 139–325 m^2 / m^3. Compact plate matrices have a lower cost of 1 m^2 of the heat-exchange surface and a higher heat-transfer coefficient.

Brazing of plate-ribbed heat exchangers is a sophisticated technological process, as it is necessary to simultaneously produce long seams (seams in heat exchangers can be hundreds or even thousands of metres long), and it is impossible to remedy defects formed inside a structure.

Composition of a brazing filler metal is an important component of the process of brazing of plate-type heat exchangers. As noted above, the heat exchangers are made from thin-sheet elements, and the erosion

© V.F. KHORUNOV and S.V. MAKSYMOVA, 2008

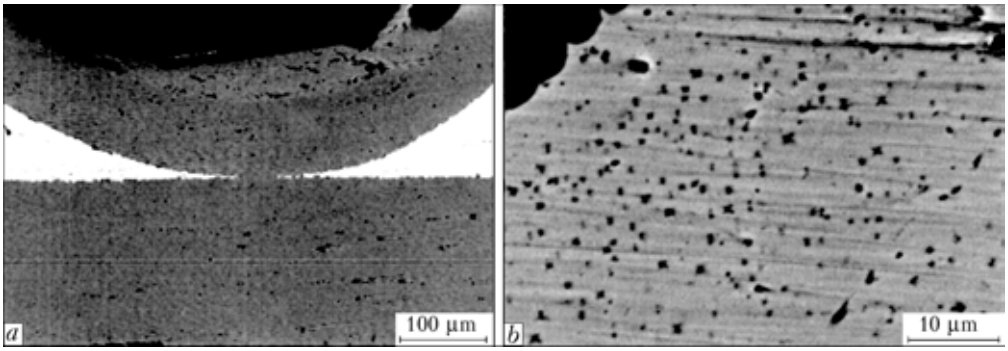

Figure 1. Microstructure of joints produced by brazing using copper: *a* — general view; *b* — fillet region

activity of a filler metal should be minimal. In this connection, it is desirable to use filler metals with a narrow solidification range. This study was conducted by using copper as a filler metal, eutectic amorphous filler metal of the Ni–Cr–Si–B system, and powder filler metals of the Ni–Mn system developed by the E.O. Paton Electric Welding Institute. Stainless steel 10Kh18N10T (Fe–(17–19)Cr–(9–11)Ni–(1–2)Mn–≤0.8Si–≤0.8Ti–≤0.12C) with a hardening temperature of 1100 °C was used as a base metal for the investigations.

To avoid substantial grain growth and deterioration of mechanical properties of the metal brazed, the brazing temperature should not exceed 1100 °C [1].

Scanning electron microscope «CamScan» equipped with the «Link» system X-ray microanalyser was used for metallographic examinations and investigation of chemical heterogeneity of the brazed joints.

Traditionally, brazing of stainless steel heat exchanging devices is performed by using copper as a filler metal [2], which is applied in the form of foil or by the electrolytic method in a thin layer 10–20 μm thick to the metal to be brazed. Using optimal coating thickness and brazing parameters, it flows well into the capillary gaps to form the defect-free joints (Figure 1). Copper has a limited solubility in iron at a high temperature, and no clearly defined diffusion zone can be revealed in this case [3]. At the same time, diffusion occurs between the filler and base metals, and the resulting seam consists of a copper matrix reinforced with dispersed particles, which contain iron, chromium, manganese and nickel (Table 1, Figure 2).

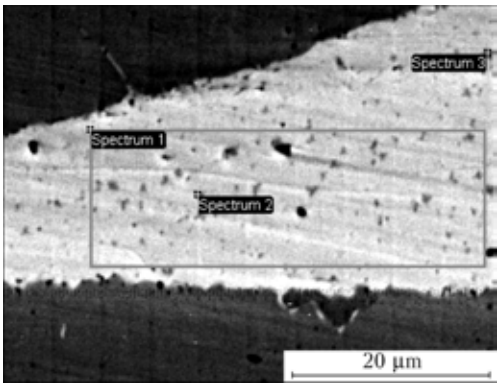

Figure 2. Microstructure of fillet region of the joint brazed by using copper, with marking of regions (spectra) being analysed

Drawbacks of copper used as a filler metal include its penetration along the grain boundaries into the base metal, which leads to its embrittlement, low heat and corrosion resistance. This is the main reason why copper is not used as a filler metal for brazing high-temperature plate-ribbed heat exchangers, e.g. aircraft ones. However, because of wide availability and low cost, this filler metal is suitable for other applications (e.g. in automobile and tractor industries).

The work on making heat exchanging devices is under way in many countries of the world as part of a global strategy of transfer of high technologies to industry. The experience of the E.O. Paton Electric Welding Institute in the field of vacuum brazing of plate-ribbed heat exchangers turned out to be very helpful, including for the manufacture of high-efficiency equipment.

Transition to nickel alloys in brazing of compact heat exchangers is a complicated and painful process, which has no unambiguous solution as yet. There are two main ways of addressing it: one provides for utilisation of thin amorphous filler alloys with a high content of boron and silicon and, hence, high erosion activity; and the second provides for utilisation of low-erosion active filler metals, e.g. on the Ni–Mn system base.

It is reported [4, 5] that filler metals with a high content of boron and silicon are unsuitable for brazing thin-walled (0.1–0.2 mm) stainless steel structures. However, in the opinion of some authors, utilisation of filler metals 0.03–0.04 mm thick in the amorphous state can provide joints containing no brittle phases. As shown by the investigations, in brazing of stainless steel with boron-containing nickel filler metals, the boron-containing phases, e.g. chromium borides (Figure 3, *a*), solidify in the seam, and these phases deteriorate plastic properties of the brazed joints and

Table 1. Content (wt.%) of chemical elements in fillet region of the joint brazed by using copper

Spectrum No.	Cr	Mn	Fe	Ni	Cu
1	–	1.25	2.70	1.67	94.38
2	2.22	1.03	10.76	2.33	83.66
3	1.81	0.96	9.05	2.09	86.08

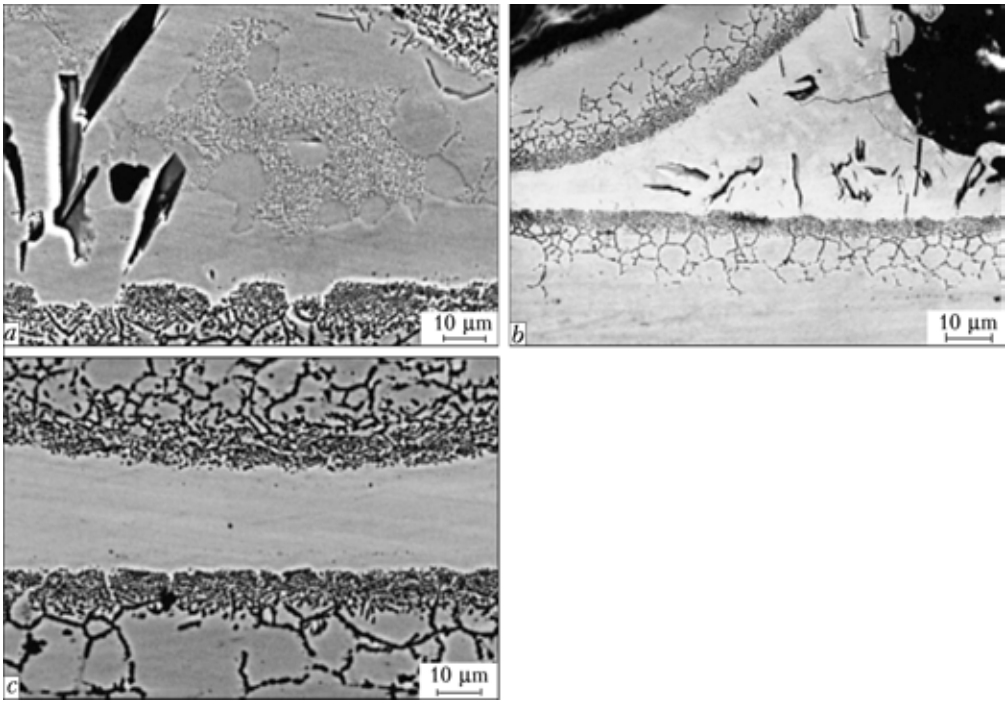

Figure 3. Microstructure of 10Kh18N10T steel brazed joints on heat exchanger produced by using filler metal Ni–7Cr–4.5Si–3Fe–3.2B: *a*–*c* — see in the text

lead to formation of cracks in fillet regions (Figure 3, *b*).

Boron actively diffuses from the seam metal into stainless steel with increase in the time of holding at high temperature. As it does not dissolve in the nickel matrix of the seam and in the material being brazed, the boride phase precipitates along the grain boundaries of the base metal (Figure 3, *c*), which has a negative effect on mechanical properties and corrosion resistance of the brazed joints.

Study [6] offers a special filler metal with an increased silicon content and decreased boron content for brazing plate-ribbed heat exchangers. While the wish of the authors to decrease the boron content is quite understandable, it should be noted that increase of the silicon content may also cause problems: silicides dissociate very slowly even at high temperatures and long holding times. As follows from study [6], when using the boron-containing filler metals, e.g. Ni–15Cr–1.4B–7.25Si, the probability of formation of the boride phase can be reduced, or it can be dissolved by using the multi-stage brazing conditions, such as heating to 1190 °C and holding for 2.5 h, cooling to 1100 °C and holding for 3 h, and cooling in nitrogen to 70 °C for 30 min.

However, the above heat treatment conditions may have a pernicious effect on properties of stainless steel. Moreover, in terms of cost effectiveness, this long and energy-consuming process is unacceptable for manufacturers of plate-type structures. In this connection, the work is now under way to develop filler metals with a decreased content of boron, or even boron-free filler metals.

On this basis, the Ni–Mn system was selected as a basis for the development of filler metals. Alloys of this system are characterised by low erosion activity, have a fusion diagram with a temperature minimum, and structure of solid solution of a differing concentration. The effect of extra alloying of the Ni–Mn system alloys with chromium, iron, boron, silicon, vanadium, etc. was investigated. Alloys of the Ni–Mn system with the 19–35 wt.% Mn were studied, the effect of silicon on structure and their melting ranges was evaluated, and position of the eutectic point for each group of the alloys was determined (Figure 4).

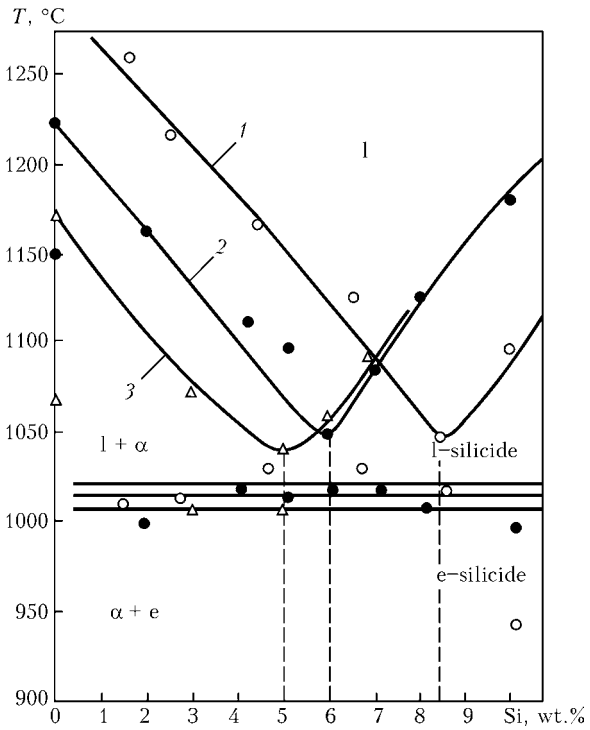

Figure 4. Liquidus and solidus surfaces on polythermal sections of Ni–Mn–Si system alloys, located on isoconcentrates with 19 (*1*), 28 (*2*) and 35 (*3*) % Mn

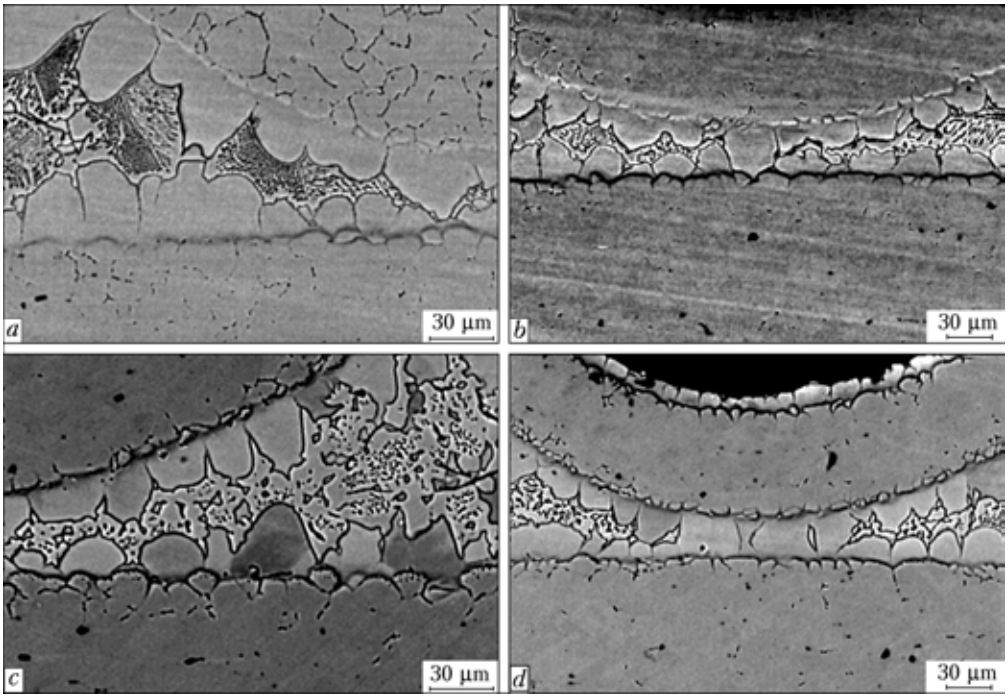

Figure 5. Microstructure of brazed joints produced by using Ni–Cr–Mn–Si system based filler metals PR-N58 (*a*, *b*) and PN-6 (*c*, *d*): *a*, *c* — fillet region; *b*, *d* — seam

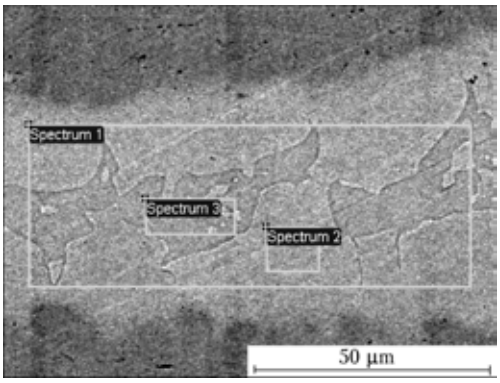

Figure 6. Microstructure of brazed joint produced by using filler metal PR-N58 and designation of spectra of the joint

Filler metals PR-N56 and PNS-6 based on the Ni–Mn–Cr–Si–Fe system were developed by using results of these investigations for brazing of stainless steel.

Investigations of peculiarities of formation of brazed joints on models of heat exchanging devices, produced by using boron-free filler metals PNS-6 and PR-N58, showed the quality formation of the seams, absence of cracks and other defects (Figure 5).

Investigations of chemical heterogeneity of the brazed joints showed that in brazing with filler metal PR-N58 the seam metal, which is a nickel-base solid solution, is enriched with elements of the base metal, i.e. iron (up to 17 wt.%) and chromium (up to 8.5 wt.%) (Table 2, Figure 6).

The amount of structural components in metal of the brazed seam depends upon its thickness, in other words, upon the brazing gap. For example, at a gap that is no more than 30–40 mm, metal of the brazed seam contains only one structural component, i.e.

Table 2. Content (wt.%) of chemical elements in the seam produced by using filler metal PR-N58

Spectrum No.	Si	Cr	Mn	Fe	Ni
1	4.39	5.80	28.05	11.50	50.26
2	2.78	8.50	24.06	17.12	47.54
3	6.76	3.03	32.23	4.83	53.15

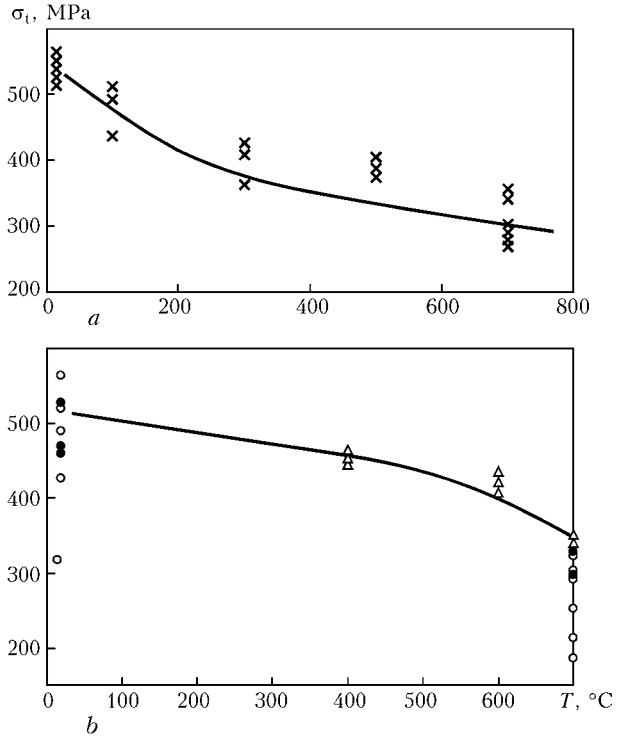

Figure 7. Dependence of strength of butt brazed joints in steel 10Kh18N10T on test temperature: *a* — filler metal PR-N58 (brazing temperature T_b = 1100 °C, 3 min); *b* — filler metal PNS-6 (○ — T_b = 1080 °C, 3 min; ● — T_b = 1080 °C, 10 min; Δ — T_b = 1100 °C, 3 min)

nickel-base solid solution. The fillet region, comprising a large amount of the liquid filler metal during brazing, contains the crystallising structural components that are characteristic of the filler metal, i.e. in addition to solid solution, it contains also the eutectic consisting of silicides (manganese, nickel) and nickel-base solid solution.

Results of mechanical tests of the butt joints in steel 10Kh18N10T produced at room and increased temperature proved a high potential of application of the said filler metals (Figure 7, *a*). For example, tensile strength of the butt joints at 500 °C (filler metal PR-N58) is 370–400 MPa, and it decreases to some extent (280–290 MPa) at 700 °C. As heat exchangers operate for a long time at high temperatures, the long-time strength tests were also conducted. At a temperature of 600 °C and load of 200 MPa, the brazed joints exhibited good performance, and they did not fracture for 1358 h. Strength of the brazed joints produced with filler metal PNS-6 is approximately at the same level (Figure 7, *b*).

The plate-ribbed heat exchangers made from stainless steel by using filler metal PR-N58 successfully passed the tests to leakage, efficiency of heat exchange and corrosion resistance in a heat-carrying environment [7]. The heat carrier in that case retained its optical transparency. Such heat exchangers are capable of staying in operation for a long time in the off-line mode at remote facilities under the observation by attending personnel.

Drawback of the brazing technology is that powder filler metals were used in the form of paste or suspension, the alternative to which should be filler metal in the amorphous form.

CONCLUSIONS

1. Application of eutectic amorphous filler metals of the Ni–Cr–B–Si system leads to a risk of formation of brittle phases and cracks even at a decreased (1.4 wt.%) boron content. Elimination of undesirable consequences of this situation by heat treatment in brazing of thin-walled metal is hardly possible.

2. The most suitable filler metals for brazing thin-walled stainless steel structures, in particular, plate-ribbed heat exchangers, are the low-activity ones of the Ni–Mn system. An important drawback of such filler metals is that they are used in the form of powders, which involves problems, particularly in vacuum brazing. Further investigations are necessary to optimise chemical composition of these filler metals in order to increase their sensitivity to amorphisation.

3. Copper used as a filler metal is still a promising material for brazing a wide range of heat exchanging devices operating at a temperature of no more than 500 °C.

1. Khimushin, F.F. (1967) *Stainless steels*. Moscow: Metallurgiya.
2. (2006) *Machine-building:* Encyclop. Ed. by B.E. Paton. Vol. III-4: Technology of welding, brazing and cutting. Moscow: Mashinostroenie.
3. (1997) *Constitutional diagrams of binary metallic system*: Refer. Book. Vol. 2. Moscow: Mashinostroenie.
4. Lugscheider, E., Partz, K. (1983) High temperature brazing of stainless steel with nickel-base filler metals BNi2, BNi5 and BNi7. *Welding J.*, 62(**6**) 160–164.
5. Lamb, S., Miller, F. (1969) The effects of aggression by nickel-base filler metals. *Ibid.*, 48(**7**), 283–289.
6. Rabinkin, A., Wenski, E., Ribaudo, A. (1998) Brazing stainless steel using a new NBF-series of Ni–Cr–B–Si amorphous brazing foils. *Ibid.*, **2**, 66–75.
7. Khorunov, V.F., Maksymova, S.V. (2006) Vacuum brazing of thin-sheet metals. In: *Proc. of 7th Int. Conf. on Vacuum Nanotechnologies and Equipment* (Kharkov, Oct. 2–6, 2006). Vol. 1. Kharkov: NNTs KhFTI, 62–65.

CURRENT CAPABILITIES OF SIMULATION OF AUSTENITE TRANSFORMATIONS IN LOW-ALLOYED STEEL WELDS

G.M. GRIGORENKO, V.A. KOSTIN and **V.Yu. ORLOVSKY**
E.O. Paton Electric Welding Institute, NASU, Kiev, Ukraine

Mathematical models describing the CCT and TTT diagrams plotted for the welds on low-alloyed steels are analyzed with a purpose of their possible experimental verification in «Gleeble-3800» system for physical simulation of metal welding and heat treatment process.

Keywords: arc welding, low-alloyed steel, weld metal, diagram of austenite transformations, simulation of phase composition

Diagrams of isothermal (TTT) and anisothermal (CCT) decomposition of austenite are widely used in practical operations of steel treatment [1, 2]. TTT diagrams provide a lot of information on the nature of transformations, but in practice it is rather difficult to achieve the isothermal condition. In the case of a very fast transformation, austenite decomposition occurs directly at the stage of achievement of the specified temperature [3]. Therefore, TTT diagrams for soaking time below 10 s are inaccurate. At treatment of large-sized items the main condition required for plotting TTT diagrams, namely rapid cooling to the specified temperature, is not achieved. In this connection, for practical purposes, TTT diagrams were replaced by CCT diagrams (non-isothermal).

At present the conditions of cooling of the welds are well-studied [4, 5]. Experimental results were the basis to plot the mathematical models, adequately describing the cooling temperatures and rates in different parts of the weld. Therefore, under laboratory conditions it is possible to simulate cooling of a small sample, the temperature mode of which corresponds to cooling at different kinds and modes of welding, different size of the items, and influence of different media.

Allowing for TTT and CCT diagrams, plotted for low-alloyed steels, is an important factor for forecasting the structural-phase condition of the welds. Numerous experiments were conducted for plotting such diagrams [6, 7]. Nonetheless, the wide range of application of alloying elements in steels alongside the strong sensitivity of CCT diagrams to the change of their composition and influence of grain size mean that it is impossible to plot a sufficient quantity of diagrams for their practical application.

Over the last decade a large scope of work has been performed on development of mathematical models which would allow calculation of CCT and TTT diagrams for steels. Almost all the models without exception are limited to their use for carbon and low-alloyed steels.

There exist numerous publications, describing the transformations in steels, but only a small part of them is suitable for calculation of CCT and TTT diagrams. In [8, 9] it is shown that it is quite possible to accurately calculate CCT and TTT diagrams for low-alloyed steels. In this model no difference was made between the diffusion and intermediate transformation. Modifying the equations proposed by Zener and Hillert [10, 11], Kirkaldy [12] plotted a model, which allowed calculation of the quantity of ferrite and pearlite, and derived the following expression for the time isothermal transformation:

$$\tau_{TTT} = \frac{1}{2^{(N/8)}(\Delta T)^3} \exp\left\{\frac{Q_{\text{eff}}}{RT}\right\} \sum_{j=1}^{m} \alpha_j C_j, \qquad (1)$$

where N is the grain point in ASTM system; Q_{eff} is the effective energy of diffusion activation; ΔT is the overcooling value, below which the austenite becomes unstable (A_{c3} temperature); C_j is the concentration of j-th element; α_j is the constant for each element.

Q_{eff} and α_j values were established experimentally by fitting curve (1) to the observed TTT transformation curve. As a result, the formula looked as follows [12] (quantity of each element is assumed in wt.%):

$$\tau_{0.1\,\%} = \frac{\exp\{2000/T\}}{2^{(N/8)}(Ae_3 - T)^3} \times \qquad (2)$$

$$\times (60 \cdot \%\,\text{C} + 90 \cdot \%\,\text{Si} + 160 \cdot \%\,\text{Cr} + 200 \cdot \%\,\text{Mo}).$$

Furtheron [12] the model was expanded for simulation of C-curves of pearlite and bainite transformation (Figure 1), and allowed calculation of the quantity of transformation products as a function of time and temperature:

$$\tau_{\text{F}} = \frac{60 \cdot \%\,\text{Mn} + 2 \cdot \%\,\text{Ni} + 68 \cdot \%\,\text{Cr} + 244 \cdot \%\,\text{Mo}}{6 \cdot 2^{(N/8)}(\Delta T)^3 D_{\text{F}}} I, \qquad (3)$$

$$\tau_{\text{P}} = \frac{1.8 + 5.4(\%\,\text{Cr} + \%\,\text{Mo} + 4 \cdot \%\,\text{Mo} \cdot \%\,\text{Ni})}{6 \cdot 2^{(N/8)}(\Delta T)^3 D_{\text{P}}} I, \qquad (4)$$

© G.M. GRIGORENKO, V.A. KOSTIN and V.Yu. ORLOVSKY, 2008

$$\tau_B = \frac{(2.3 + 10 \cdot \%\,C + 4 \cdot \%\,Cr + 19 \cdot \%\,Mo)10^{-4}}{6 \cdot 2^{(N/8)}(\Delta T)^2 D_B} I, \quad (5)$$

where $I = \int_0^X \frac{dX}{X^{2(1-X)/3}(1-X)^{2X/3}}$; X is the volume fraction of structural components; D_F, D_P, D_B are the diffusion coefficients of ferrite, pearlite and bainite, respectively.

If TTT diagram is calculated, then according to Kirkaldy additivity rule [13] it can be transformed into CCT diagram.

Later on Bhadeshia [14, 15] used another procedure for determination of points of the start of ferrite and bainite transformation, and compared his model with the experiment (Figure 2). Furtheron Lee improved Bhadeshia model [16], in order to expand its applicability limits to somewhat higher concentrations than those used in low-alloyed steels.

One of the disadvantages of these models was application of thermodynamics of diluted solutions at calculation of the transformation temperatures for medium-alloyed, tool and stainless steels.

Work [17] is an attempt to combine the more general thermodynamic models with the kinetic models in order to determine the capabilities of widening the range of steel compositions at forecasting their CCT diagrams. The Kirkaldy model was selected as a basis, and the empirical parameters could be easily adjusted and changed.

In addition to the above models, allowing to varying degrees for the real processes, which are connected to the thermodynamics and kinetics of transformation, there exist a number of purely empirical models based on processing the experimental results. A number of researchers [18, 19] are using Avrami equation for description of the structural components:

$$M = 100\,(1 - \exp(-k_i w^{n_i})), \quad (6)$$

$$FP = 100 \exp(-k_F w^{n_F}), \quad (7)$$

$$B = 100 - M - FP, \quad (8)$$

where M, FP, B is the quantity of martensite, ferrite-pearlite, bainite in the structure, wt.%; w is the cooling rate; k_M, k_F, n_M, n_F are the constants (for low-alloyed steels of 10G2FB type $k_M = 0.0021$, $k_F = 1.2$, $n_M = 0.487$, $n_F = 0.8$).

Having analyzed more than one hundred thermokinetic diagrams of austenite decomposition in low-alloyed steels [7, 20], models were proposed for assessment of the fraction of structural components in the structure of the HAZ metal:

$$M(\tau) = 1 - F[(\ln \tau - \ln \tau_i)/\ln S_i], \quad (9)$$

$$FP(\tau) = F[(\ln \tau - \ln \tau_{FP})/\ln S_{FP}], \quad (10)$$

$$B(\tau) = 1 - M(\tau) - FP(\tau), \quad (11)$$

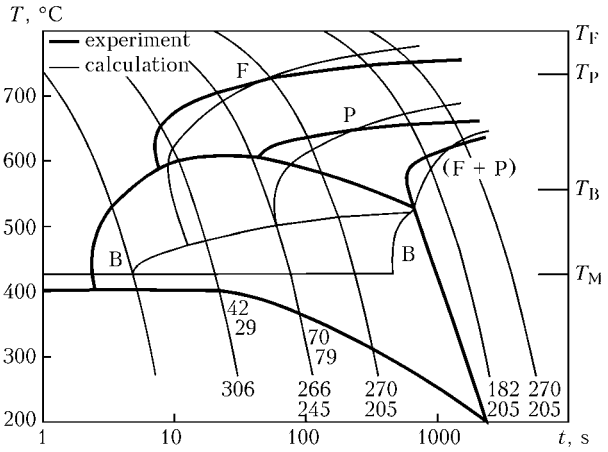

Figure 1. Comparison of the calculated (36Cr6 steel) and experimental [12] CCT diagrams

where τ is the duration of cooling from 800 to 500 °C; $F(z) = 0.5[1 + \mathrm{erf}\,(z/\sqrt{2})]$ is the integral function of normal distribution; τ_M, τ_{FP} are the cooling durations, at which 50 % of martensite or ferrite-pearlite structure form, respectively; S_M, S_{FP} are the constants characterizing the steepness of the curves of variation of the content of martensite or ferrite-pearlite structure at increase of the cooling time, respectively.

From summing up of all the above-said it follows that plotting a model of austenite decomposition, adequately describing the processes of decomposition in the weld metal of low-alloyed steels, requires obtaining a significant number of experimental results both for determination of temperatures of the start and end of formation of the structural components forming during austenite decomposition, and for metallographic determination of the quantity of the decomposition products. Great material and time consumption often makes this a difficult-to-perform task. However, availability of the currently most advanced «Gleeble-3800» system at the E.O. Paton Electric Welding Institute allows successfully solving it.

«Gleeble-3800» system is a complex (Figure 3) designed for physical simulation of the processes of welding, hot deformation of metals (rolling, forging,

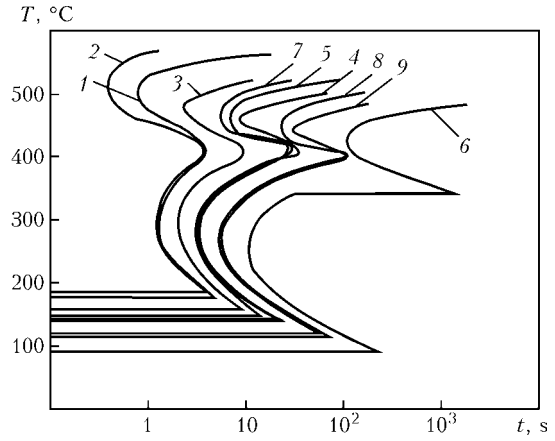

Figure 2. Calculated curves of isothermal transformation for a number of steels [15]: *1* — Fe–0.4C; *2* — Fe–0.4C–2Si; *3* — Fe–0.4C–1Ni; *4* — Fe–0.4C–2Ni; *5* — Fe–0.4C–1Mn; *6* — Fe–0.4C–2Mn; *7* — Fe–0.4C–2Cr; *8* — Fe–0.4C–1Mn–1Cr; *9* — Fe–0.4C–1Mn–1Ni

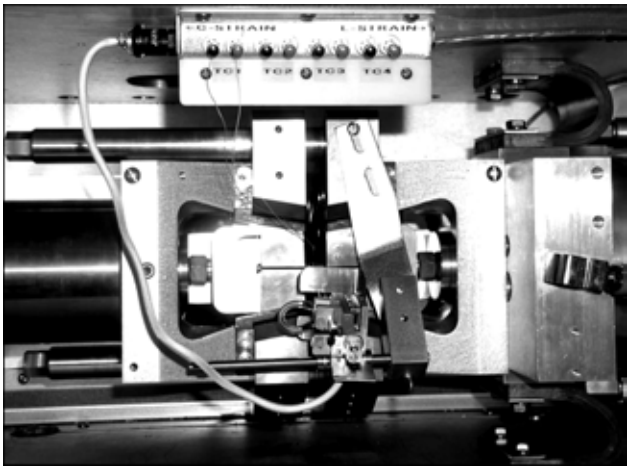

Figure 3. Appearance of working chamber of «Gleeble-3800» system

upsetting), as well as simulation of metal heat treatment. Testing for hot compression and tension can be conducted both at direct and alternating value of the applied force, the maximum compression force can momentarily reach 20 t, and the maximum force of tension of the samples is up to 10 t at up to 2000 °C temperatures of metal heating. Test data allow determination of not only the degree of metal deformation, depending on the applied force and temperature, but also the process parameters, at which development of hot cracks becomes possible. Deformation rate at compression can be up to 1 m / s.

At simulation of the processes of metal heat treatment, as well as investigation of the melting and solidification processes, the maximum heating temperature can briefly reach 3000 °C, rate of heating and cooling is up to 10,000 °C / s. Sample cooling is conducted both from inside and from the outside of the samples, cooling media being water and air. All the investigations can be conducted in a controlled atmosphere.

Availability of a high-speed dilatometer with an induction high-sensitivity sensor in the system allows plotting diagrams of thermokinetic transformation in the automatic mode, this greatly accelerating the time for obtaining and processing the experimental results.

Thus, all the prerequisites are in place now for successful construction and development of a mathematical model of austenite decomposition. Results obtained using «Gleeble-3800» system will be the basis of the database on the kinetics of thermokinetic decomposition of austenite in welds on low-alloyed high-strength steels, in order to determine both the empirical coefficients, used for description of the decomposition kinetics, and for more precise determination of temperature intervals of transformation of the characteristic structural components, duration of the transformations and final structural-phase state of weld metal.

1. Gulyaev, A.P. (1960) *Heat treatment of steel*. Moscow: Mashinostroenie.
2. Novikov, I.I. (1978) *Theory of heat treatment of metals*. Moscow: Metallurgiya.
3. Gulyaev, A.P. (1986) *Metals science*. Moscow: Metallurgiya.
4. Grabin, V.F. (1982) *Metals science of fusion welding*. Kiev: Naukova Dumka.
5. Rykalin, N.N. (1951) *Calculations of thermal processes in welding*. Moscow: Mashgiz.
6. Popov, A.A., Popova, L.E. (1965) *Isothermal and thermokinetic diagrams of overcooled austenite decomposition*. Moscow: Metallurgiya.
7. Seyffarth, P., Meyer, B., Scharff, A. (1992) *Grosser Atlas Schweiss-ZTU-Schaubilaer*. Duesseldorf: DVS.
8. Kirkaldy, J.S., Tomson, B.A., Baganis, E.A. (1978) *Hardenability concepts with applications to steel*. Warrendale, PA: AIME.
9. Kirkaldy, J.S., Venugopolan, D. (1984) *Phase transformations in ferrous alloys*. Ed. by A.R. Marder, J.I. Goldstein. Warrendale, PA: AIME.
10. Zener, C. (1946) Kinetics of the decomposition of austenite. *Transact. of AIME*, **167**, 550–555.
11. Hillert, M. (1957) Thermodynamics and kinetics isothermal transformation in steel. *Jerkont. Ann.*, **141**, 758–767.
12. Kirkaldy, J.S. (1991) Diffusion-controlled phase transformation in steel. Theory and applications. *Scand. J. Met.*, **20**, 51–61.
13. Kirkaldy, J.S. (1988) *Advances in phase transformation*. Oxford: Pergamon Press.
14. Bhadeshia, H.K.D.H. (1981) Developments in martensitic and bainitic steels: role of the shape deformation. *Metal Sci.*, **15**, 175.
15. Bhadeshia, H.K.D.H. (1982) A thermodynamic analysis of isothermal transformation diagrams. *Ibid.*, **16**, 159–165.
16. Lee, J.-L., Bhadeshia, H.K.D.H. (1993) Computer simulation of microstructural evolution in thermomechanical processing of steel plate. *Mater. Sci. Eng. A.*, **171**, 223.
17. Saunders, N., Guo, Z., Li, X. et al. *The calculation of TTT and CTT diagrams for general steels*. http: / / www.msm.cam.ac.uk
18. Zakharova, I.V. (2001) *Decrease of defectiveness of low-alloy welded joints by optimization of welding technology*: Syn. of Thesis for Cand. of Techn. Sci. Degree. Mariupol.
19. Pekarska, V. (2002) Mathematical simulation of HAZ metal structure in laser welding. In: *Proc. of Int. Conf. on Mathematical Modeling and Information Technologies in Welding and Related Technologies* (Katsiveli, Sept. 16–20, 2002), 114–117.
20. Seyffarth, P., Kasatkin, O. (1982) Calculation of structural transformation in the welding process. *IIW Doc. IX–82*.

IMPROVEMENT OF SERVICE RELIABILITY OF DOUBLE-WALL WELDED TANKS

A.Yu. BARVINKO
E.O. Paton Electric Welding Institute, NASU, Kiev, Ukraine

The problem of improving the reliability of oil storage double-wall tanks is considered. It is shown that installing special bands at lower flanges of the main and auxiliary wall does not solve the problem in its full scope. It is suggested that reliability of the main wall should be improved by applying to assessment of rolled plate quality the deformation defect tip displacement criterion K_c which is met by the new generation of steels, i.e. controlled-rolling niobium-containing steels. Substantial improvement of toughness properties of the wall plates will guarantee detection and removal of defects in the main wall in the subcritical condition.

Keywords: welded structures, double-wall tanks, niobium-containing steels, cracking resistance, tough fracture, brittleness criteria

Increase of the capacities of petroleum-processing plants during their upgrading following the most recent technologies and insufficient stability of oil prices in the world market dictate the need to increase the capacity of the existing charging stock tank farms. On the other hand, continuous increase of land prices and constricted nature of the territories adjacent to the petroleum storage depots, makes it necessary to look for non-traditional methods of increasing the oil tank farm capacity without increasing their building areas.

Over the last years, a tendency has been observed to eliminate making earth or concrete diking around the tanks by construction of double-wall tanks of «sleeve-in-sleeve» type [1]. In this case, the facility consists of two tanks: inner (main) and outer (protective). The latter tank prevents oil spills beyond the protective wall at local or avalanche failures of the main tank. If the question of localization of oil spills within the protective tank wall at local failures of the main wall raises no doubt, the question of the protective wall performance at extended tough (avalanche) failure of the main wall requires a separate consideration.

Hypothetically, the instantaneous failure of the main tank wall along its height can be brittle or tough. Brittle fracture is characterized by absence of deformations at rupture edges in steels with low values of impact toughness. The motive force of brittle fracture is the wall elastic energy (Hook's energy). High requirements to minimum values of impact toughness (Charpy), method of production and composition of steels for the tank wall and welded joints in the current codes of leading countries [2–4] allowed a practically complete elimination of brittle fractures. Initiation and development of a brittle crack in the wall is possible only in local sites with low toughness properties or in sections where the high toughness properties cannot be implemented. In particular, these can be the regions of bulk stressed state, characteristic for sites with surface layer work hardening due to impact actions, weld sections with crack-like defects or quenching structures. In the case of a biaxial and particularly triaxial stressed state in the tip of a defect in a weld favourable conditions are in place for brittle crack initiation and development. In this case the constrained conditions for strain development do not permit realization of high ductile properties of the wall material.

During development the brittle crack goes beyond the defect limits. High ductile properties of the wall material and its welded joints begin to be manifested here. The crack develops into a quasibrittle crack, and then into a tough crack. The rate of tough crack growth and its critical length are determined by the impact toughness values of wall material specified by the standards currently in force. Many years of operation of the tank farms in Ukraine, Russia and other countries shows that the rules of selection of the steel grade and its impact toughness accepted in codes [2–4] in combination with the rules of tank operation ensure the required performance during the entire guaranteed service life of tanks of regular design. In the presence of diking around the tanks the technical supervision personnel has a good opportunity of performing daily visual inspection of all the tanks, which allows with a sufficient degree of probability to visually reveal on the wall outer surface through-thickness defects of 10–50 mm length, i.e. before their critical values.

Application of tanks of a design of «sleeve-in-sleeve» type essentially impairs the conditions of scheduled daily monitoring of the technical condition of the inner (main) tank.

The Figure gives the schematic of some design solutions of double-wall tanks of 20,000 and 50,000 m^3 capacity. A 20,000 m^3 tank has the main wall of H_m = = 22.5 m height and protective wall of H_{pr} = 18.1 m height at $L_3 \approx 2$ m distance between them. In 50,00 m^3 tank H_m = 20.0 m and H_{pr} = 13.5 m are assumed at distance $L_3 \approx 5.4$ m between them. If in 50,000 m^3 tank the conditions for visual inspection of the main wall from a circular platform located on top of the protective wall can be regarded acceptable to a certain extent, it is extremely difficult to perform thorough inspection of the wall of 20,000 m^3 tank at $L_3 \approx 2$ m. The possibility of gas contamination of the interwall

© A.Yu. BARVINKO, 2008

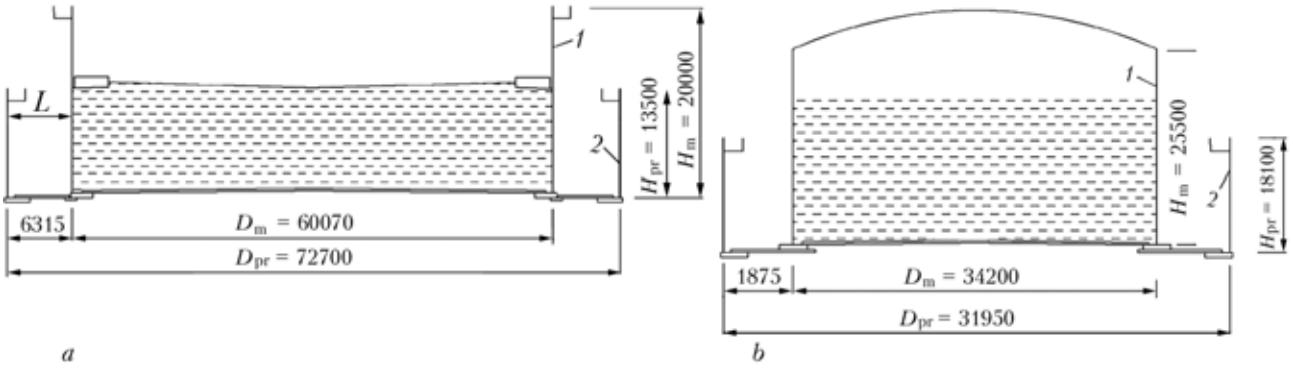

Schematics of tanks of «sleeve-in-sleeve» design of 50,000 (*a*) and 20,000 (*b*) m^3 capacity: *1, 2* — wall of the main and protective tank, respectively; *L* — interwall spacing

space and presence of snow deposits in winter, makes it more difficult to examine the manhole nozzles and supply piping in the lower flange.

Changes of the steady-state conditions of technical supervision of the main tank wall performance should be taken into account at development of its main engineering designs and rules of operation.

It is widely believed that the protective wall can not only localize the oil spill at local damage to the main tank, but also withstand the hydraulic shock at an avalanch failure of the main wall. In a number of cases during design such an ability of the protective wall is substantiated by calculations and mounting special bands. The fact that at avalanche failure the load is applied to the auxiliary wall in a local fashion, along one of the generatrices to the entire height, is not fully taken into account. The motive force of the tough crack after a critical length has been achieved, will be the pressure of the column of flowing out liquid (oil or other stored product) located above the crack on the crack lips. At opening of the crack lips a yield core forms in the crack tip, in which the wall material successively flows, is strenghthened and fails after σ_{ult} has been achieved. Then a new cycle starts with formation of a new ductility zone [5, 6]. The rate of tough crack propagation in the tanks depends on pressure of out-flowing oil on its lips, and in the line pipelines ---- on the pressure of outflowing gas [5]. Full-scale testing of the main gas pipelines showed that at 6–7 MPa pressure in the pipe the crack rate is 250–300 m / s [7]. For tanks there are no such direct data. Based on description of individual cases of avalanche failure of tanks [7] at 0.10–0.15 MPa pressure on the tough crack lips, fracture occurred within 1 s. The stored product outflowing from the opening crack, will make a dynamic impact on the auxiliary wall along one of its generatrices. Being a thin-walled shell, at such a loading the wall immediately looses its stability, and takes the shape of an elongated ellipse. This may well lead to wall rupture along the generatrix. Search for solutions to give additional rigidity and strength to the wall to take up the dynamic impact of outflowing liquid, in our opinion, may only lead to considerable loss of metal, without getting sufficient guarantees of the auxiliary wall performance at the avalanche tough fracture of the main wall.

The objective of this study is substantiation of an improvement of reliability of double-wall tanks by complementing the normative requirements on selection of steel grades for the main tank wall and greater capacity tanks of a regular design, allowing for the criterion of crack resistance ---- characteristic of crack tip opening δ_c. The proposed characteristic allows for plastic deformations preceding achievement of a critical length by the crack, and will guarantee self-arresting of the process of initiating crack development before it has reached a critical value. In [8] it is shown that at δ_c = 0.17–0.18 mm the subcritical values of a through-thickness crack reach 60 mm, this allowing their guaranteed detection after outflow of the stored product. The given δ_c values correspond to impact toughness values at $KCV_{-20} \geq 80$ J / cm^2 [8, 9]. The issues of detection of tough cracks at their subcritical development in the wall of main gas pipes are considered at a sufficiently high level by O.M. Ivantsov [10, 11], D. Broek [9], etc. The stresses in the wall crack tip were assessed by K_c criterion ---- stress intensity factor (SIF). The difference in the approaches consists in that δ_c definition is derived allowing for plastic deformations in the crack tip, and K_c is determined proceeding from the presence of an elastic and highly insufficient share of plastic deformation in δ_c. Dependencies $\delta_i \rightarrow KCV$ and $K_c \rightarrow KCV$ have a similar form [9]. Accumulated experimental data allowed establishing the above dependencies for controlled-rolled niobium-containing steels as the best complying with the required values δ_c and K_c [9, 10]. Transition from δ_c and K_c criteria to KCV value generally-accepted in metallurgical production for sheet rolled stock allows using the derived results in practice. The Canadian company Nova norms the impact toughness on Charpy samples, tolerating the presence of a through-thickness defects of a certain length at working hoop stresses, which do not exceed the stresses corresponding to 80 % of the minimum yield point of steel of X70 class (Table 1) [11].

Let us consider the possibility of application for the main wall of tanks of «sleeve-in-sleeve» type of controlled-rolled steels of the type of X70 class, widely applied for pipes of the main gas pipelines. Steels of X70 class belong to niobium-containing low-alloyed steels. Modern technology of thermomechanical treatment of low-alloyed steels of a higher strength became

Table 1. Requirements of Nova Company, Canada, to pipes of X70 steel [11]

Outer diameter, mm	KCV, J / cm^2	Size of critical through-thickness defect, mm (90 % of maximum possible defect)
914	47	14
1067	55	135
1219	69	155
1422 ($Ð_{work}$ = 8.4 MPa)	69	165

Table 2. Mechanical characteristics of steels of strength classes C355–C440 to TU U 27.1-05416923-085:2006 [14]

Steel grade, (strength class)	σ_y, MPa	σ_t, MPa	δ_5, %	ψ, %	$KÑV_{-40}$, J / cm^2
	Not less than				
06GB (355)	355	450	22	55	98
06GB (390)	390	490	22	55	98
06G2B (440)	440	540	22	55	98

possible to a great extent owing to the use of microalloying niobium additives. Steels have values KCV_{-20} < < 88 J / cm^2. A wide application of niobium-containing steels for construction of the main gas pipelines and extensive experience of their successful operation allowed metallurgists of Russia and Ukraine proposing new steels of thermomechanical rolling for welded building structures, mechanical engineering products and other branches. Specification TU 14-1-4083–86 [12] was developed specifically for the welded metal structures with supply of 8–50 mm thick rolled stock of steels 09G2FB and 10G2FB. Russian codes [2] recommend the above steel grades for the oil tank walls. The disadvantage of these steels is the need for application of preheating in many cases [13].

New capabilities for increasing the reliability and guaranteed performance of tanks are opened up owing to development by UkrgosNIIKM «Prometej» and PWI of a new range of niobium-containing steels according to TU U 27.1-05416923-085:2006 [14] with 0.04–0.09 % C content. Table 2 gives the main characteristics of the above steels. With a wide variation of σ_y values from 355 to 490 MPa and preservation of high value of impact energy KCV_{-40} = 98 J / cm^2, all the steels fully meet the requirements of Table 1 and have a critical through-thickness crack-like defect not less than 100 mm long. On the other hand, a low content of carbon in steels allows their welding to be performed without edge preheating.

Application for walls of large-capacity tanks (more than 20,000 m^3) of increased and high strength steels, the toughness properties of which guarantee seft-braking of the initiating tough crack before it has reached a critical value, equal to approximately 100 mm, raises its reliability to a qualitatively new level and with daily examination practically eliminates the possibility of avalanche failure development.

The design of the wall eliminating avalanche failures is particularly necessary for the main (inner) wall of a double-wall tank. Such a design allows eliminating the mounting of bands as avalanche crack arresters on this wall and on the outer wall. In case of deterioration of the conditions of daily visual examination of the main wall surface, the controlled development of the through-thickness defect before it has reached the critical value equal to approximately 100 mm, actually guarantees a timely detection and repair of the defect.

Ukraine now has positive experience of application of niobium-containing steels for oil tank walls. Steel 06G2B of 440 MPa strength was used for lower flanges of walls of a double-wall tank of 75,000 m^2 capacity at LPDS «Brody». Steel 10G2FB is successfully applied at complete replacement of the lower flange in 50,000 m^3 capacity tanks and for special inserts for replacement of vertical site butt joints. Welded joints were performed without edge preheating and had the impact toughness KCV on the level of base metal.

CONCLUSIONS

1. Owing to development and mastering of commercial production of a new generation of niobium-containing steels of C355, C390 and C440 strength class, having the impact toughness values KCV_{-40} = 98 J / cm^2, in Ukraine the crack resistance of the wall of oil tanks under construction is essentially improved.

2. Proceeding from the criterion of the condition of self-braking of a tough crack (δ_c = 0.17–0.18 mm) it is necessary to complement in the current codes the item specifying the impact toughness values in transverse samples for sheet rolled stock of lower flanges of the wall of a tank of more than 20,000 m^3 capacity by not less than KCV_{-20} = 80 J / cm^2. It is necessary to extend these requirements also to the inner walls of double-wall tanks.

1. Beloev, M., Konstandinov, J., Staneev, S. et al. (1996) Nieto're problemy budowy zbiorniko'v o podwo'jnym korpusie i podwo'jnym dnie. *Biuletin Institutu Spawalnictwa w Gliwicach*, **3**, 50–54.
2. *PB 03-605–03* Russia: Rules for arrangement of vertical cylindrical steel tanks for oil and oil product storage. Moscow.
3. *VBN V.2.2.28-58-2–94* Ukraine: Vertical steel tanks for oil and oil product storage.
4. *API Standard 650*: Welded steel tanks for oil product storage. 9th ed. May, 1993.
5. Shumejker, A.K., MacKortni, R.F. (1974) Pipeline deformation at propagation of shear fracture. In: *AOIM*. Serier D: Theoretical principles of engineering calculations, 73–81.
6. Shumejker, A.K., MacKortni, R.F. (1974) Analysis of displacements at propagation of shear fracture along the pipeline. *Ibid.*, **4**, 86.
7. Rozenshtejn, I.M. (1995) *Accidents and reliability of steel tanks*. Moscow: Nedra.
8. Paton, B.E., Trufyakov, V.I., Kirian, V.I. (1981) Requirements to toughness of steel for the main pipelines at mounting extensive fracture arresters in them. *Avtomatich. Svarka*, **12**, 5–9.
9. Broek, D. (1980) *Principles of fracture mechanics*. Moscow: Vysshaya Shkola.
10. Ivantsov, O.M., Kharitonov, V.I. (1978) *Reliability of the main pipelines*. Moscow: Nedra.
11. Ivantsov, O.M. (1985) *Reliability of structural units of the main pipelines*. Moscow: Nedra.
12. *TU 14-1-4083–86*: Rolled sheets of niobium-containing and other low-alloyed steels with improved weldability and cold resistance. Introd. 04.02.2007.
13. *VSN 2-124–80*: Instructions on the technology of welding the main pipelines. Moscow.
14. *TU U 27.1-05416923-085:2006*: Sheet welded products of quality steel of 355–590 strength grades for machine-building.

CARBIDE PHASES AND DAMAGEABILITY OF WELDED JOINTS OF STEAM PIPELINES UNDER CREEP CONDITIONS

V.V. DMITRIK[1], **A.K. TSARYUK**[2] and **A.I. KONYK**[3]
[1]Ukranian Engineering-Pedagogical Academy, Kharkov, Ukraine
[2]E.O. Paton Electric Welding Institute, NASU, Kiev, Ukraine
[3]OJSC ZEMI, Kharkov, Ukraine

Regularities of ageing of welded joints of steam pipelines from heat-resistant 12Kh1MF steel operating under creep conditions are considered. A connection is established between the damageability of welded joints and the carbide transformation kinetics, and recommendations are given on optimization of the initial structure of base metal.

Keywords: heat-resistant steels, welded joints, pores, life, carbides, structure, creep, steam pipelines

Damageability of welded joints of steam pipelines from heat-resistant pearlitic steels under the creep conditions at their operation for more than 250,000 h is due to the features of transformation of welded joint metal structures [1–3]. These transformations are characterized by different level of deformation of α-phase grains, quantity and degree of coagulation of carbide phases of the 1st group (predominantly $M_{23}C_6$), as well as the amount of carbide precipitates of the 2nd group. Structural transformation are due to carbide reactions $M_3C \rightarrow M_7C_3 \rightarrow M_{23}C_6 \rightarrow M_6C$, investigation of which in the damageability mechanism appears to be urgent. Structural transformations run with the highest intensity in the HAZ incomplete recrystallization zone, which is exactly what accounts for its higher damageability at long-term operation than that of other HAZ sections, as well as the weld and base metal.

Studying the regularities of the ageing process, as well as the principles determining its kinetics is necessary to more precisely determine the mechanism of damageability of these welded joints operating under the creep conditions.

Investigations were conducted on samples of 159 × × 18 mm size cut out of welded joints of 12Kh1MF steel of hot re-heating steam pipelines of Zmievka TPP, which were produced by standard technology using manual arc welding, as well as the respective reference samples. After welding the above joints were subjected to high tempering at the temperature of 750 °C for 3 h.

The steam pipeline was partially in operation before 2002 at the temperature of 545 °C and pressure of 24 MPa, and after 2002 –– at the temperature of 510 °C and the same pressure. The overall duration of operation was equal to 275,637 h. In such a condition the steam pipeline material had the following mechanical properties: σ_t = 775 MPa; σ_y = 270 MPa; δ = 19.5 %; ψ = 77%; KCV = 18 J / cm^2.

© V.V. DMITRIK, A.K. TSARYUK and A.I. KONYK, 2008

Appropriate chemical microetching was used to detect M_3C, M_7C_3, $M_{23}C_6$, M_6C carbides, as well as pores [4, 5]. Etchant of the following composition: 1 g KOH; 4 g $KMnO_4$; 100 ml H_2O was used to reveal M_3C carbide. Duration of etching in the boiling solution was 5–10 min. Addition of tartaric acid to the above etchant allowed identifying only M_7C_3, $M_{23}C_6$ and M_6C carbides.

Carbide phases were studied by qualitative microstructural analysis using powder diffractometer Siemens-D500 in monochromatic radiation. Diffractograms were taken in the region of angles $10 \le 2\theta \le \le 140°$ with scanning pitch of 0.02° and pulse accumulation time of 75 s in each point. In order to detect pores and identify the carbide phases JSM-820 scanning microscope with a system of X-ray microanalyzer Link AN10185S and 10 nm resolution in secondary electron mode and about 2 μm locality of microanalysis was used. Optical and electron microscopy were used for structural analysis, and standard equipment was applied for mechanical property determination.

The initial (as welded) structure of welded joint metal demonstrates characteristic non-uniformly distributed through the body and the boundaries of α-phase grains dispersed carbides of cementite type (Figure 1), having the composition of substitutional solid solution as to chromium. Dimensions of cementite precipitates are equal to 20–500 nm. Calculation of electronographs showed that they have an orthorhombic lattice, the parameters of which are equal to a = = 0.45 nm, b = 0.512 nm, c = 0.680 nm (with the accuracy of ±0.005 nm). These data are close to those given in [6]. The shape of such carbides is close to the spherical or elliptical one. The content and uniformity of carbide distribution in the sections of the HAZ structures, as well as in the area of weld metal and base metal of welded joints, differs noticeably, which is related to the intensity of structural transformations.

In the structure of welded joints of 12Kh1MF steel under the creep conditions metastable carbides of the 1st group M_3C, M_7C_3, $M_{23}C_6$ and M_6C, as well as stable MC and M_2C carbides of the 2nd group, are

found after operation for 275,673 h (Figure 2). It is rational to consider the general regularities of formation of carbide transformations, characteristic for structures of the studied welded joints.

The intensity of transformations of carbides of the 1st group located in the body of α-phase grains, is much lower than along the grain boundaries, which is confirmed by their quantity. For instance, after operation for 275,637 h the revealed quantity of M_3C carbides located in the grain bulk, was equal to about 20–30 %, and along their boundaries to approximately 5–7 % of the total amount of carbides of the 1st group.

A crystal of cementite grain alloyed by chromium consists of a certain quantity of octahedrons, having mutually oriented axes located at angles [6, 7]. In the structure of the studied welded joints chrome cementite $(Fe, Cr)_3C$ forms at a local content of 2.0–2.3 wt.% Cr. Molybdenum in M_3C dissolves to 1 %. In M_3C cell chromium may substitute up to 25 % of iron atoms, which is their saturation limit.

Termodynamic activity of chromium in carbides and along the boundaries of α-phase grains is lower than in the grains proper, thus promoting its directional diffusion under the creep conditions. Diffusion processes (at long-term operation) lead to an increase of the degree of chromium segregation along the boundaries of α-phase grains and in the zone of grains adjacent to their boundaries. Diffusion rate in α-phase grains depends on their dimensions, shape and structure. Saturation of cementite type carbides by chromium atoms under the creep conditions occurs not only due to their volume diffusion from α-phase grains

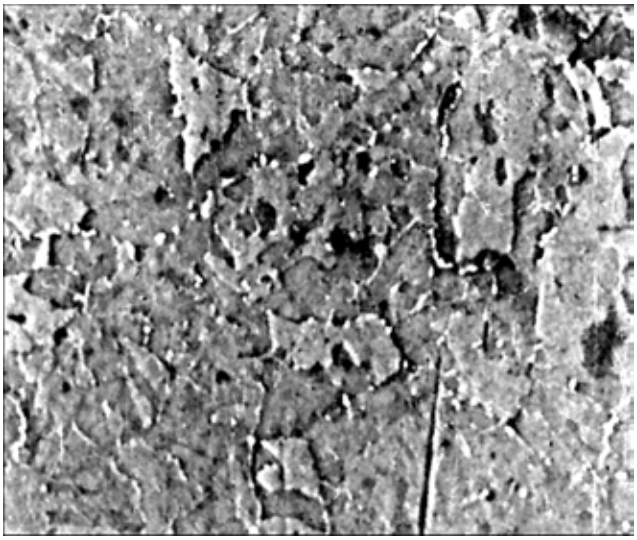

Figure 1. Microstructure of weld metal with characteristic cementite precipitates (×2500)

to the interphase, but to a greater extent — due to diffusion along the boundary (boundary diffusion), as well as dislocation displacement. Grains of α-phase form Guinier–Preston zones adjacent to their boundaries, where chromium concentration can be 2–12 times higher than their average concentration. Cementite type carbides located along the boundaries of α-phase grains (see Figure 2), can be considered in the presence of heterogeneous fluctuations (by Frenkel) as subcritical nuclei [6]. When local concentration of chromium becomes critical, heterogeneous fluctuations cause the respective phase transformations provided the growth of the subcritical nuclei is characterized

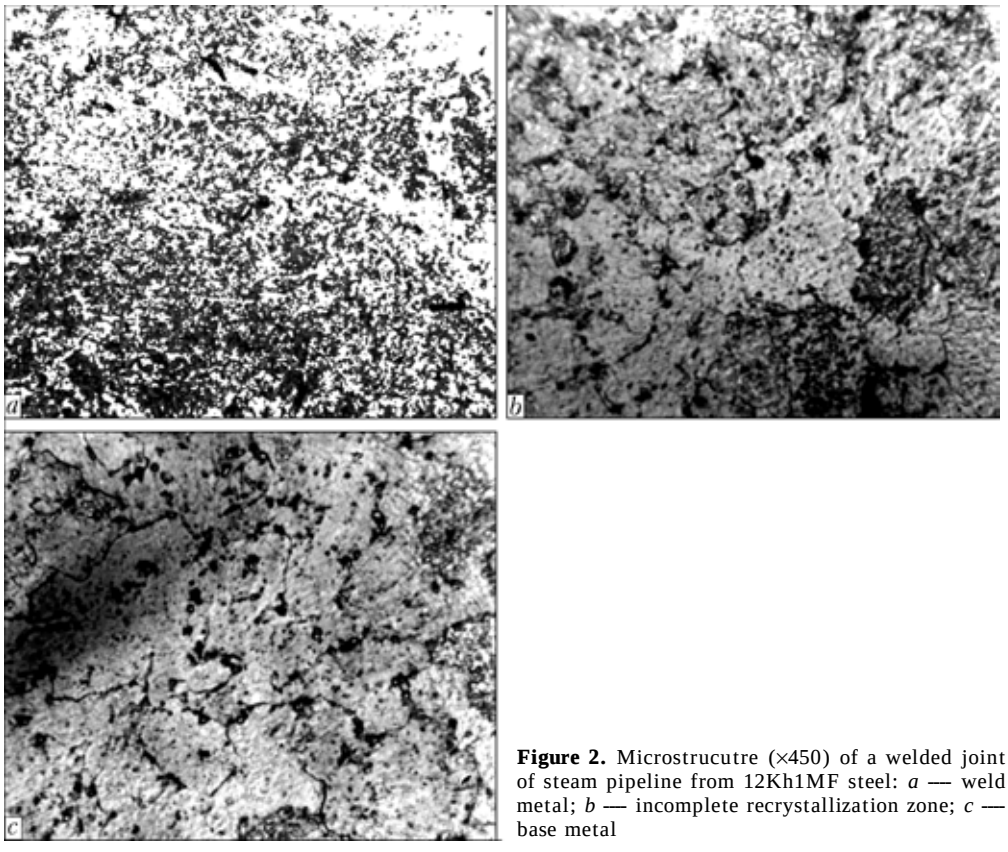

Figure 2. Microstrucutre (×450) of a welded joint of steam pipeline from 12Kh1MF steel: *a* — weld metal; *b* — incomplete recrystallization zone; *c* — base metal

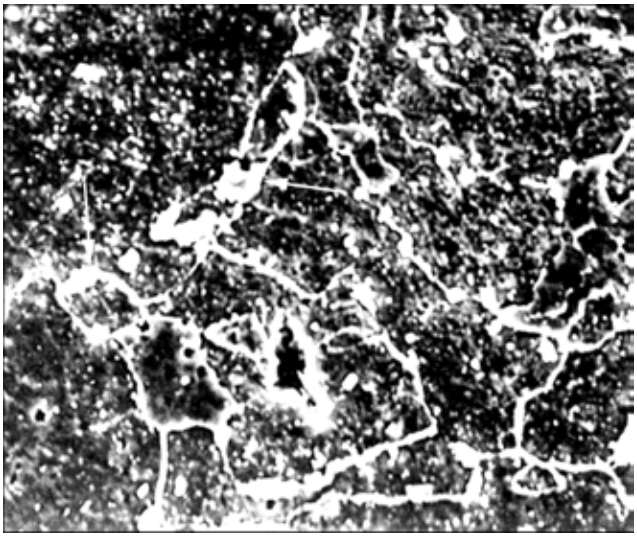

Figure 3. Microstructure of metal of the HAZ incomplete recrystallization zone with precipitates of $M_{23}C_6$ carbides (shown by arrows) in welded joints of steam pipelines from 12Kh1MF steel (×1500)

first by increase of the cell energy level, and then its lowering.

At achievement of about 3.5–5.5 % local concentration of chromium in Guinier–Preston zones, a limit oversaturation of cementite by chromium up to 5 % occurs, which is exactly what provides its transformation into trigonal carbide $(Cr, Fe)_7C_3$. It may be shown that such transformations are the most characteristic for the period of welded joint operation from 80,000 to 150,000 h, during which the greatest number of these carbides is noted.

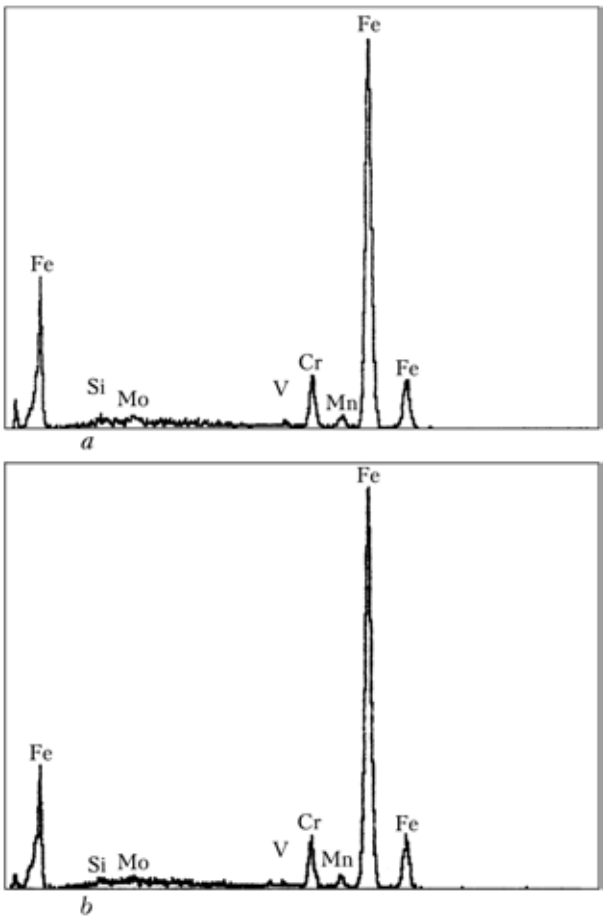

Figure 4. Spectra of $M_{23}C_6$ carbide precipitates located along boundaries of α-phase grains: *a* — incomplete recrystallization zone; *b* — fusion zone

Both the segregation level and atom mobility have a marked influence on carbide transformations. L.I. Mirkin showed [8] that for formation of trigonal carbide $(Cr, Fe)_7C_3$ of the size of 20 metallic atoms, the number of fluctuations in 1 cm^3 of steel containing 2 wt.% Cr, is equal only to several tens. In the metal of HAZ incomplete recrystallization zone at increased level of segregation compared to other structure sections, the number of fluctuations is also high. Quantity of M_7C_3 carbide phases after operation for 100,000–150,000 h is approximately 30 % greater here than in other sections, which is provided by a higher rate of $M_3C \rightarrow M_7C_3$ reaction.

At establishment of a local concentration of chromium in the grains and on grain boundaries above 5.5 % a limit saturation of trigonal M_7C_3 carbide by chromium occurs, this leading to its transformation into cubic carbide $M_{23}C_6$ (Figure 3). After operation for 275,673 h it is established that an elementary $M_{23}C_6$ cell consists of hollow cubes and tetrahedrons, which have metal atoms in their center. Tetrahedral edges between the cubes are essentially longer than the cube edges. Cell size is as follows: a = 1.0572 nm, which differs from the data of [4, 5, 9], where a = = 1.0595 nm. The difference in cell parameters is due to chromium atom substitution by molybdenum and manganese atoms, which have a larger atomic radius: for chromium 0.127 nm, for molybdenum — 0.139, for manganese — 0.130 nm [10]. Substitution occurs under the conditions of additional building of the lattice of $M_{23}C_6$ carbides, also at their coalescence. M_7C_3 precipitates in welded joint structures noticeably differ by their composition (Figure 4), for instance, in the zone of incomplete recrystallization as to chromium — by 15, and as to molybdenum — by 25 and as to manganese — by 30 %. Such a difference results from the presence of different levels of segregation of the above elements, which is due to the diffusion processes dependent on the operation conditions and operation time.

A regularity is confirmed [11] of $M_{23}C_6$ nucleation occurring, as a rule, on the contact boundaries of three α-phase grains. This is exactly where the segregation level rises the most intensively, which depends on the structure and conditions of ageing. For instance, after operation for 200,000 h the quantity of $M_{23}C_6$ carbides (fusion zone) was equal to about 40 % of their total quantity, after operation for 275,637 h — to 60 % and after operation for 300,000 h (experimental data) — to about 63 %.

Lowering of the steam pipeline working parameters (temperature and pressure) after operation for 250,000 h, in order to increase their life allowed lowering the diffusion process rates in the welded joint metal. However, the lowering did not have any noticeable influence on the intensity of dislocation

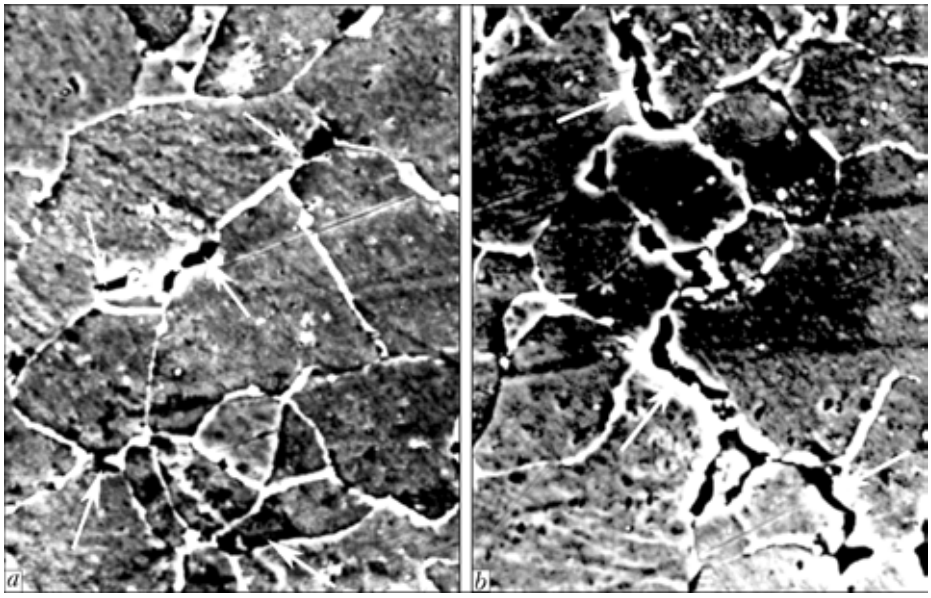

Figure 5. Grain boundaries of α-phase grains damaged by pores and microcracks (shown by arrows): *a* — incomplete recrystallization section; *b* — fusion zone (×2500)

mechanism of damageability at the steady-state level of structural transformations and respective operating conditions [12]. In the presence of local concentration of chromium (above 10 wt.%) $M_{23}C_6 \rightarrow M_6C$ reaction proceeds. Average chromium content in the segregation zones after operation for up to 150,000 h in the incomplete recrystallization section rose approximately from 1.5 (initial averaged segregation) to 5 wt.%, and after operation from 150,000 to 275,673 h ---- from 5 to 6 wt.%, which is confirmed by lowering of the diffusion process rate at increase of operation period. Local increase of the concentration of chromium in the segregation zones (above 10 wt.%) and of M_6C carbides (about 5 wt.%) can be considered an exception, and it is due to an increased content of chromium in the pipe billet metal.

Intensity of pore initiation in welded joints of 12Kh1MF steel under the creep conditions is essentially related to stability of carbide phases of the 1st group. Pores initiate in the most intensive manner in the HAZ incomplete recrystallization zone. Duration of welding heating in the intercritical temperature range (A_{c_1} – A_{c_2}) promotes increase of initial segregation of chromium on α-phase grain boundaries (1.5–2.0 %), which rises essentially during welded joint operation and leads to an increase of $M_3C \rightarrow M_7C_3 \rightarrow$ $\rightarrow M_{23}C_6 \rightarrow M_6C$ reaction rate.

$M_{23}C_6$ carbides (approximately 60 %), as well as M_3C, M_7C_3, M_6C, VC, Mo_2C carbides (the rest), are present in the metal of incomplete crystallization zone at the second creep stage (after operation for 275,637 h). Content of $M_{23}C_6$ carbide precipitates in the metal of the weld, HAZ zones, as well as in the base metal, differs essentially. For instance, in the base metal $M_{23}C_6$ content was equal to about 4 %, in the weld metal to 45 % and in the overheated zone to 5 % of their total content, respectively. It is established that in the incomplete recrystallization section pore density is greater by about 70 % than in the base metal, by 30 % than in the weld metal and by about 40 % than in the HAZ fusion zone.

The detected quantity of pores agrees with the statistics [1]. Assuming about 0.05–0.10 μm pores as the nucleus ones [1, 13, 14], it was taken into account that their initiation and propagation occurs during the entire operation of welded joints. During pore propagation their shape develops from an ellipsoidal or spherical into an elongated ramified one of a variable cross-section (Figure 5), this allowing them to be formally regarded as microcracks. In the metal of incomplete recrystallization zone damageability develops the most intensively along bainite–pearlite boundaries (about 280 pores / mm^2), where pearlite is a new product of austenite decomposition, which is close to the data of [13], and it is the least intensive (about 140 pores / mm^2) along bainite–bainite boundaries (new product of austenite decomposition). During pore development their coalescence occurs along the grain boundaries, they form a net, linear porosity, and also give rise to microcracks (see Figure 5).

It is established that most of the pores and microcracks initiate on the contact surface of coagulating

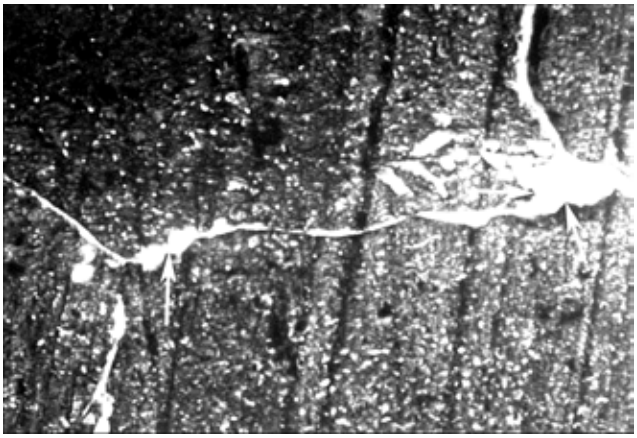

Figure 6. Pore formation in incomplete recrystallization section near coagulating $M_{23}C_6$ carbides (shown by arrows) (×4500)

precipitates of $M_{23}C_6$ (Figure 6) with boundaries of α-phase grains normal to the applied loads (or close to normal) (see Figure 5). Pore formation is largely dependent on the shape and dimensions of carbide precipitates, as well as their coherence with α-phase grains, which needs to be determined more precisely.

In the studied welded joints fatigue microcracks are detected, which initiated along the grain boundaries, in particular near coagulating $M_{23}C_6$ carbides, and which propagate normal to the working loads (see Figure 5). Such cracks cause transverse fracture of elongated $M_{23}C_6$ carbides.

Intensity of damageability by pores of the metal of incomplete recrystallization zone essentially depends on new products of austenite decomposition, controlling the rate of carbide reactions. It is also established that welded joint damageability can be reduced by producing in the structure of incomplete recrystallization zone the new products of austenite decomposition in the form of bainite, troostite or sorbite.

1. Khromchenko, F.A. (2002) *Life of welded joints of steam pipelines*. Moscow: Mashinostroenie.
2. Zemzin, V.N., Shron, R.Z. (1978) *Heat treatment and properties of welded joints*. Leningrad: Mashinostroenie.
3. Dmitrik, V.V., Tsaryuk, A.K., Bugaets, A.A. et al. (2006) Evaluation of remaining life of welded joints of pipelines for thermal power plants. *The Paton Welding J.*, **2**, 6–10.
4. Pigrova, G.D. (2003) Influence of long-term service on carbide phases in Cr--Mo–V steels. *Metallovedenie i Term. Obrab. Metallov*, **3**, 6–9.
5. Kiffer, R., Bonezovsky, F. (1968) *Solid materials*. Moscow: Metallurgiya.
6. Blanter, M.E. (1984) *Theory of heat treatment*. Moscow: Metallurgiya.
7. Gulyaev, A.P. (1978) *Metals science*. Moscow: Metallurgiya.
8. Mirkin, L.I. (1968) *Physical principles of strength and plasticity*. Moscow: MGU.
9. Rodriguez-Carvajal, J., Roisnel, T. (1998) FullProf.98 and WinP-LOTR: New Windows 95 / NT applications for diffraction. *Commission for powder diffraction: Int. Union on Crystallography Newsletter*, **5–8**, 159.
10. (1976) *Tables of physical values*: Refer. Book. Ed. by I.K. Kikoin. Moscow: Atomizdat.
11. Chuistov, K.V. (1985) *Ageing of metal alloys*. Kiev: Naukova Dumka.
12. Dmitrik, V.V., Bartash, S.N., Shelepov, I.G. (2007) On the features of damage of steam pipeline welded joints in creep conditions. *Energosberezhenie. Energetika. Energoaudit*, **3**, 78–184.
13. Berezina, T.G., Bugaj, N.V., Trunin, I.I. (1991) *Diagnostics and prediction of fatigue life of power units metal*. Kiev: Tekhnika.
14. Mints, I.I., Khodykina, L.E., Shulgina, N.G. et al. (1989) Study of fracture peculiarities in creep of Cr–Mo–V steels. *Metallovedenie i Term. Obrab. Metallov*, **7**, 33–36.

NON-DESTRUCTIVE TESTING

DETERMINATION OF CRACK DIMENSIONS IN WELDED JOINTS USING ULTRASONIC DIFFRACTION WAVES*

E.A. DAVYDOV

E.O. Paton Electric Welding Institute, NASU, Kiev, Ukraine

A feasibility of measurement of the height of crack-like discontinuities using diffraction of ultrasonic waves formed on the edges is considered.

Keywords: ultrasonic testing, change of discontinuity size

Traditional approach to ultrasonic flaw detection does not allow an accurate estimate of the dimension of crack-like discontinuities**. Therefore, it is impossible to perform a quantitative estimate of the criticality of the found defects using the calculation methods of fracture mechanics and the usually conducted analysis of the criticality of a discontinuity and prediction of further operation of the equipment (without repair) essentially is only of a qualitative nature. For sophisticated and critical equipment, the repair of which cannot be performed (it can only completely replaced), or involves great difficulties, such an approach leads to unjustified expenses or its unpredictable failure ---- accident. Therefore, safe operation of critical equipment requires quantitative analysis of the criticality of the detected discontinuities. This problem can be solved only if the precise geometrical dimensions of discontinuities are known. At present the problem of determination of the geometrical dimensions of discontinuities does not have a satisfactory solution, which is indirectly confirmed by absence of any normative documents (GOSTs, regulations, in-

*The paper is prepared by the results of fulfillment of purpose-oriented comprehensive program of the NAS of Ukraine «Problems of residual life and safe operation of structures, constructions and machines» (2004–2006).

**Davydov E.A., Troitsky V.A. (2002) Determination of the dimensions of internal discontinuities of metal structures by ultrasonic testing methods. In: Proc. of 5th National Sci.-Techn. Conf. «Nondestructive Testing and Technical Diagnostics» (Kiev), 23–36.

© E.A. DAVYDOV, 2008

structions, etc.), regulating assessment of the actual dimensions.

It is known that diffracted waves, formed on the sharp edges of the discontinuity, allow determination of the co-ordinates of these edges, and, therefore, also the dimensions of the discontinuity. Work of a number of researchers shows the good prospects of this research direction. On the other hand, there is no clear methodology of application of diffraction waves for assessment of the dimensions of discontinuities at ultrasonic nondestructive testing. Issues of precision limits of the method, optimization of ultrasonic circuit characteristics and some other have not studied.

Development of comprehensive, scientifically-grounded principles and methods of determination of the dimensions of crack-like discontinuities based on analysis of the diffraction fields allows improvement of the validity of the prediction (residual life) of reliable operation of critical equipment.

The purpose of the work is establishment of a scientifically-grounded base for determination of the dimensions of crack-like discontinuities (defects) using ultrasonic diffraction waves, suitable for practical application with the existing technology base of ultrasonic testing (UT). In order to achieve the defined objective, analysis of the complete acoustic circuit of the flaw detector and optimization of its parameters to achieve the greatest amplitude of the signal from ultrasonic waves diffracted from the crack edge, have been performed, as well as determination of the coordinate of the diffracted wave «source» and assessment of the result error (dependence of measurement error on the control schematics and methods of coordinate determination).

Technology of crack sizing. UT technology for determination of the height of crack-like discontinuities in welded joints was proposed on the basis of the performed research. The main technological sequence of control and the corresponding sequence of the received ultrasonic signals are given in Figures 1 and 2.

The schematic shown in Figure 1 allows measurement of the crack size by two methods.

1. If the diffracted wave can be received by the same transducer, which emits the initial wave, crack size by height ΔH is determined by the following formula:

$$\Delta H = H_2 - H_1, \tag{1}$$

where

$$H_1 = \sqrt{L_{12}^2 - \left[\frac{S^2 + L_{12}^2 - L_{11}^2}{2S}\right]^2}, \tag{2}$$

$$H_2 = \sqrt{L_{22}^2 - \left[\frac{S^2 + L_{22}^2 - L_{21}^2}{2S}\right]^2}, \tag{3}$$

$$L_{11} = C_L(t_{11} - \Delta t_1), \tag{4}$$

$$L_{12} = C_L(t_2 - t_{11} + \Delta t_1/2 - \Delta t_2/2), \tag{5}$$

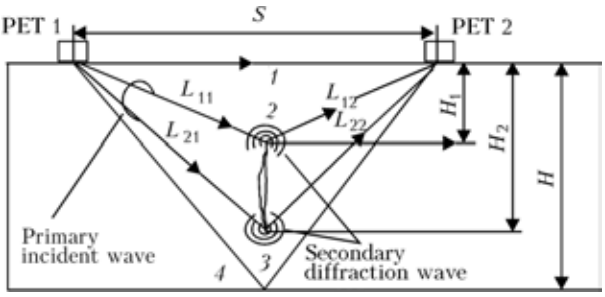

Figure 1. Schematic of crack sizing: *1* — head wave signal; *2, 3* — diffraction signals from the upper and lower crack edge, respectively; *4* — «backwall» reflection

$$L_{21} = C_L(t_{22} - \Delta t_1), \tag{6}$$

$$L_{22} = C_L(t_3 - t_{22} + \Delta t_1/2 - \Delta t_2/2), \tag{7}$$

where C_L is the longitudinal velocity of the ultrasonic wave in the material of control object; t_{11} is the time delay in propagation of the ultrasonic wave along the path of PET 1 — upper edge of the crack — PET 1; Δt_1, Δt_2 is the time delay of ultrasonic wave propagation in PET 1, PET 2, respectively; t_2 is the time delay of ultrasonic wave propagation along the path of PET 1 — upper edge of the crack — PET 2; t_{22} is the time delay of ultrasonic wave propagation along the path of PET 1 — crack lower edge — PET 1; t_3 is the time delay of ultrasonic wave propagation along the path of PET 1 — crack lower edge — PET 2.

2. If it is possible to perform transverse scanning (in the Figure plane) the center position of the transducers for the upper and lower edges (tip) of the crack separately is sought. The centered position corresponds to minimum value $t_{2\,\min}$ (or $t_{3\,\min}$), crack size by height ΔH is determined from formula $\Delta H = H_2 - H_1$, where according to designations in Figure 1

$$H_2 = \sqrt{\left(\frac{C_L}{2}(t_{3\,\min} - \Delta t_1/2)\right)^2 - \left(\frac{S}{2}\right)^2}, \tag{8}$$

$$H_1 = \sqrt{\left(\frac{C_L}{2}(t_{2\,\min} - \Delta t_1/2)\right)^2 - \left(\frac{S}{2}\right)^2}. \tag{9}$$

Determination of crack tip coordinates by the first realization is more difficult to implement in technical terms, because of decrease of the amplitude of diffracted wave emitted in the reverse direction. On the practical level of realization, this is related not only

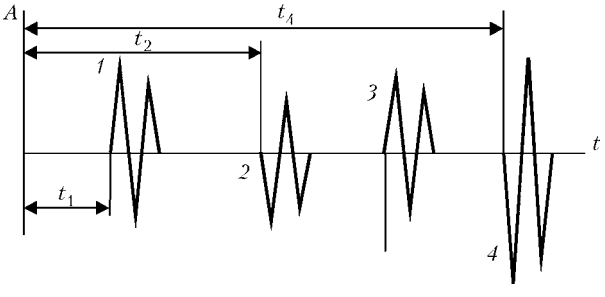

Figure 2. Pulse sequence by the schematic in Figure 1: *t* — time delay between emission and reception of signals from the respective ultrasonic waves

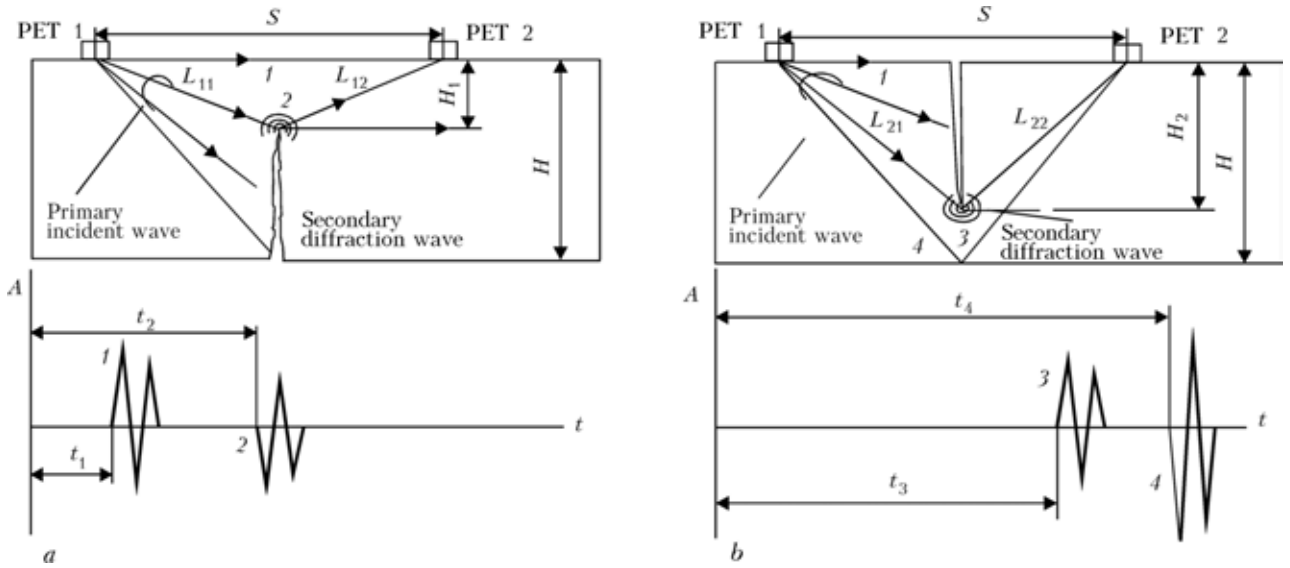

Figure 3. Schematic of sizing the crack coming to the surface of the object of control: *a*, *b* — for the lower and upper surfaces, respectively; *1–4* — same as in Figure 1

to the features of amplitude dependence, but also to the presence of reverberation noises in the combined transducer. Decrease of reverberation time is known to be a quite complicated task, and a reliable solution of this problem is possible only with application of combined transducers. Without dwelling on the advantages or disadvantages of this solution, let us note that application of combined transducers makes the requirements to the hardware somewhat more complicated. It is sufficient to note the fact that the traditional manual flaw detectors have just one receiving channel, which does not allow direct application of the available fleet of manual flaw detectors. Therefore, the second solution should be regarded as more rational for sizing the crack-like defects.

For the case when the crack reaches one of the surfaces of the object of control, the signal sequence is given in Figure 3. Attention should be given to signal phases, which differ by a half-period and, therefore, are an indication of where diffraction occurred — on the upper or lower edge of the crack. The latter is important for identification of signals from «hanging» cracks, as a correct correspondence of the phases is an indirect confirmation of the fact that these are signals from the crack, and they correspond to the upper and lower crack edge.

The proposed technology of sizing the crack-like discontinuities can be adapted to welded joints of a more complex shape. Schematics of measurements for the most widely used welded joint types shown in Figure 4, can be given as a example. Amplitude analysis is much more serious (among the given examples this concerns, primarily, the schematic given in Figure 3, *a*). In most of the cases this problem can be most easily solved experimentally on specific technological samples.

Verification of UT technology of discontinuity sizing. The procedure was tried out on welded joints

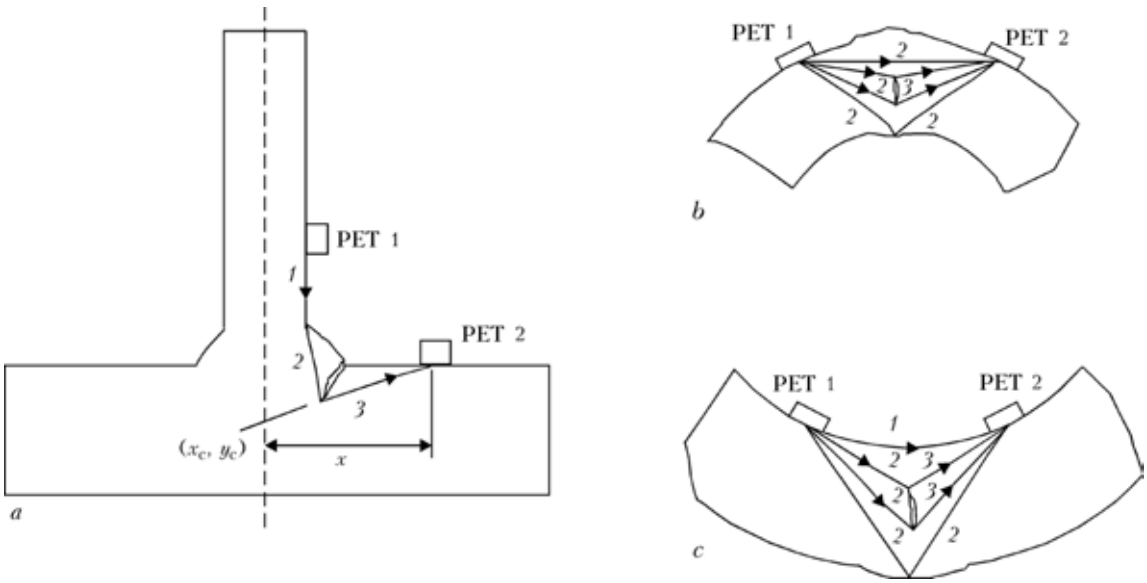

Figure 4. Examples of schematic variants for sizing of discontinuities in objects of a complex (non-flat) geometry (*a–c*): *1* — head (surface) wave; *2* — longitudinal; *3* — diffraction

Results of determination of the height of discontinuities in the welds of «Druzhba» oil pipeline, mm

Welded joint No.	No.	Pig	UT I (by the results of RII)	UT II («Orgtekhdiagnostika»)	UT II («Diascan»)	UT III (PWI) (diffraction waves)	Metallographic examination	Note
«Samara–Unecha» oil pipeline, «Nikolskoe–Stalnoj Kon» section								
195370	1	7.2	6	1–2		3.7	4	–
202810	2	10.8	0	1–2		4	4	Edge misalignment
202730	3	10.8	0	1–2		3		Same
202640	4	10.8	8	1–2		4	4.5	–
	5	8.9	0	1		3		Edge misalignment
195350	6	10.8	4	1–2		0	0	Features of weld section formation
	7	10.8	9	1–2		3	4	–
195340	8	10.8	5–6	1–2		2		–
	9	7.6	0	1		0		Edge misalignment
	10	7.3	4–5	1		1		–
95710	11	10.8	4–8	1–2		0		Welded joint 12 + 20 mm
95650	12	10.8	5–8	1–3		4	4.5	–
«Surgut–Polotsk» oil pipeline, «Lysva–Perm» section								
105670	13	6.6	Unstudied		5–3	3		–
107210	14	4.8	Same		7–4	0		5 mm edge misalignment
89490	15	7.6	0		0	0		Bulk discontinuity at the depth ≈ 7 mm
77410	16	9.6	Unstudied		0	4		3 mm edge misalignment
64930	17	10.8	12		7–1	4.5		–
	18	10.8	9		7.5–3.0	5.1		–
	19	10.8	Unstudied		Unstudied	5.9		–
	20	10.8	Same		Same	5		–
	21	10.8	»		»	4.7		–
	22	9	»		»	4.4		–
4720	23	12	10		9–7	8.5		Pipe thickness of 14 and 15 mm
12050	24	8.9	Unstudied		0	3		
12150	25	6.7	Same		0	4		
12210	26	5.6	»		8–6	5		
	27	7.9	»		0	5		

of the main pipeline «Druzhba». As a result of running a pig through the pipeline section, some welded joints were found to have cracks of inadmissible sizes, which were determined more accurately using the UT technology of discontinuity sizing.

In addition, an independent expert control was also conducted by specialists of «Orgtekhdiagnostika» («Skaruch» system, mechanized control to VSN 012–88), «Diascan» (USN 50 flaw detector, manual inspection to VSN 012–88), PII company (pig supplier,

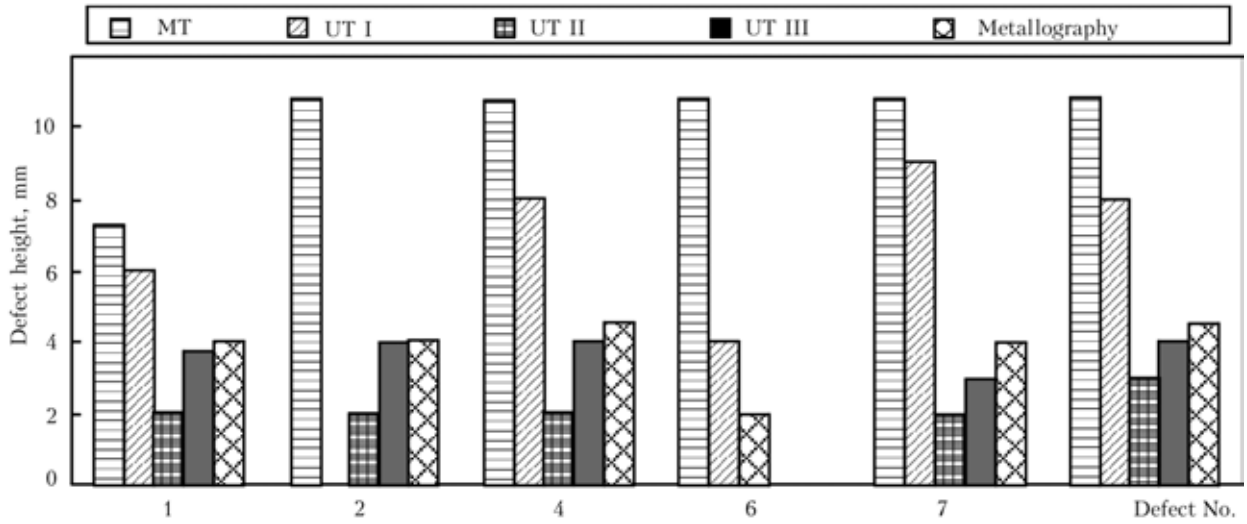

Figure 5. Comparison of the results of measurement of the height of defects by the methods of nondestructive testing and metallographic data

USL-38 flaw detector, manual control to a British standard).

The summary Table gives the results of all the measurements, made by different organizations. By the results of ultrasonic and magnetic inspection some welded joints were cut out for destructive testing, this allowing metallographic examinations to be performed.

Figure 5 gives the histogram of measurement results in comparison with the metallographic data (for welded joints of «Nikolskoe–Stalnoj Kon» section by the Table data).

Results of measurements obtained by different methods differ essentially from each other. Based on the given data it should be admitted that the errors in measurement of defect height by the amplitude methods can be up to hundred of percent. Measurement accuracy depends not only on the nature and features of the discontinuity, but also on the criteria of the procedure of height evaluation proper.

Average error by height of the defects found with the diffracted wave method is 0.4 mm, and the maximum error of height determination, by the data of metallography, is not more than 1 mm.

Thus, the performed package of work allows determination of the real geometric dimensions of crack-like discontinuities and assessment of the performed measurements using ultrasonic waves diffracted at the crack edge. Developed procedure allows rather simple assessment of the geometrical dimensions of crack-like discontinuities using the existing UT technological base and with an accuracy sufficient for practical purposes.

FROM HISTORY OF WELDING

TRANSITION TO INTEGRATED DEVELOPMENT OF WELDING PRODUCTION

A.N. KORNIENKO[1] and **A.P. LITVINOV**[2]
[1]E.O. Paton Electric Welding Institute, NASU, Kiev, Ukraine
[2]Priazovsky State Technical University, Mariupol, Ukraine

Creation of an integrated program of welding production development by the initiative of Evgeny O. Paton in 1930–1932 is considered. Foundation of a research institution with the structure providing realization of scientific-and-technical ideas into specific technologies and equipment, as well as their commercial application, is described. Brief review of the priority science-intensive developments of the Electric Welding Institute, performed under the leadership of E.O. Paton, is given.

Keywords: welding production, arc welding, automatic welding, integrated development, fundamental researches, bridge engineering, history of engineering

Welding started to intensively oust rivet and bolt joints during the first decades of the XX century in manufacturing of metal constructions. Welding had obvious advantages over riveting, yet the metal quality at that was not stable. Wide introduction of welding into industry was particularly urgent for the USSR as technical revolution and industrialization of production dictated the necessity of metal economy and increasing the assembling and welding operation efficiency. Welding equipment was bought abroad and urgent measures were taken on local equipment manufacturing, for which purpose personnel training was organized, specialized design and branch research organizations were created. However, the research and design, carried out in these organizations and in the chairs of higher education institutes, were aimed only at solution of individual tasks of welding production. Neither in the USSR, nor abroad there were no institutions that could consolidate and solve the whole complex of problems, appearing in the path of further development of welding.

In 1929, Evgeny O. Paton, a well-known bridge builder, organized the Electric Welding Laboratory in the system of All-Ukrainian Academy of Sciences (AUAS) at the Chair of Engineering Constructions. It should be noted that E.O. Paton, as a specialist in the field of metal structures and bridge builder, knew all the disadvantages of rivet joints [1, 2] and understood that welding would open the new trends in designing and building the engineering structures. The scientist deployed research of welding structures workability under the influence of static and dynamic loads, developed rational types of welded structures, provided assistance in construction design and welding introduction at the enterprises. More than 60 articles [3–6] were published by E.O. Paton and his colleagues during the 1930s. Some of these works were published in the American Welding Society Journal [7, 8]. Monograph on designing welded structures [9] was published in 1933. At the same time E.O. Paton was involved in organizational issues: in autumn 1930 he set up the Electric Welding Committee that can be considered as a prototype of inter-branch center of research coordination and assistance in implementation [10]. In 1931 he set one more task — to automate the welding process, and started to form the design unit.

In 1932 E.O. Paton elaborated the program of integrated welding production development for the first time in the world. As far back as two decades before as he started working on welding, specialists from different countries tried to coordinate their efforts to solve the problems of new welding process development within the framework of societies, associations, companies, etc. However, the participants of such voluntary associations (American Welding Society [11], All-Union Scientific Engineering Welders Society [12], German Welding Society [13], etc.) worked in their laboratories and at the chairs independently on comparatively narrow problems (within the framework of their interests and possibilities), often ignoring even the related problems. The members of the societies met from time to time and shared the obtained results. Equipment and technology development taking the results to the industrial implementation stages progressed very slowly. General Electric Company, where research laboratory and design team [14, 15] were organized by E. Tomson, can be named among the few exceptions. E.O. Paton realized that solution of such a complicated range of scientific-technical problems that were encountered in the path of welding production development, requires participation of metallurgists, electrical engineers, mechanical-designers, specialists of some branches of engineering and would be the most effective under single person leadership in the frame of one

© A.N. KORNIENKO and A.P. LITVINOV, 2008

organization with all the necessary subdivisions. The results of scientific studies should become the basis for technological and design developments that would accelerate the new technologies application in production.

From the beginning of 1932 discussion of the research subjects for the next five-year plan of the USSR national economy development was started at AUAS. In-situ sessions were held in Kharkov and Donbass. E.O. Paton made reports in these meetings, in which he gave an analysis of the country's demand for welding equipment and a prediction of the volumes of welded products [16–18]. Evgeny Paton stated: «The main problem of electric welding in the 2nd Five-Year Plan Period is as complete as possible mechanization of the welding process. This measure will yield a big saving of welding equipment, time and labor force... It follows from here that development of automatic machines should be placed on the agenda in our country. We cannot rely on imported automatic machines, it is necessary to develop the Soviet ones ...» [18, p. 7].

In November 1932, the Ukr. SSR Government allocated funds for development of the Electric Welding Laboratory [19], and on February 2, 1933, AUAS Presidium passed a Resolution on transformation of the Electric Welding Laboratory into the Electric Welding Institute (EWI) [20]. E.O. Paton was appointed the director and scientific leader of the Institute [21]. The Government of the Ukr. SSR approved this Resolution on January 3, 1934 [22]. Evgeny Paton continued realizing the idea of a total integration of scientific research, technological developments, design, and manufacturing of pre-production models of equipment and participation in implementation of institute's works, this time within the frame of the Institute. EWI structure was formed in accordance with these tasks. Specialists of different scientific directions were selected. E.O. Paton organized the Welding Department at the Kiev Polytechnic Institute for training engineers of welding production in 1936. Considering that transformers are cheaper and simpler than generators in operation, E.O. Paton chose alternating current as the direction of arc welding development [23]. The group of technologists and designers managed to master automatic welding head and develop a coating with high stabilizing properties (with titanium dioxide) in a short time, and also find a method of welding current supply to the electrode wire. The first introduction of automatic welding took place at Bezhetsk Wagon Works «Krasny Profintern» for fifty ton tanks manufacturing, the designs of all the equipment for the production line being developed at EWI [23].

The Conference on automatic welding was called in Kiev in spring 1936 by E.O. Paton initiative. Special attention at the Conference solutions was paid to comprehensive study of the problems by EWI that were connected to arc welding automation. Six sites were selected for automatic welding implementation. The Peoples' Commissariat of Heavy Industry Order # 860 on automatic welding development dated May 23, 1936 was favorable for welding production progress, in which it was noted that «... the advances of the Electric Welding Institute of the Academy of Sciences of the Ukr. SSR at comprehensive solution of the task of electric arc welding automation (designing the automatic head, electrode study, development of coated electrode manufacturing method, designing machine tools for automatic machines)...», and thanks were extended to E.O. Paton and P.P. Bushtedt. It was noted in the Order: «To request the Academy of Sciences of the Ukr. SSR to organize at the Institute a permanent design and consulting office on the matters of welding automation with the aim of providing the technical assistance to the interested plants of the Ukr. SSR by the Electric Welding Institute at automation of welding processes» [24]. Thus, one more necessary element –– the implementation department for carrying out the continuous work cycle (from research to implementation of new equipment) appeared in EWI structure in 1937.

Submerged-arc welding by nonconsumable (carbon) electrode of low-carbon steels of up to 18 mm thickness was developed under the direction of E.O. Paton in 1938–1939. The technology and equipment were introduced for welding flat-car beams at Bezhetsk Wagon Works. N.G. Slavyanov [25] already used flux for shielding the weld pool, however this task was not solved for the device that moves during welding. A number of foreign companies and organizations in the USSR actively worked on designing the mechanisms for feeding the wire and creating of new means of shielding during the first decade of the XX century. Welding methods with paper wire braiding, with flux «pressing» into slots during wire feeding, a method of shielding by a layer of sawdust, etc. were patented. An acceptable quality of the weld and efficiency of welding operations were achieved by employees of Linde Company, USA, who developed the composition of granulated flux for welding steels and the technique of submerged-arc automatic welding with consumable electrode [23, 26].

EWI staff consolidating the success achieved in mechanization and automation of arc welding processes, managed to independently complete the solution of all tasks connected with consumable electrode submerged-arc welding application [27]. The first local fused flux (AN-1), electrode wire compositions, original designs of welding head and welding transformers were developed. The results of exploratory research package were generalized by E.O. Paton in the first monograph about submerged-arc welding in the world literature, published in 1940 [28]. The monograph set forth the basic principles of a new scientific direction –– welding metals science. In June 1940 submerged-arc welding of structural steel sheets of more than 10 mm thickness with 30 m / h speed was demonstrated to the participants of All Union Conference on automatic welding. The new welding method

turned out to be 11 times more efficient than manual welding. Such tempo of the new method and equipment design became possible due to an efficient organization of research and design work that was consistently conducted by E.O. Paton.

Resolution of USSR Sovnarkom and TsK VKP(b) about introduction of automatic submerged-arc welding at 20 major plants of the country in a six month term was issued on December 20, 1940. E.O. Paton was appointed member of the Council on Machine-Building at USSR SNK; he was entrusted with controlling the fulfillment of this Resolution [26]. Evgeny Oskarovich Paton, heading large-scale organizational and research works, visited the plants, where EWI instructors provided not only automatic welding introduction but also the feedback from the plants to the Institute.

Paton's principle of organization of new technology development was subjected to severe examination during the years of the Great Patriotic war. EWI staff under the leadership of E.O. Paton managed to overcome successfully all the difficulties in the path of creation of automatic welding of armored steels and its implementation into production of tanks and other armored technique under difficult conditions in the Urals (Nizhny Tagil). The reasons of weld cracking were established, technologies of welding without defects and fluxes from local raw materials were developed, original automatic welding heads with a constant electrode feed rate and control systems, and production lines were designed [29]. B.E. Paton and A.M. Makara studied the nature of the process that takes place in the submerged-arc welding zone and experimentally proved the presence of the arc discharge for the first time in the world [30]. The experience and results of scientific research, design, technology development and implementation served as a base for creation of new welding processes. Considerable success in development of multiarc and multielectrode submerged-arc welding processes was achieved and the first welding semi-automatic machines were designed already by the middle of 1940s [31].

Focusing on automation of submerged-arc welding as the main problem of the end of 1940s, E.O. Paton extended the technology and design development of new metal joining and raising the welding speed with the aim to introduce this method into new branches of industry. The principle of comprehensive solutions was manifested completely when designing fundamentally new assembling-welding automatic machine tools for manufacturing tubs, miners' lamps, riser pipes of mine supports, etc. Automated line production of large diameter pipes by high-speed two and three arc welding was started at several plants of our country.

Method of large-sized tanks manufacturing from panels which were welded by submerged-arc automatic machines in the workshops, then rolled into transportable coils and unrolled at the site was developed at the Institute for the first time in the world. Creation of devices and technologies of making vertical, horizontal and overhead welds was one more milestone in the history of automatic submerged-arc welding. Thus, the task of full-scale submerged-arc welding application at construction of large-scale industrial facilities (blast furnaces, gasholders, pipelines) and buildings was solved [32]. It should be noted that in 1945 EWI was given the name of its founder –– E.O. Paton –– for great achievements in the field of comprehensive development of welding production.

Theoretical problems also emerged at that time without studying which the scientifically grounded technologies and new welding equipment could no longer be developed quickly and confidently. At the end of 1940s–beginning of 1950s more detailed models of consumable electrode welding process were suggested, the reasons of porosity in welds and cracks in the joints were determined [33]. Intensive development of welding metals science that emerged from welding metallurgy into an independent direction already at the stage of investigation of the structure of weld metal and HAZ of armored steels joints [34] was going on in 1941–1945. The quench hypothesis of crack formation in the joints was developed at the same time [34]. As a result of comprehensive studies scientifically-grounded requirements were worked out to chemical composition of steel and the method of its killing that in conjunction with the requirements to the composition of consumable electrode and the flux allowed guaranteeing the required performance of welded joints at low temperatures. Development of steel for welded structures was one of the results of such investigations [35]. Study of heating processes and electrode melting in automatic welding began already in the war time [36], as well as of electric parameters of welding [37], allowed defining the principles of automatic regulation of the welding process by power source [38] and led to creation of a new class of equipment.

In the second half of 1940s the scientific search, investigation and development in the sphere of welding fabrication were carried out on 35 topics that were a kind of prototype of the future integrated target programs oriented to solution of major practical problems. Development of the technology of all-welded bridge construction with application of automatic welding in site was one of the aims of such investigations. At fundamental study of any problem, Evgeny Paton was always guided by the principle according to which the front of studies was deployed much wider than the initial problem demanded. The principle of comprehensive performance of research, technological and engineering developments and pilot testing was used by E.O. Paton to a full degree during design and construction of the bridge across the Dnieper in Kiev. Mounting of the bridge of about 10,000 ton mass and 1543 m length consisting of 26 spans was completed in autumn 1953.

One of the most important components of the integrated program of welding production development,

promoted by E.O. Paton, was the fulfillment of basic theoretical and experimental investigations required for further applied engineering developments. Such organization of scientific work that combined a fundamental depth with clear purposefulness was of pioneering nature for an Institute of an academic profile [39]. The E.O. Paton EWI took the lead over all the other local and foreign organizations as to the wide range of directions of welding production development.

Thus, in 1932 E.O. Paton put forward an idea of comprehensive development of welding problems, including metallurgical, metals science, electrical engineering and many other aspects, and created a specialized research institution, where it is possible to solve independently all the problems arising in the path of welding production development and with such a structure, which provides quick realization of the whole work cycle –– from the scientific-technical idea to development and implementation of technologies and equipment. The Institute foundation was approved by AUAS Presidium in 1933, and on January 3, 1934 the official status of Electric Welding Institute was recognized by governmental resolution.

In 1930–1940s highly-productive equipment and local technologies of submerged-arc automatic welding and rational welded structures were developed for the first time in the shortest term at EWI consisting of research and design subdivisions, workshops and a team of instructors under the direction of E.O. Paton. The Institute developments allowed organizing manufacture in production lines, applying conveyor assembling and fast stack mounting with a high level of mechanization and automation of technological operations.

In 1940–1950s theoretical and experimental researches, without the results of which it was already impossible to create high technologies and new welding equipment, were deployed at a new level. A research method of a principally new level emerged, namely purposeful fundamental research. The principle of comprehensive performance of research, technological and design developments, experimental verifications and quality control was used by E.O. Paton in full when organizing the design and construction of the bridge over the Dnieper in Kiev.

1. Paton, E.O. (1905) To the problem of weakening of sheets by rivets. *Zhurnal Min. Putej Soobshcheniya*, Book 3, 143–156.
2. Paton, E.O., Kozlovsky, N.I. (1930) *Experimental comparison of electric welding and riveted fastenings of longitudinal beams to transverse beams*. Moscow: Transpechat NKPS.
3. Paton, E.O., Dyatlov, A.V. (1930) *Impact testing of electric welded and riveted beams*. Moscow: Transpechat NKPS.
4. Paton, E.O., Petrov, M.V. (1931) *Search for a rational type of electric welded trussed girders: Experimental studies*. Kiev: Electric Welding Committee.
5. Paton, E.O., Shevernitsky, V.V. (1934) *Transactions in the field of electric welded structures*. Kiev: VUAN.
6. Paton, E.O. (1935) Bridge supports of welded type. In: *Coll. on Metal Structures*. Moscow.
7. Paton, E.O. (1944) Effect of high welding current intensity on shrinkage. *Welding J.*, **1**, 60–62.
8. Paton, E.O., Gorbounov, B.M., Berstein, D.O. (1944) Behavior of residual stresses under external load and their effect on strength of welded structures. *Ibid.*, **9**, 473–480.
9. Paton, E.O., Gorbunov, B.N. (1933) *Calculation and design of electric welded structures in industrial engineering*. Moscow; Leningrad: Gosstrojizdat.
10. (1930) *Journals of Presidium of AUAS of 1930* (Central Sci. Archives of NAS of Ukraine, b. 1, inv. 1, p. 108).
11. Kornienko, A.N. (2004) Conford Every Adams and American Welding Society. *Svarshchik*, **3**, 35.
12. Kornienko, A.N. (1989) History of welding (problems and propositions). *Svarochn. Proizvodstvo*, **10**, 47–78.
13. Kornienko, A.N. (2004) At the origins of cooperation between German and national specialists in field of welding (1920–1930s of XX century). In: *Investigations of the history of enigneering*. Kiev: NTUU «KPI».
14. Kornienko, A.N. (2001) Elihew Tomson. *Svarshchik*, **3**, 38.
15. Kornienko, A.N. (2002) Irving Langmuir and atomic-hydrogen welding. *Ibid.*, **3**, 47.
16. Paton, E.O. (1932) *Paths of development of electric welding in the Second Five-Year Plan*. Kharkov: Mashbudvydav.
17. Paton, E.O. (1932) *Paths of development of electric welding in the Second Five-Year Plan Period*. Kharkiv: Mashbudvydav.
18. Paton, E.O. (1932) Paths of development of electric welding in the Second Five-Year Plan Period. *Avtogen. Rabotnik*, **1 / 2**, 7–16.
19. (1933) *Journalss of the Presidium of AUAS* (Central Sci. Archives of NAS of Ukraine, b. 1, inv. 1, p. 58).
20. *Ibid.*, p. 3.
21. *Ibid.*, p. 7.
22. *Personal history of E.O. Paton* (Central Sci. Archives of NAS of Ukraine, b. 1, inv. 1, p. 350).
23. Matijko, M.M. (1960) *Development of electric arc welding in Ukraine*. Kiev: AN Ukr. SSR.
24. (1936) Order of People's Commissariat of heavy industry on development of automatic welding # 869 of May 23, 1936. *Avtogen. Delo*, **7**, 42–43.
25. Paton, B.E. (1955) State-of-the-art of automatic submerged-arc welding –– results of development of N.G. Slavyanov's ideas. In: *Proc. of Sci.-Techn. Conf. of Welders Dedicated to 100th Anniversary of N.G. Slavyanov*. Kiev: Mashgiz.
26. Chekanov, A.A. (1963) *History of automatic electric arc welding*. Moscow: AN SSSR.
27. Paton, E.O. (1951) *On the priority of Soviet science and engineering in the field of submerged-arc welding*. Kiev.
28. Paton, E.O. (1940) *Bare electrode automatic submerged-arc welding*. Kharkov: Kharkov Techn. House.
29. Paton, B.E. (1945) Development of automatic submerged-arc welding during the war years. *Elektrichestvo*, **3**, 3–5.
30. Paton, B.E., Makara, A.M. (1944) *Experimental study of automatic submerged-arc welding process*. Kiev: EWI.
31. Paton, E.O. (1950) Development of automatic submerged-arc welding during 10 years (1940–1950). *Avtogen. Delo*, **2**, 1–3.
32. Kornienko, O.M., Litvinov, O.P. (2005) Peculiarities of development of scientific principles and applications of welding in Ukr. SSSR from 1945 up to the middle of 1950 years. *Narysy z Istorii Pryrodoznavstva i Tekhniky*, **45**, 123–131.
33. Frumin, I.I., Kirdo, I.V., Podgaetsky, V.V. (1949) Pore formation in welds and influence of flux composition on pore susceptibility. *Ibid.*, **10**, 1–11.
34. Makara, A.M., Medovar, B.I. (1948) On the nature of initial solidification of the weld pool. *Ibid.*, **12**, 25–27.
35. Paton, E.O., Shevernitsky, V.V. (1949) Steel for welded bridges. *Ibid.*, **6**, 3–7.
36. Paton, B.E. (1948) Study of electrode heating process in automatic submerged-arc welding. In: *Transact. of the E.O. Paton Electric Welding Institute*, **3**, 17–23.
37. Paton, B.E. (1944) Electrode melting process in automatic submerged-arc welding. In: *Transact. on Automatic Submerged-Arc Welding*, 22–38.
38. Paton, B.E., Lebedev, V.K. (1948) Automatic control of welding arc power. *Ibid.*, **1**, 260–281.
39. Paton, B.E. (1980) Science-engineering-production. *Voprosy Filosofii*, **10**, 22–31.

REDUCTION OF EVACUATION TIME OF LARGE-SIZED VACUUM CHAMBERS OF ELECTRON BEAM WELDING INSTALLATIONS

O.K. NAZARENKO
E.O. Paton Electric Welding Institute, NASU, Kiev, Ukraine

Results of evacuation of the UL-132 commercial installation large-sized vacuum chamber of 20 m^3 volume without application and with application of a system for freezing out water vapors are presented. It is found that time for evacuation of the vacuum chamber down to vacuum $2.66 \cdot 10^{-4}$ Pa ($2 \cdot 10^{-4}$ mm Hg) in case of freezing out of water vapors reduces 2 times (from 40 to 20 min).

Keywords: electron beam welding, evacuation, large-sized vacuum chambers, working vacuum, freezing out of water vapors

In recent years requirements to the evacuation time of large-sized vacuum chambers of electron beam welding installations got more stringent for the purpose of increasing number of working cycles per a shift. So, for example, time for achievement of working vacuum $2.66 \cdot 10^{-2}$ MPa ($2 \cdot 10^{-4}$ mm Hg) in the vacuum chamber of 20–30 m^3 volume usually should not exceed 20 min. It is known that exactly presence of water vapors in the air medium, which is removed in the course of evacuation of a chamber, significantly reduces evacuation process, because water vapors are condensed on walls of a chamber and its mechanisms. At vacuum 1 Pa (1.33^{-2} mm Hg) water vapors constitute from 65 to 95 % of the residual gas. Water vapor may form from 50 to 100 monolayers on all internal surfaces of the volume being evacuated. A significant time is needed for molecules of vapor to be torn from a solid surface and become free gas, which is then evacuated by a high-vacuum pump. Possibility of preliminary removal of water vapors by scavenging of a vacuum chamber by hot dry air for the meantime is not commercially implemented.

It is known* that for freezing out water vapor it is sufficient to use cryocoils, cooled down to the temperatures close to –100 °C. At temperature –109.1 °C partial pressure of water vapors does not exceed $2.66 \cdot 10^3$ Pa ($2 \cdot 10^{-5}$ mm Hg). A cryocoil, made from a smooth copper pipe, has optimal ratio of surface and mass, which allows ensuring quick cycle of its functioning. In process of cooling a blended cooling agent, flowing through the coil, evaporates at the temperature +90 – –150 °C. Time of a standard coil cooling from 25 to –110 °C is not more than 2 min. Practically, for equivalently quick warming hot gas, preliminarily cleaned of oil, is fed from the delivery line directly into the said coil. A freezing out system, equipped with interface for connection to a general computer control system, is added to the traditional vacuum evacuation unit of the installation without any change of the latter.

In Figure 1 general view of the cryocoil, mounted on rear wall of the KL-132 installation vacuum chamber of about 20 m^3 volume, is presented.

Figure 1. General view of cryocoil mounted on rear wall of vacuum chamber of KL-132 installation (below to the right is «cold inlet» into vacuum chamber)

One can see from Figure 2 that beginning from the instant of the freezing out system turn on, which corresponds approximately to vacuum 1 Pa (1.33^{-2} mm Hg),

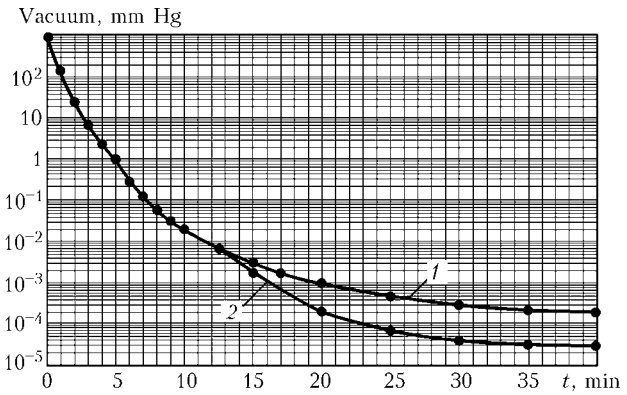

Figure 2. Time dependence of rarefaction degree of KL-132 installation vacuum chamber of about 20 m^3 volume, achieved without (*1*) and with (*2*) freezing out of water vapors

*Nesterov S.B., Podchernyaev O.N., Yudin B.V. et al. (2003) High-vacuum commercial cryogenic pumps. In: Proc. of 6th Int. Conference on Vacuum Technologies and Equipment (Kharkov, April 21–16, 2003). Kharkov: NNTs KhFTI, 231–237.

© O.K. NAZARENKO, 2008

rate of rarefaction significantly increases, and vacuum $2.66 \cdot 10^{-2}$ MPa ($2 \cdot 10^{-4}$ mm Hg) is achieved within 20 min, while when the freezing out system is turned off only within 40 min, i.e. 2 times longer.

In addition to reduction of the evacuation time, freezing out of water vapors reduces probability of moisture getting into the gap of the edges being welded, which prevents occurrence of small pores in a weld in case of welding of titanium alloys.

We have already implemented freezing out of water vapors in two commercial installations for electron beam welding.

120 kV/6 kW ELECTRON BEAM SYSTEM: GUN + POWER SOURCE + CONTROL SYSTEM

System design

- Electron beam gun with turbomolecular pump.
- X-ray shield for stationary gun version.
- Low-voltage power cabinet.
- High-voltage tank with high-voltage transformer and rectifier.
- High-voltage tank with electron tube break down protector and stabiliser.
- Control cabinet.
- Control console.
- Secondary electron visualization system of VCU type.

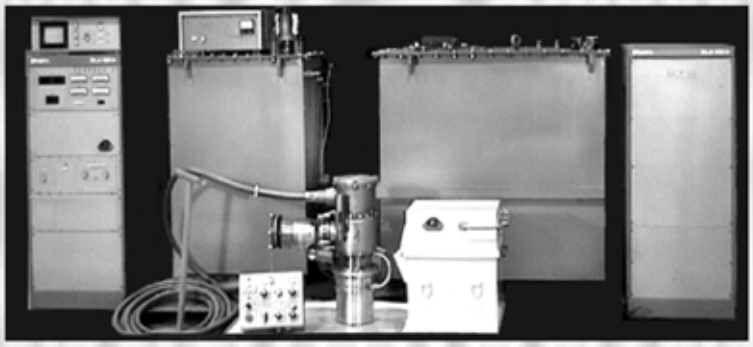

The EB gun permits welding in continuous and pulse modes; it may be used inside a vacuum chamber in any position. As the gun has a small mass, it may be installed on a robot-type manipulator.

The triode electron-optical system provides smooth adjustment of beam power. Cathode replacement takes only 10 min.

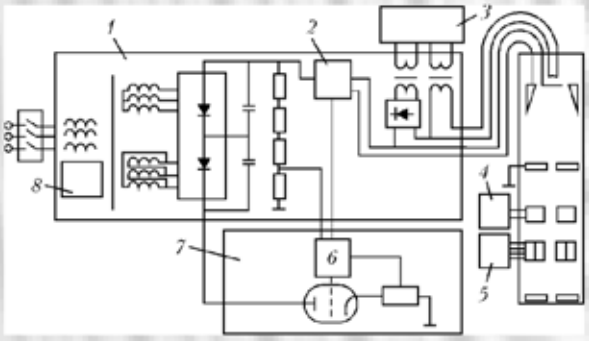

Electric circuit diagram: *1* — high-voltage source; *2* — welding current stabilizer; *3* — bombardment current stabilizer; *4* — focus current stabilizer; *5* — beam deflection current source; *6* — accelerating voltage stabilizer; *7* — control tube unit; *8* — current limiter

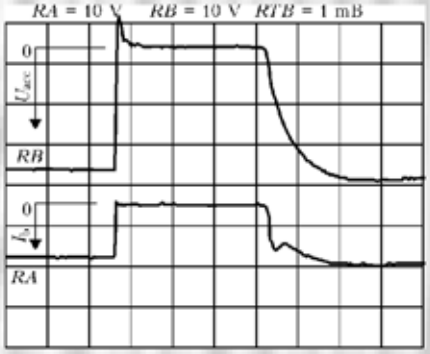

Oscillogram of the real discharge in the electron gun: U_{acc} — accelerating voltage; I_b — beam current

High quality welds and reliable performance are provided by the high-voltage unit, where a special electron tube in the high-voltage circuit enables preventing spark discharges from transition into arc discharges; ensuring quick response of the stabilizer, high stability, small ripple and possibility of pulse modulation; eliminating weld defects caused by gun discharges.

Contacts: Prof. Nazarenko O.K.
E-mail: nazarenko@technobeam.com.ua

NEWS

EQUIPMENT AND TECHNOLOGY FOR HIGH-FREQUENCY MECHANICAL PEENING OF WELDED JOINTS

The E.O. Paton Electric Welding Institute developed technology and equipment for hardening high-frequency mechanical peening (HFMP) of welded joints, which is further development of the technologies of surface plastic deformation of metals and is used for improving service characteristics of welded joints of the structures of various designation and, first of all, for increasing their resistance to fatigue. Surface plastic deformation of a metal in HFMP is achieved due to mechanical pulsed action of impact elements of a manual tool, excited by an ultrasonic generator. For hardening of welded joints for the purpose of increasing resistance to fatigue in HFMP only zone of the weld fusion with the base metal of 4–7 mm width is subjected to plastic deformation.

HFMP of fusion zone of the joints, carried out according to the recommendations, causes:

- formation of a characteristic groove of up to 0.5 mm depth, formation of which removes sharp undercuts along the weld and reduces coefficient of stress concentration, stipulated by geometry of a welded joint;
- strain hardening of the plastically strained metal;
- formation of residual compression stresses in near-surface layers of the cold-worked metal at the depth up to 1 mm;
- change of the metal structure of this zone up to the fine-grain one.

Depending upon mechanical properties of the metal, type of a welded joint, characteristics of the alternate loading cycle and level of residual welding

stresses, HFMP increases cyclic working life of joints 7–10 times, and unlimited ultimate fatigue strength by 30–200 %.

Ultrasonic installation for performance of HFMP consists of the following main parts: a power source and an ultrasonic generator *1*, a manual impact tool with a piezoceramic converter *2*, and a demountable head with different number of block heads *3*.

In comparison with other methods of surface plastic deformation of welded joints, HFMP is characterized by high productivity and cost effectiveness; compactness and mobility of the equipment; insignificant area of treatment (zone of transition from the weld metal to the base metal); possibility of treatment in any spatial position; possibility of the treatment efficiency forecasting; it is used at the stages of production and operation of the structures.

DEMONSTRATION HALL OF WELDING EQUIPMENT NOVELTIES

The «Shtorm-ITS» company (Ekaterinburg, Russia) opened hall for demonstration of the welding equipment novelties and the most claimed models of imported welding equipment of high-tech class, which recommended themselves well on Russian market.

«Shtorm-ITS» is one of the leading companies in Urals region, which is engaged in complex deliveries of equipment for welding and cutting and its adjustment and warranty and post-warranty servicing.

An experienced welding instructor will demonstrate equipment, which represents interest for a customer, in operation and carry out experimental welding and cutting works on specimens of a customer.

The following equipment is demonstrated in the demonstration hall:

- wide nomenclature of mechanisms for movement of torches of welding semi-automatic machines of the «Noboruder» series. This equipment is a means for

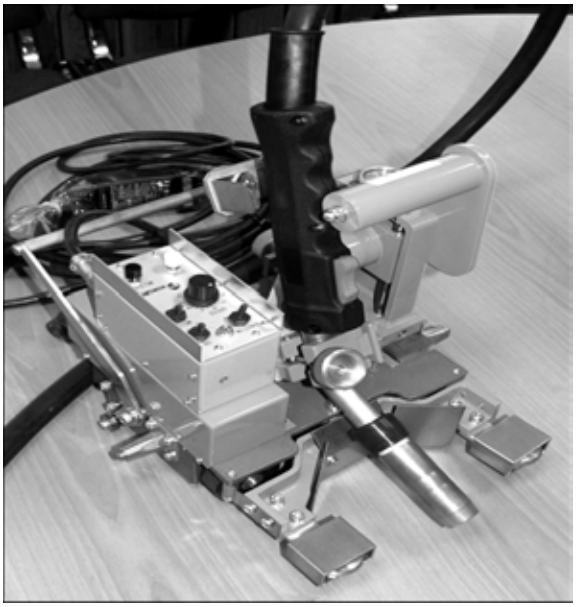

Figure 1

mechanization of the semi-automatic welding process; it is used for fulfillment of welds in different spatial positions. It allows getting high and stable quality of a weld with significantly lower labor input than in a manual method (Figure 1);

• state-of-the-art inverter welding machines for manual arc, semi-automatic, argon-arc and plasma welding with digital processing of data (produced in Germany). Ergonomic design and simplicity in operation of this equipment allow producing quality welded joints even by a welder of low qualification (Figure 2);

Figure 2

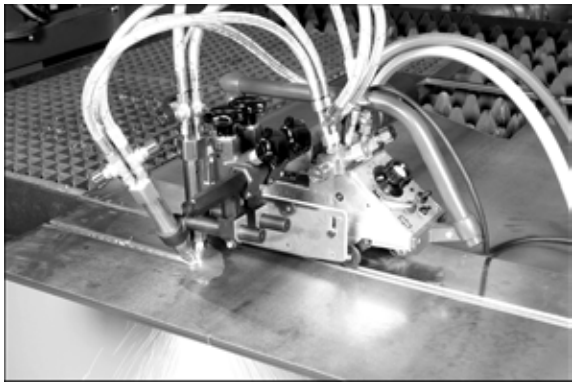

Figure 3

• the whole assortment of gas equipment «Messer» ---- from reducers and cutters to small-size machines for thermal cutting. This equipment recommended itself as quality, extremely simple in operation, reliable, and long-lasting one (Figure 3);

• welding rotators, means for individual protection of visual and respiratory organs of a welder, and filtering-ventilation equipment for removal of welding fumes from the welding zone (Figure 4).

Opening of the demonstration hall in Ekaterinburg allowed improving quality of work of «Shtorm-ITS» with customers and making new high-tech equipment more accessible for demonstration and approbation.

Figure 4

There is no need anymore to wait till next meeting at the exhibition; doors of the demonstration hall are always open for those wishing to be convinced in practice in quality of the supplied equipment!

FLAW DETECTION OF METAL PRODUCTS AT TEMPERATURE ABOVE 900 °C

In the E.O. Paton EWI DB experimental check of possibility of flaw detection of a metal at the temperature above 900 °C by means of laser acoustic-magnetic method was carried out. The check was performed on two specimens with artificial and natural defects. First specimen represented a steel parallelepiped of $80 \times 100 \times 320$ mm size with a treated surface and applied artificial defect in the form of a rectangular groove of $1 \times 1 \times 30$ mm size. Second specimen represented a fragment of $54 \times 220 \times 240$ mm size of a continuously cast slab of a rectangular section with a natural defect. Preliminarily presence of a natural defect was confirmed by the magnetic-powder method. The defect represented a crack in a near-rib zone in a recess of a surface of a wavy relief (a wavy profile is formed due to swinging of a mould during casting).

The specimens were heated up to temperature 1000 °C and installed on a flaw detection stand, on which scanning of surface of the specimens was performed by the sensor of the acoustic-magnetic flaw detector. Air gap between surface of the sensor and scanned surface of the specimens was not less than 10 mm.

Signals from artificial and natural defects were registered at the signal / noise ratio not less than 20 dB. On basis of the experimental check results application of laser acoustic-magnetic method for on-line flaw detection of solid metal at outlet from continuous steel casting unit was recommended.

SIMONA — NEW SYSTEM FOR MONITORING OF STRESS-STRAIN STATE OF MAIN PIPELINES AND VESSELS UNDER PRESSURE

The system, developed by «NPF Diagnostika» Ltd. (Minsk) and Institute of Applied Physics of the NAS of Belarus, is designed for registration, collection, transfer, real-time indication, and storage of multisensor information about change in the process of operation of local strains and stresses in elements of vessels under pressure, loaded metal structures of gas-compressor stations and main pipelines and other structures.

Original strain-measuring sensors are based on principle of frequency change of own oscillations of a string depending upon its tension. The interfacing unit controls over communication line reading of information from a group of sensors and its transfer to the dispatcher terminal. From a group of the interfacing units, located in the control-measurement columns, local deformation data in the places, where the sensors are installed, are fed to the dispatcher terminal, where they are analyzed.

On basis of fed to the terminal data judgment is made about possibility of occurrence in elements of the structures of critical strains and stresses because

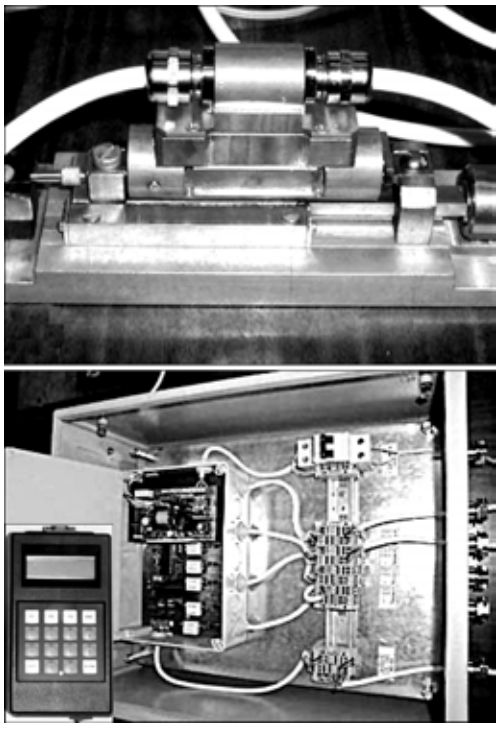

of motion of soil, corrosion losses of the metal, inadmissible development of cracks, occurrence of peak over loads, etc.

In contrast to existing systems of stress-strain state control, SIMONA ensures continuous monitoring of state of the structure within the whole cycle of its operation.

«INTROSCAN-M» — ANALYZER OF STRESSES AND STRUCTURE OF FERROMAGNETIC MATERIALS

«NPF Diagnostika» Ltd. and Institute of Applied Physics of the NAS of Belarus (Minsk) developed instrument INTROSCAN on basis of application of Barkhausen effect. It is the forth generation of magnetic-noise analyzers of stresses and structure of metals, supplementing possibilities of earlier produced instruments RMShA, INTROMET and INTROMAT.

Due to original technical solutions and availability of an inbuilt computer with operational system Windows CE, the instrument provides new possibilities and has no analogues in CIS and abroad.

It ensures:

- automatic construction and storage of unlimited number of the graduation curves;
- independence of the measurement results upon changes within wide range of a gap sizes between poles of a sensor and a controllable surface and upon state of the surface;
- presentation of information in relative and true units;
- construction of a diagram of stresses within 180° sector (in case of application of a 4-pole sensor);
- automatic selection of optimal control conditions;
- dialogue mode of operation, a convenient user interface, and visual presentation of scanning results in the form of linear or circular diagrams;
- simplicity of expansion of the instrument possibilities and adaptation to specific tasks of a user due to application of new user programs.

It may be used for:

- control and measurement of residual and applied stresses with application of special methodology for estimation of stress-strain state;
- control of surface plastic deformation;
- determination of a hardened layer thickness;
- assessment of stresses in near-surface layers at different depths up to 1 mm;
- control of thickness, width and profile of transitional zone of surface layers, hardened by laser, plasma and other kinds of treatment;
- control and detection of grinding burns;
- control of hardness of carbon and alloyed steels.

NEW EMISSION SYSTEM WITH TABLET LaB_6 CATHODE

Tablet LaB_6 cathodes have been used for many years in welding guns of the E.O. Paton Electric Welding Institute, which are also manufactured by Sumy PA «Elektron».

PWI is currently supplying to the customers a new emission system, in which the design of the molybdenum cathode holder and control electrodes has been changed, and fused single-crystal tablets of a special shape are used.

Previously used transition bushing

As-assembled unchanged heater component

New transition bushing

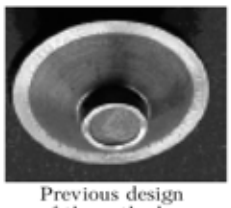

Previous design of the cathode–holder assembly

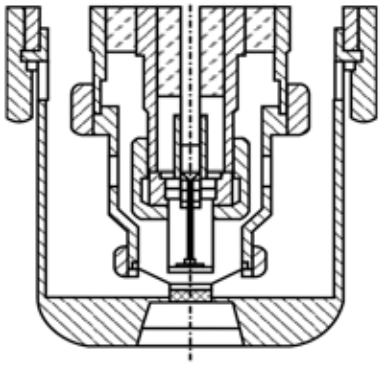

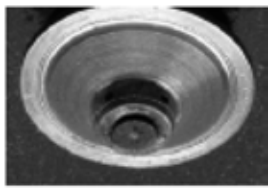

New design of cathode–holder assembly

Previously used control electrode

New control electrode

Development of a new emission system was necessitated primarily by a comparatively short cathode life (10 h). This is attributable to the fact that the emitting surface of a hot-pressed tablet is significantly disrupted because of the recrystallisation processes and ion bombardment. A large contact surface between the tablet and molybdenum holder intensifies the diffusion and evaporation processes leading to reduced dimensions of the tablet, change of its position and increase of the beam peripheral part. Such tablets are also prone to fracture because of cracking.

In order to replace the previously used emission system by a new system it is necessary to use only a new transition bushing, cathode assembled with the holder and control electrode. No other changes in the gun or power source are required. Cathodes and heating spirals are no longer delivered separately, in view of the impossibility of precision assembly of these elements with the holders under the conditions of a non-specialized plant, as well as because of the need for vacuum training of the assembled components.

Cathodes and heating elements are supplied only as-assembled with the holders:

Diameter of the cathode emitting surface, mm	Beam current, mA
1.50	0–50
3	0–250
3	0–500
4.25	1000

Application. New emission systems are designed for welding guns with accelerating voltage of 30, 60 and 120 kV (U-250A, ELA-15, ELA-30, ELA-60 / 60, ELA-60B, ELA-120-6, etc.).

Advantages of the new emission system:

• cathode life has been extended to 40 to 70 h due to application of single-crystal cathodes and a new design, preventing LaB_6 interaction with the molybdenum holder;

• specific beam power has been increased not less than 2 times due to elimination of its peripheral part, thus providing more narrow and deep welds;

• high reproducibility of welds has been ensured and possibility of beam deflection from the welding gun geometrical axis, and, hence also from the plane of the butt of the edges being welded has been eliminated, due to precision assembly and vacuum training of emission system components.

RANGE OF KL-109, KL-110 AND KL-111 UNIVERSAL MACHINES FOR EBW OF LARGE AND HEAVY WORKPIECES

• PC and programmable controllers are used.

• Electron beam parameters analysis and «black box» type selfdiagnostics of machine by PC.

• Real-time seam tracking and monitoring of EBW process by RASTR system on the basis of the secondary electron emission.

• Gun power source with electron tube flashless system.

Mobile type 15, 30 or 60 kW electron beam gun at accelerating voltage of 60 kV.

Design

The work chamber has two sliding doors. The workpiece table is moved out of the work chamber onto the runout platform of EBW process. The table acommodates rotators with horizontal and vertical axis, and also back centre. The electron gun 3-axis-manipulator has the travelling distance in *Õ*-direction up to 3000 mm, in *Y*-direction up to 730 mm and in *Z*-direction up to 1500 mm. Precision of the guidance and drive system equals that of precision machine tools operation with tolerances in the hundredth-of-a-millimeter range.

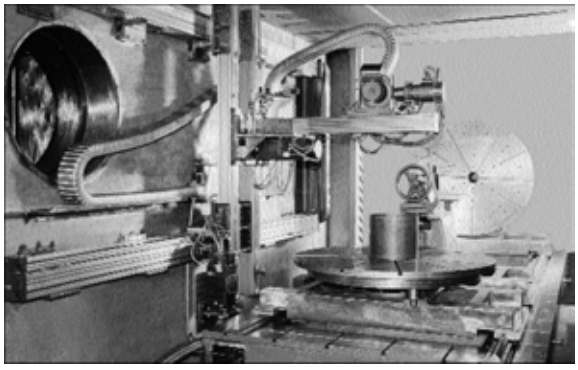

Technical data

Vacuum chamber inner dimensions, m:	
KL-109 and KL-110	$2.5 \times 2.5 \times 5.0$
KL-111	$2.0 \times 2.0 \times 5.5$
Time of evacuation up to the vacuum of $5 \cdot 10^{-4}$ Torr, min	≤ 45
Workpiece weight, kg	max 2500

KL-113 UNIVERSAL MACHINE FOR EBW OF LARGE WORKPIECES

- PC and programmable controllers are used.
- Electron beam parameters analysis and «black box» type selfdiagnostics of the machine by PC.
- Real-time seam tracking and EBW process monitoring by RASTR-5 system on the basis of the secondary electron emission.
- Gun power source with electron tube flashless system.

Machine design

The work chamber has two sliding doors. The workpiece table is moved out of the work chamber onto the charging car. The table acommodates the rotators with horizontal and vertical axis, also the tailstock. The mechanism of electron gun movement has three moving axes *Õ–Õ*, *Y–Y*, *Z–Z*. The gun moves by means of standard linear modules, equipped ball-and-screw gears. The gun is placed on a plate in the rotating support. Rotation may be performed in specified range of 0–90°. Rotation is visually controlled by limb / dial accurate up to 1°, as well as display of rotation angle on the monitor screen.

Vacuum system is assembled on the basis of two roughing-down pumps with capacity of 320 m^3 / h, a single two-rotor ROOTS pump with capacity of 4860 m^3 / h, two high-vacuum pumps D630 with capacity of 16000 l / s each, and turbo-molecular pump with capacity of 110 l / s.

Automated control system (ACS) is a program and hardware complex intended to control the EBW machine equipment (vacuum system, high-voltage source, positioner drive and rotators, RASTR-5M system) both during preparatory operations and EBW performance.

The ACS structure is hierarchic two-level (upper and lower control levels) distributed system. The upper control level (realized in operation medium Windows NT) performs the following functions:

- giving tasks to the lower level subsystems;
- representation of the ACS operation results;
- image of the weldment surface, weld and pool and tracking a joint (RASTR-5M system).

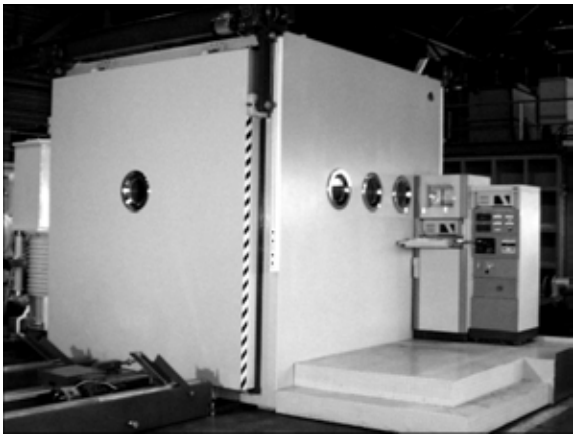

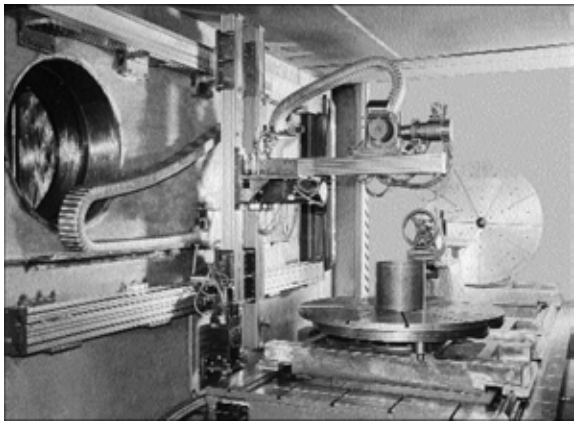

The lower level subsystems software is realized in MS DOS operation medium. The lower level function is direct control of the EB machine equipment. The realized software structure allows using MS DOS realiability at direct control of the machine in real time mode and Windows graphic possibilities (graphic interface) to create a friendly interface for a welding operator with visualization of the EBW processes. The ACS noise immunity is greatly increased due to the lower level subsystems location directly at control objects. Network interchange between the levels is realized by Fast Ethernet network line.

Main technical parameters for KL-113 machine

Overall machine sizes (l × w × h), mm	8450 × 280 × 3470
Weight without high voltage power source, t	32.5
Vacuum chamber internal sizes (l × w × h), mm	3000 × 2500 × 2700
Working pressure in chamber, Torr	not worse than $2 \cdot 10^{-4}$
Time before working pressure in chamber and gun is obtained, min	max 30
EB gun movements with positioning accuracy ±0.1 mm along the coordinates *X*–*X*, *Y*–*Y*, *Z*–*Z*, mm	1800, 800, 1000
Gun tilt angle with 1° accuracy in *X*–*Y* plane, deg	90
EB gun traveling speed along linear coordinates, mm / s	1.66–25
EB gun and source power, kW	15
Accelerating voltage, kV	$60 \pm 0.5 \cdot 10^{-2}$
Beam current, mA	1–250
Beam deflection angle, deg	±3.5
Technical parameters, provided by the Buyer:	
mains	380 V, 50 / 60 Hz
consumed power, kV·À	max 60
cooling water flow rate at temperature of 25 °Ñ and pressure of 2 kg / cm^2, l / h	min 1550
compressed air pressure, kg / cm^2	min 4

Prof. Nazarenko O.K.
E-mail: nazarenko@technobeam.com.ua
http: / / www.nas.gov.ua / pwj / beam
http: / / paton.kiev.ua / eng / inst / ntkstructure / deplist / 571.html